Forecasting Research

Met O 11 Technical Note No. 13

A theoretical study of the information content of the ERS-1 Scatterometer data

by

R. J. Purser

August 1988

Mete... 11)
London Road, E... 2 2SZ, England

MET O 11 TECHNICAL NOTE NO. 13

A THEORETICAL STUDY OF THE INFORMATION CONTENT OF THE ERS-1 SCATTEROMETER DATA

R. J. Purser

LONDON, METEORDLOGICAL OFFICE.
Met.O.11 Technical Note (New Series) No. 13

A theoretical study of the information content of the ERS-1 scatterometer data.

02580988 FH2A

Met O 11 (Forecasting Research)
Meteorological Office
London Road
Berkshire RG12 2SZ
ENGLAND

August 1988

ABSTRACT

When the random errors of an observing system and those of a background field are distributed according to known distributions then, given sample data, the information about parameters on which the true observational values depend is contained entirely in the implied likelihood function of these parameters. In the case of radar scatterometry only two parameters, the velocity components u and v, are sought from the measurements of backscattered power and background wind data. The likelihood function is therefore well displayed using a conventional contour plot.

Using anticipated error variances of the ERS-1 scatterometer we compute the likelihood functions on a grid in (u, v)-space for a variety of simulated data and assorted beam configurations. The resulting contour plots vividly display the essential problems relating to the appearance of two or more ambiguities in the velocities that locally maximise the likelihood. We find that at least a two-fold ambiguity is present in the standard three-beam configuration corresponding to equal speeds but approximately opposite directions. In the two-beam configuration that will be used near coasts, up to four modes of the likelihood function appear but with directions that are generally less well defined than those of the three-beam configuration. The inclusion of background information, even if it is of unexceptional quality, greatly increases the chances of correctly selecting the proper alias and a probabilistic quantification of the available choices can be provided to ascertain the degree of certainty associated with the selection adopted. Given the correct choice is made, the resulting precision is potentially very high with implied standard-deviations of about half a metre per second.

1. INTRODUCTION

There is a prospect of a wealth of new data in the form of ERS-1 scatterometer winds expected to become available in the early nineteen-nineties (Offiler, 1987). In their raw form the data comprise calibrated radar backscatter returns from fairly small patches of the sea surface. The sampling arrangement is designed to ensure that over open ocean the same patch of sea is observed from three different azimuth angles as the satellite passes by. The backscatter is caused by Bragg interference from small wind-sensitive wavelets and, not surprisingly, is dependent on (among other things) both the speed of the wind and its direction relative to the azimuth of the beam. As a consequence, it is possible in principle to infer from the backscatter measured at different azimuths the mean wind velocity affecting the patch of sea surface sampled, although in practice the retrieved wind can only be narrowed down to from two to four distinct ambiguities.

In practice, we should expect a number of sources of noise, in addition to the ordinary measurement noise whose amplitude is approximately known. These might include defects in our "forward model" that expresses backscatter as a function of geometrical variables and wind speed, possibly the effects of intense precipitation within the area observed (although this should be less of a problem than in the case of the Seasat scatterometer which used a radar with much shorter wavelength than that of the ERS-1 instrument). Also there is the possibility of an inhomogeneous sea state over the area (approximately 50 Km square) sampled by the instrument, which might appear as an effective noise component. The effect of noise in the observations is to blur the points in velocity component (u, v) space considered consistent with the observations. Given a probability model for the distribution of errors of each measurement it is possible, as will be demonstrated in Section 2, to construct for each point (u, v) of velocity space the "likelihood function" which objectively quantifies the degree to which each velocity vector can "explain", or be considered consistent with, the backscatter actually observed. Moreover, no relevant information is lost by considering the likelihood function as a surrogate for the raw observations, since any Bayesian estimate of velocity

(i.e., combining the observational data with prior probabilistic information) is effected by multiplying the prior probability for (u, v) by the likelihood to get the posterior probability. We shall expand on these statistical concepts in the next section.

For practical purposes it is usually more convenient to work with the logarithm of the likelihood (and in Bayesian estimation with the logarithm of the probability densities). Then, since the likelihood contributions of independent measurements combine multiplicatively, the log-likelihoods can simply be added. In the simulations presented in Section 3 we assume that the errors in each beam are distributed independently, both from each other and from the error in the background when the latter is used.

We then find that with plausible distributions for the measurement error and without the use of the background field a three-beam configuration gives two principal aliases of almost equal likelihood, but with velocities very sharply defined once the correct alias is known. In the two-beam configuration, four aliases are typical although they may often merge to give ill-defined maxima ("modes") of the likelihood. The curvature or "Hessian" of the log-likelihood at the modes gives a measurement of the effective precision of the combined data (the "information matrix"). The principal standard deviations from the information matrix show high precision but a significant anisotropy (by a factor of about two or three) with the velocity being more accurately defined in magnitude than in the sense orthogonal to the inferred direction. The inclusion of background data greatly assists in the selection of the proper alias, even if the standard deviation of this background is comparable with the true wind speed itself. Assuming a known distribution for the prior probability of the background error it is possible to estimate the proportion of occasions when the background information will actually mislead - i.e., causing the wrong alias to be given preference. Not only is this proportion very small for plausible statistics but, on those occasions when the background does tend to mislead the relative likelihoods of the two competing aliases tend to be sufficiently close that this information itself can be used to alert an analysis system to the possibility of a persisting ambiguity in the data provided.

2. THE LIKELIHOOD FUNCTION AND ESTIMATION THEORY.

If a probability function used to model the frequency of occurences of a certain number of observations is believed to belong to a family of such functions, each identified by N unknown parameters, $u_1, u_2, .., u_N$, the actual observations are normally better explained by some vectors $\underset{\sim}{u}$ of parameters than by others. Suppose for example that, prior to obtaining measurements, it is known that the u components themselves are random variables distributed jointly according to some probability density function,

$$P(\underset{\sim}{u}) \quad , \tag{2.1}$$

and that, given $\underset{\sim}{u}$, the probability of P imprecise measurements, $\underset{\sim}{\sigma} = \sigma_1, .., \sigma_P$, is

$$P(\underset{\sim}{\sigma} | \underset{\sim}{u}) \quad . \tag{2.2}$$

Then since the probability of both $\underset{\sim}{\sigma}$ and $\underset{\sim}{u}$ is given by the joint density (in a space of dimension N+P):

$$P(\underset{\sim}{\sigma}, \underset{\sim}{u}) = P(\underset{\sim}{\sigma} | \underset{\sim}{u}) P(\underset{\sim}{u}) \quad , \tag{2.3}$$

which is clearly equal to

$$P(\underset{\sim}{u}, \underset{\sim}{\sigma}) = P(\underset{\sim}{u} | \underset{\sim}{\sigma}) P(\underset{\sim}{\sigma}) \quad , \tag{2.4}$$

we conclude that the conditional probability of $\underset{\sim}{u}$ given measurements $\underset{\sim}{\sigma}$ is

$$P(\underset{\sim}{u} | \underset{\sim}{\sigma}) = \frac{P(\underset{\sim}{\sigma} | \underset{\sim}{u}) P(\underset{\sim}{u})}{P(\underset{\sim}{\sigma})} = \frac{P(\underset{\sim}{\sigma} | \underset{\sim}{u}) P(\underset{\sim}{u})}{\int P(\underset{\sim}{\sigma} | \underset{\sim}{u}) P(\underset{\sim}{u}) \prod_{i=1}^{N} du_i} \quad , \tag{2.5}$$

which is Bayes' theorem.

The important point to observe is that, given two possible vectors $\underset{\sim}{u}_1$, $\underset{\sim}{u}_2$, to compare, their relative probability or "odds", expressed as a ratio, on the evidence provided by $\underset{\sim}{\sigma}$, takes the form:

$$\frac{P(\underset{\sim}{u}_1 | \underset{\sim}{\sigma})}{P(\underset{\sim}{u}_2 | \underset{\sim}{\sigma})} = \frac{P(\underset{\sim}{\sigma} | \underset{\sim}{u}_1)}{P(\underset{\sim}{\sigma} | \underset{\sim}{u}_2)} \cdot \frac{P(\underset{\sim}{u}_1)}{P(\underset{\sim}{u}_2)} \quad . \tag{2.6}$$

Thus, regardless of the prior probability distribution $\underset{\sim}{u}_1$ and $\underset{\sim}{u}_2$ happen to belong to, the effect of the data $\underset{\sim}{\sigma}$ is to modify the odds of $\underset{\sim}{u}_1$ versus $\underset{\sim}{u}_2$ being the true parameters by the multiplication of the "likelihood ratio":

$$\frac{P(\underset{\sim}{\sigma} | \underset{\sim}{u}_1)}{P(\underset{\sim}{\sigma} | \underset{\sim}{u}_2)} \quad . \tag{2.7}$$

Clearly the likelihood function, defined within arbitrary multiplicative factors by

$$L(\underset{\sim}{u}) = P(\underset{\sim}{\sigma}_m | \underset{\sim}{u}) \quad , \tag{2.8}$$

expresses completely the information from measurements $\underset{\sim}{\sigma}_m$ that could be relevant to the estimation of the parameters $\underset{\sim}{u}$. Equivalently, we may take the log-likelihood function,

$$\ell(\underset{\sim}{u}) = \log L(\underset{\sim}{u}), \tag{2.9}$$

and use it to modify additively the log-prior, yielding (within arbitrary additive constant) the log-posterior probability density from which final inferences would be drawn. A thorough discussion of the use of the likelihood function as a tool for statistical inference can be found in the monograph by Edwards(1972).

3. SIMULATION AND ASSESSMENT OF SCATTEROMETER DATA.

a) Likelihood functions for Gaussian statistics.

In applying the theory of section 2 to scatterometer data, the "parameters" we aim to estimate are the two velocity components orthogonal

to and parallel to the track of the satellite,

$$u_1 = u$$
$$u_2 = v \,. \qquad (3.1)$$

The measurements, $\underset{\sim}{\sigma}$, are the calibrated radar-backscatter returns from the portion of sea observed. When a background value B is included, then formally this value becomes equivalent to yet another measurement as far as the analysis of one patch of sea is concerned. The method of simulation of the data is to choose a "true" value of the two wind components, $\underset{\sim}{u}_T$. Then to compute from these, the corresponding "true" backscatter values $\underset{\sim}{\sigma}_T$ using a forward model provided by Met O 24 based on Long (1986). The beam directions are taken to be 45°, 90° and 135° relative to the track of the spacecraft. The zenith angle is taken to be 45° for the studies presented although strictly it will be different for each beam direction. Figure 1 shows a schematic depiction of the satellite and beam arrangement. The observed values $\underset{\sim}{\sigma}$ are generated by adding a pseudo-random noise component to the true value $\underset{\sim}{\sigma}$. In most of the examples presented here we use Gaussians for the error distributions with standard deviations, s_σ, 9% of the corresponding true $\underset{\sim}{\sigma}$ (this proportion is expected to increase slightly for larger zenith angles):

$$\left\langle (\sigma_m - \sigma_T)^2 \right\rangle^{1/2} = s_\sigma = 0.09\,\sigma_T \,. \qquad (3.2)$$

In a similar way, random errors can be added to the true wind, $\underset{\sim}{u}_T$, to generate a plausible background field, $\underset{\sim}{u}_B$, and again we use a Gaussian model for most of our simulations. The log-likelihood for a given selection of data is computed according to the same probability model used to simulate the data. Thus, the log-likelihood function for a single beam with measurement σ_m is

$$\ell_m(\underset{\sim}{u}) = \frac{-\left[\sigma_m - \sigma(\underset{\sim}{u})\right]^2}{2s_\sigma^2} \,, \qquad (3.3)$$

and is the sum of such terms for multiple beam measurements. Similarly the contribution from the background field is a term,

$$\ell_b(\underset{\sim}{v}) = \frac{-|v_b - v|^2}{2 s_b^2} \quad , \qquad (3.4)$$

where s_b is the standard deviation of a single wind component of the background field error. For display it is convenient to add a constant to the likelihood function that brings the maximum value to zero. The relative likelihood of subsidiary modes can then be quickly assessed. In each figure we display eleven charts using the same format for easy comparison. Each of the eleven shows a log-likelihood function contoured in unit intervals in the range [0,-10] (actually, the values contoured are the negatives of the log-likelihoods, i.e., "cost functions", since this avoids the congestion of redundant "-" prefixes by each contour label). Velocities with log-likelihood less than -10 are shown hatched and are not considered relevant in the estimation of $\underset{\sim}{u}$. The scatterometer beams are numbered 1,2,3 representing the relative azimuth angles 45°, 90°, 135° respectively. The contributing data of each of the eleven charts of a figure are listed in table 1.

The "nth" chart of figure "m" will be referred to as "figure m.n". Figure 2.1 shows the log-likelihood for the background value simulated using a Gaussian distribution of errors in each component with a standard deviation s_b=5 ms^{-1}. The true velocity (shown by a cross in each illustration) is directed 260° to the track of the satellite and has a magnitude of 5 ms^{-1}. Charts 2, 3 and 4 show the individual contributions to the log-likelihood from the three respective beams taken singly. Note the characteristic oval shape to the loci of maximum likelihood and the approximate symmetry of each pattern when rotated 180° degrees. Combining two beams (1 and 2) gives the log-likelihood contribution shown in chart 5 with the typical four-fold ambiguity in wind manifested in the four equal modes of the likelihood. As a consequence of the approximate symmetry referred to above these aliases tend to occur in diametrically opposing pairs. On adding the information from the third beam (chart 6) it is usually possible to eliminate one pair of ambiguities leaving two almost equally likely aliases. On the basis of scatterometry alone it is clearly very difficult to justify giving preference to one alias at the expense of

the other, and this is especially true at low wind speeds where the approximation to 180° symmetry is relatively good. The remaining charts 7 to 11 are like charts 2 to 6 respectively except that now we add in the contribution from the background. Even each impoverished configurations of one beam (charts 7, 8, 9) now provides a unique mode in roughly the correct part of (u, v)-space in this particular example. The two-beam (chart 10) and three-beam (chart 11) configurations still display the same ambiguities as before but with a preference or "ranking" among the modes according to how close each one is to the background. In the two beam arrangement the proper alias is now preferred to its nearest competitor by a margin of approximately 0.78 units of log-likelihood, corresponding to a likelihood ratio of roughly 2:1. With three beams, although the likelihood margin remains about the same the number of possible aliases is now reduced to only two. In the case of such slack winds only a modest advantage is gained by the use of a background.

Figure 3 shows another sequence of charts, this time from a simulation with a true wind of the same speed of 5 ms^{-1} but now blowing at 180° to the satellite track. Although the patterns of the likelihood-charts are different in detail from figure 2 (for example charts 5 and 10 show that the two pairs of ambiguities are now less distinct from each other in the two-beam configuration), we still see the characteristic four aliases with two beams, two aliases with three beams. As in figure 2, the background, while not positively misleading, only weakly supports the proper alias, being displaced from "truth" towards the origin. Figure 4 shows another randomly generated simulation, again with the same Gaussian statistics and true wind speed, but in which the background happens to be displaced relative to the truth away from the origin. At this orientation, with the true wind at 120°, the four ambiguities of the two-beam configuration become degenerate - there are apparently only three distinct modes in figure 4.5. As expected from the displacement of the background, its presence lends support to the choice of proper alias relative to the false one in the three-beam arrangement (figure 4.11), this time by a log-likelihood margin of just over four units (a likelihood ratio of 64:1). However, with two beams (figure 4.10) the two almost degenerate modes near the truth are

about equally supported by the background. This nicely illustrates the advantage of possessing three beams over two.

At higher true wind speeds, but retaining the same assumed background errors, the patterns expand as we would expect and the value of the background as an aid in discriminating aliases increases. Figure 5 shows the simulation with a 10 ms^{-1} wind at 260° to the satellite track. As previously mentioned, there does appear to be slightly less of the 180° symmetry present in the scatterometer-only contours (charts 2 to 6), but not to the extent that the true alias in chart 6 enjoys obvious preference over its opposite. The inclusion of background information with a standard deviation now less than the actual wind speed has more pronounced effect on the likelihood charts, usually confering a strong preference for the proper mode relative to other modes. Even in the single beam configurations (charts 7 to 9) the location of the true wind is narrowed down to effectively a single elongated region of the (u, v)-plane in each case. If we compare figures 5.10 and 5.11 for the 10 ms^{-1} wind with the corresponding figures 2.10 and 2.11 for the 5 ms^{-1} wind at the same orientation it is clear that at the larger wind speed the modes are not quite as sharply defined. However, the ability to discriminate the good mode using the background is enhanced, as exemplified by figure 5.11 in which the likelihood ratio of the true to the false alias is approximately 400:1. At a true wind direction of 180° figure 6 shows another example of degeneracy of the modes of the two-beam configuration (chart 5) resulting now in a single pair. In the three-beam configuration, figure 6.6, we see just a hint of a positive discrimination between the good mode and the bad by consistency among the beams themselves, but a likelihood ratio of only about 3:1 and the risk of making a 20 ms^{-1} error hardly warrant reliance on scatterometry alone to de-alias the winds in a case such as this. As in figure 5, the background gives very definite support to the true alias in the two- and three-beam arrangements. Figure 7 shows a simulation for a 15 ms^{-1} wind of 260°. With the inclusion of background data, the false alias does not even register on the likelihood charts so, provided our statistical assumptions are valid, we can be virtually certain that the alias selected is the correct one. The 5 ms^{-1} standard deviation of the background components is a somewhat arbitrary assumption. If we were to

choose s_b=2.5 ms^{-1} instead, then the shape in the sequence of figure 2 would resemble the present figure 5, while if we chose s_b=7.5 ms^{-1} then figure 7 would resemble the present figure 5 (except in scale, of course). The important point is that a background is helpful in de-aliasing and is more reliable in this role the more precise it is in comparison with the true wind speed.

It is a simple procedure to extract from the gridded log-likelihood functions used in the construction of the preceding figures the "precision" or "information" matrix associated with the chosen alias. This is defined as the Hessian matrix of second derivative coefficients of the negative-log-likelihood at the mode. The inverse square-roots s_1, s_2, of the eigenvalues of this matrix are like standard deviations of the contributing data in the directions defined by the two respective eigenvectors. In table 2 these numerically estimated principal standard deviations, together with the orientation θ of the more precise component, are listed for the examples illustrated in figures 2 to 7 and for those charts representing data combinations $\{\sigma_1, \sigma_2\}$, $\{\sigma_1, \sigma_2, \sigma_3\}$, $\{B, \sigma_1, \sigma_2\}$, $\{B, \sigma_1, \sigma_2, \sigma_3\}$, (i.e., charts 5, 6 , 10 , 11). The relative coarseness of the (u, v)-grid makes the first three rows of entries of this table somewhat unreliable - the missing value results from an erroneous appearance of a negative eigenvalue of the numerically estimated information matrix for that entry. Note that in each case the orientation of the dominant principal component of the precision matrix is roughly in line with the actual wind, and the accuracy in this direction tends to be a factor of about two times better than the accuracy of the transverse component - i.e., speed is measured better than azimuth. With these idealised assumptions even the larger standard deviations are still well within the normal requirements of numerical weather prediction.

b) Estimating the frequency of misleading background values.

It is useful to be able to estimate (at least roughly) the proportion of occasions when the background misleads us in the selection of the proper alias. In a simple statistical model of the ambiguities, where each has the same (true) speed and equal likelihood and the aliases appear in exactly opposing pairs, then assuming the error of the proper alias is negligible compared to that typical of the background, the background is misleading

whenever it is closer to a false alias than it is to the true one. With the Gaussian background statistics assumed in the experiments above the probability of the background misleading can be computed for both the standard three-beam and the two-beam configurations if, for the latter, the angle 2α between the lines of the two alias-pairs is known.

Define

$$f(x) = \int_x^\infty \frac{1}{\sqrt{2\pi}} \exp\left(-\frac{x'^2}{2}\right) dx' \quad , \tag{3.5}$$

i.e., the probability of a Gaussian random variable exceeding its mean by more than a proportion x of its standard deviation. Then if $|\underset{\sim}{u_t}|$ is the true wind speed, the background will mislead in the three-beam case on a proportion of occasions,

$$P_1 = f(u') \quad , \tag{3.6}$$

where

$$u' = \frac{|\underset{\sim}{u_t}|}{s_b} \quad , \tag{3.7}$$

and where s_b is the component standard deviation of background error as before. We may also generalise this estimate to the proportion P_r of occasions where the background "seriously" misleads by not only being closer to a false alias but also by supporting it at the expense of the true alias by a likelihood ratio exceeding r. In the schematic figure 8a this occurs when the background lies within the shaded half-plane with

$$\exp\left[\frac{1}{2}\frac{(d_1^2 - d_2^2)}{s_b^2}\right] = r \quad . \tag{3.8}$$

Since

$$d_1 + d_2 = 2|u_t| \quad , \tag{3.9}$$

then

$$d_1 = s_b\left(v' + \frac{\log r}{2v'}\right) , \qquad (3.10)$$

and hence

$$P_r = f\left(v' + \frac{\log r}{2v'}\right) . \qquad (3.11)$$

Table 3 lists a selection of these probabilities assuming $s_b = 5\ ms^{-1}$, P_1 for those cases that are generally misleading and P_{10} for those seriously misleading with an adverse likelihood ratio of ten associated with the latter.

For the configurations with four aliases of equal likelihood and speed shown in the schematic diagram of figure 8b, P_r is obtained from the frequency at which the background is found in the shaded region, where the dimensions satisfy,

$$\exp\left[\frac{1}{2}\frac{(a_1^2 - a_2^2)}{s_b^2}\right] = \exp\left[\frac{1}{2}\frac{(b_1^2 - b_2^2)}{s_b^2}\right] = \exp\left[\frac{1}{2}\frac{(d_1^2 - d_2^2)}{s_b^2}\right], \qquad (3.12)$$

with,

$$\begin{aligned} a_1 + a_2 &= 2|v_t| \cos\alpha \ , \\ b_1 + b_2 &= 2|v_t| \sin\alpha \ , \\ d_1 + d_2 &= 2|v_t| \ . \end{aligned} \qquad (3.13)$$

This probability, P_r , is then computed numerically by the appropriate double integration.

Table 4 lists the pairs of such probabilities, P_1, P_{10}, for angles 2α = 30°, 60°, 90°, using statistical assumptions similar to those used for table 3. We clearly see that the chances of a misidentification of the proper alias are decreased by using three beams instead of two, also these mistakes are more likely when the wind is slack (when it fortunately matters less). Furthermore, it is clear that a seriously misleading

background (corresponding to P_{10}) occurs with a very much smaller frequency than a generally misleading one (P_1).

c) Non-Gaussian statistics

The discussion so far has centred on simulations that assume Gaussian error statistics. In particular, the magnitudes of probabilities in tables 3 and 4 depend critically on the weight in the tails of the distribution of errors. For Gaussian distributions, which tend to have thinner tails than those of more realistic distributions of observational error (which have their tails fattened by the sporadic appearance of gross errors) the probabilities of the background selecting a false alias are probably underestimated. The general appearance of sequences of likelihood charts can be dramatically altered by seemingly minor modifications of the probability distribution of error. To illustrate this, figure 9 shows a sequence following the format used in the earlier simulations, where again we assume a true speed of 5 ms^{-1}, directed 260° to the satellite track but now with fat-tailed distributions assumed for all errors. Each error is simulated by assigning a proportion, 0.9, to the previously used Gaussian but the remaining 0.1 assigned to a Gaussian with ten times the width. Although the particular errors of the random simulation shown in figure 9 do not obviously belong to the outlier portion of the new distributions, we observe a striking change in the appearance of the log-likelihood contours, especially away from the immediate vicinity of the principal aliases. Now we find structures for the likelihood distribution that become progressively more complicated as more information is assembled. The loci of maxima of the individual contributions become ridges of the likelihood function linking numerous modes when observations are combined. It is not claimed that the simple form of fat-tailed distribution employed in this example is realistic - the example is included just to underline the point that one should be aware of the often sensitive dependence of objective inferences on the particular set of statistical assumptions constituting the framework within which these inference are being made. Thus it is better to regard the implicit assumption of Gaussian statistics often made in data assimilation not as a fact but rather as the starting point for further refinement when real data eventually become available and their statistics accumulated.

4. SUMMARY

The theory of likelihood estimation was discussed in section 2 and applied in section 3 to the examination of the effective information content of scatterometer observations. The assumption of Gaussian statistics for the measurement and background errors leads to the following general characteristics concerning the retrieved winds.

i) The normal three-beam insrument configuration generally leads to two aliases of approximately equal speed but opposite direction; a two-beam configuration usually leads to four aliases of roughly comparable speeds occurring in two opposing pairs. In certain orientations of the two-beam configuration relative to the true wind the aliases can merge, corresponding to three, or even two, degenerate modes of the likelihood function.

ii) Having scatterometer data alone is not sufficient to yield a reliable discrimination of the true alias from the false one(s).

iii) The provision of a background value, i.e., a wind extracted from the most recent forecast, is a valuable source of independent data that is in most cases sufficient to enable a reliable selection of the true alias to be made.

iv) In the majority of those rare cases when the background happens to mislead, the degree of preference it confers on a false alias relative to the true, as quantified by the likelihood ratio, is minor, so the likelihoods themselves can be used as indicators of a potential persisting ambiguity.

v) The effective precision of retrieved winds for scatterometry, once external information has successfully selected the proper alias, is very high. Although the precision is anisotropic, speed being better determined than azimuth, even the larger component of effective standard deviation is sufficiently small that in practice the anisotropy in precision can safely be neglected in an operational assimilation scheme.

The considerations above suggest that for data assimilation it is important to be able to use forecast background information in the selection of the appropriate alias, which means that either the raw measurements $\underset{\sim}{o}$ or the principal aliases are needed to effect this decision.

However, since the effective precisions of retrieved winds, given the correct alias, are so high, there seems very little to be gained operationally from working with the raw σ data if the complete set of principal aliases are already available. In the non-operational monitoring of data quality and the validation of the parameters of the "forward model" there is of course considerable value in having access to the raw data. The problems of quality control can generally be interpreted in statistical terms as the identification and special treatment (e.g., rejection) of occasional outliers. Accounting for such "rogue" observations objectively requires a reasonably representative model for the tails of the error distributions. The final experiment of section 3 demonstrates the dramatic change in the information content of the given measurements when fat-tailed distributions are substituted for the Gaussians used in the previous simulations. The actual form for the error distributions will only be ascertained by the painstaking accumulation of statistics from real scatterometer measurements and forecast backgrounds.

The present study is deliberately restricted to consideration of essentially "spot" observations. While some emphasis has been placed on the importance of background information, another source of external data for de-aliasing arises from considerations of horizontal consistency of the wind field. Such consistency should be particularly vital in cases where the background field errors take the form of a broadly coherent displacement from the true field (e.g., a forecast timing error). In this case it is possible to imagine a contiguous region of significant extent within the swath of scatterometer data being consistently misled by background field winds that are closer to the false aliases than to the true ones. Inevitably, there will be sparsely observed locations where the resulting errors will pass undetected but it is nevertheless important to seek ways by which the frequency of such mistakes is minimised. In the absence of other independent observations the only hope seems to be to exploit the spatial statistics of the surface wind field in order to detect likely inconsistencies and, if possible, correct them. Constraints of smoothness and the smallness of divergence are candidates for the kind of constraining assumptions that might be used within a variational method to ensure regional consistency (Hoffman, 1982). A study has begun of the

variational techniques that might be used objectively in such awkward situations to identify and correct partially erroneous swaths using both background data and spatial constraints and the results from this study are expected to form the contents of a future technical note

ACKNOWLEDGMENT

The code for the forward model used in these simulations was kindly supplied by David Offiler. Considerable assistance was provided by Dr. Brian Barwell in setting up the code for the graphical output used in the figures.

References

Edwards, A. W. F., 1972: "Likelihood". Cambridge University Press, 235pp.

Hoffman, R. N., 1982: "SASS wind ambiguity removal by direct minimization". Mon. Wea. Rev. 110, 434-445.

Long, A. E., 1986: "Towards a C-band radar sea-echo model for the ERS-1 scatterometer". In proceedings of the conference on spectral signatures of objects in remote sensing. Les Arcs, 16-20 December 1985. Paris, ESA No SP-247.

Offiler, D., 1987: "Wind measurements from the Earth Resources Satellite (ERS-1)". Met. Mag., 116, 279-285.

CHART	BACKGROUND	σ_1	σ_2	σ_3
1	/			
2		/		
3			/	
4				/
5		/	/	
6		/	/	/
7	/	/		
8	/		/	
9	/			/
10	/	/	/	
11	/	/	/	/

Table 1: data contributing to log-likelihood charts

		$\{\sigma_1, \sigma_2\}$			$\{\sigma_1, \sigma_2, \sigma_3\}$			$\{B, \sigma_1, \sigma_2\}$			$\{B, \sigma_1, \sigma_2, \sigma_3\}$		
Spe.	Dir.	s_1	s_2	θ	s_1	s_2	θ	s_1	s_2	θ	s_1	s_2	θ
5	260°	0.38	0.61	317°	0.29	0.42	267°	0.24		242°	0.22	0.42	267°
5	180°	0.17	0.34	254°	0.21	0.37	159°	0.17	0.34	254°	0.21	0.37	159°
5	120°	0.28	0.84	107°	0.19	0.60	107°	0.28	0.71	103°	0.19	0.60	107°
10	260°	0.79	0.99	271°	0.40	0.65	271°	0.50	1.21	243°	0.47	0.70	272°
10	180°	0.31	1.46	224°	0.41	0.52	173°	0.41	0.97	220°	0.40	0.53	162°
15	260°	0.54	2.01	244°	0.70	1.07	276°	0.86	1.98	239°	0.69	1.05	276°

Table 2. Principal component standard deviations and orientations for various combinations of data used to construct figures 2 through 7.

$\|u_t\|$	P_1	P_{1o}
2.5	0.31	0.0025
5.0	0.16	0.016
7.5	0.067	0.012
10.0	0.023	0.005
12.5	0.0062	0.0015
15.0	0.0014	0.00036

Table 3. Probabilities of misleading, and seriously misleading, background values when their errors are Gaussian with standard deviation s_b=5 ms^{-1} for the case of two opposing aliases.

	$2\alpha=30°$		$2\alpha=60°$		$2\alpha=90°$	
$\|u_t\|$	P_1	P_{1o}	P_1	P_{1o}	P_1	P_{1o}
2.5	0.62	0.0059	0.60	0.0090	0.59	0.010
5.0	0.50	0.041	0.44	0.068	0.42	0.080
7.5	0.40	0.047	0.30	0.077	0.27	0.084
10.0	0.32	0.044	0.19	0.064	0.15	0.064
12.5	0.26	0.041	0.12	0.048	0.076	0.043
15.0	0.22	0.040	0.071	0.035	0.034	0.028

Table 4. Probabilities as in table 3 but for four aliases occurring in pairs oriented at angle 2α to each other, as depicted in figure 8b.

Figure captions

Figure 1: Schematic view of ERS-1 satellite and its three scatterometer beams.

Figure 2: A sequence of log-likelihood charts from a random simulation of background and observations when the true wind is 5 ms^{-1} and directed towards 260° azimuth relative to the satellite orientation. The component- standard deviation of the background (chart 1) is 5 ms^{-1}. Charts 2 to 4 show log-likelihoods from the three beams individually, charts 5 and 6 show those from the beam combinations (σ_1, σ_2), (σ_1, σ_2, σ_3). The remaining sequence repeat in order the combinations of charts 2 through 6 but with the background data now added.

Figure 3: As for figure 2 but with true wind of 5 ms^{-1} at 180°.

Figure 4: As for figure 2 but with true wind of 5 ms^{-1} at 120°.

Figure 5: As for figure 2 but with true wind of 10 ms^{-1} at 260°.

Figure 6: As for figure 2 but with true wind of 10 ms^{-1} at 180°.

Figure 7: As for figure 2 but with true wind of 15 ms^{-1} at 260°.

Figure 8: Geometry of region (shaded) of (u, v)-space corresponding to a "seriously" misleading background value, (a) for two aliases situated symmetrically about the velocity origin, (b) for four aliases of equal speed situated in pairs aligned at an angle 2α to each other.

Figure 9: As for figure 2 with a true wind of 5 ms^{-1} at 180° but with fat-tailed non-Gaussian error-statistics.

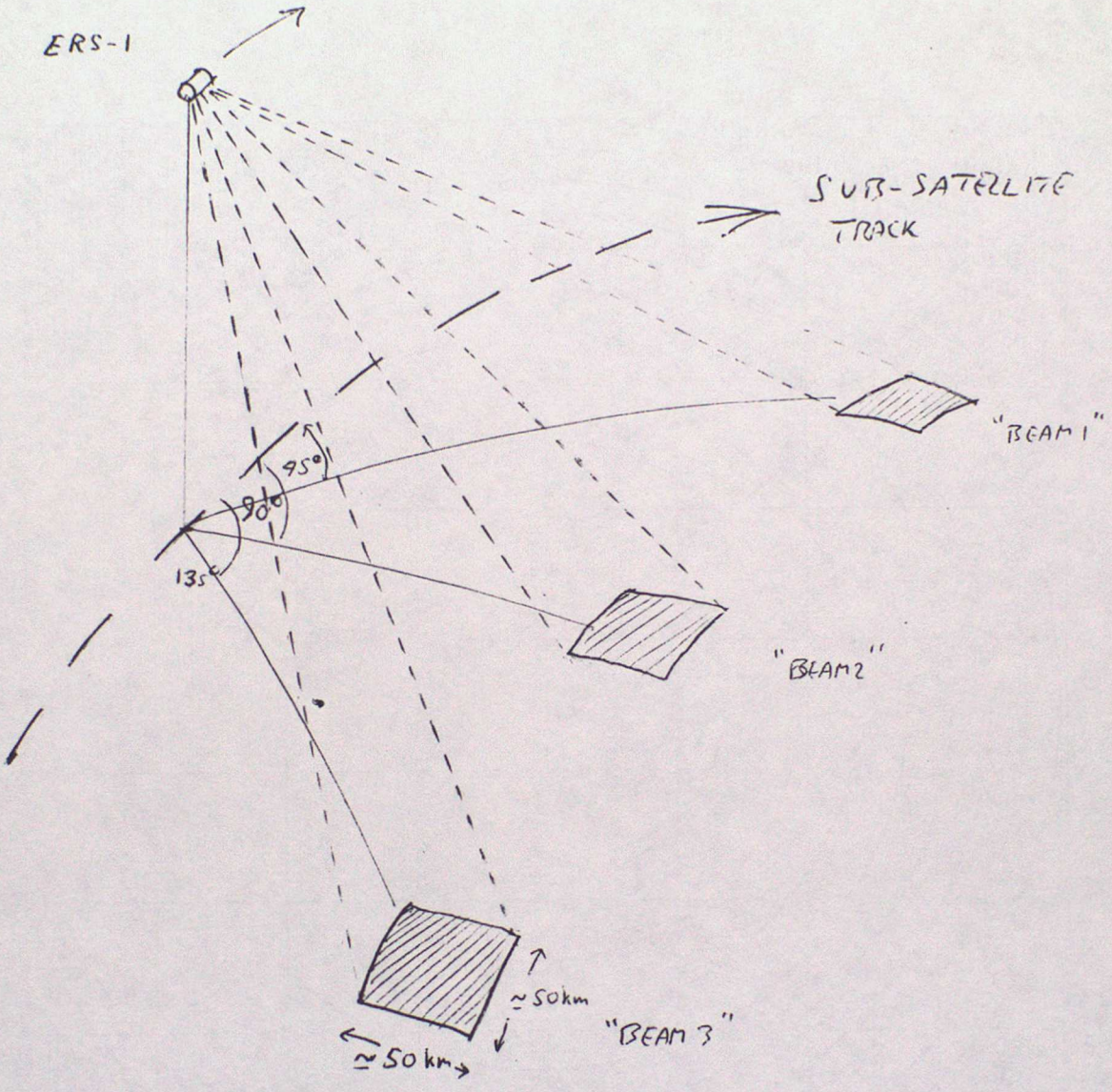
ERS-1
SUB-SATELLITE TRACK
"BEAM 1"
95°
90°
135°
"BEAM 2"
≃ 50km
≃ 50 km
"BEAM 3"

FIGURE 1

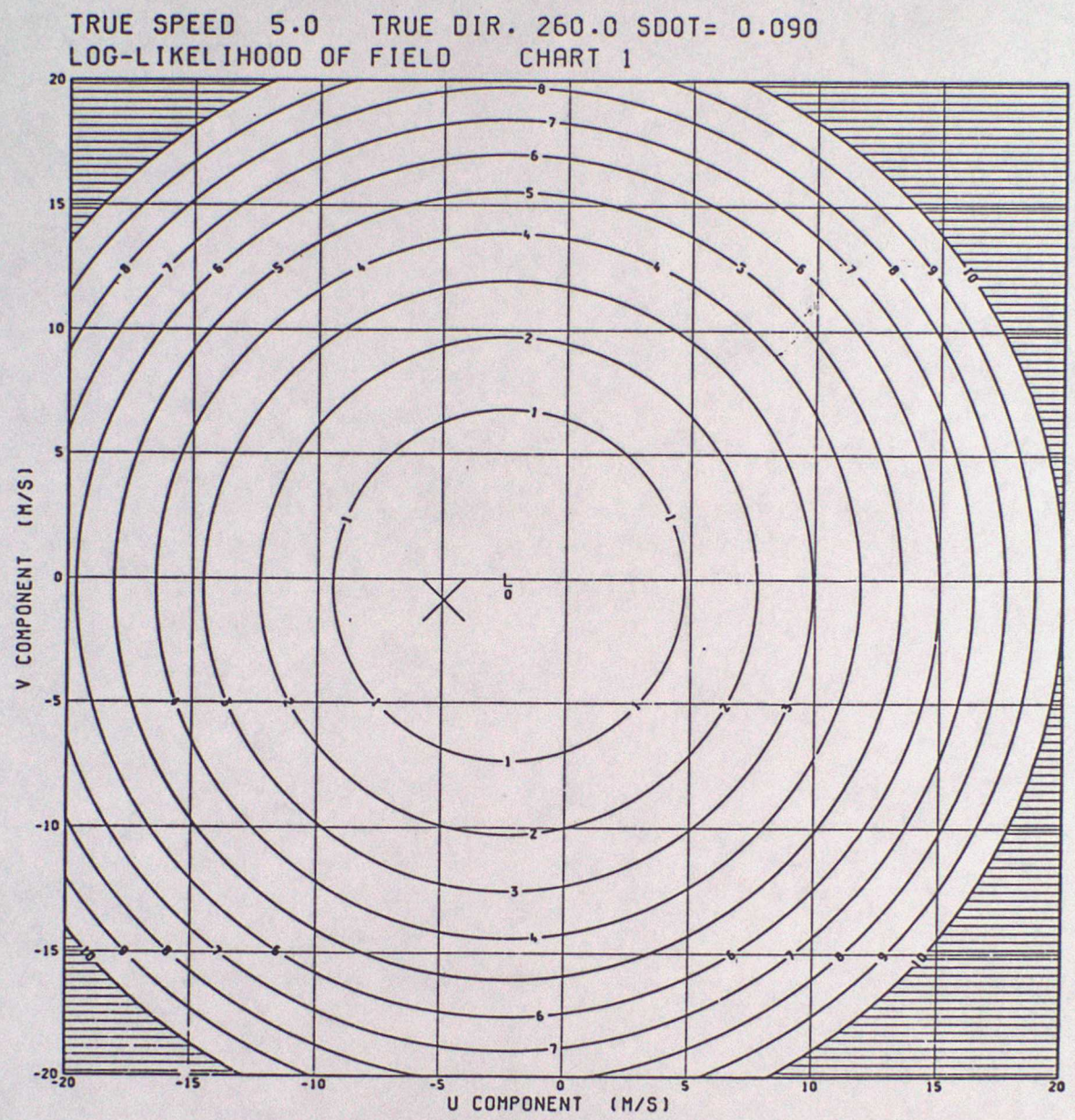
TRUE SPEED 5.0 TRUE DIR. 260.0 SDOT= 0.090
LOG-LIKELIHOOD OF FIELD CHART 1
V COMPONENT (M/S)
U COMPONENT (M/S)
20
15
10
5
0
-5
-10
-15
-20

FIGURE 2.1

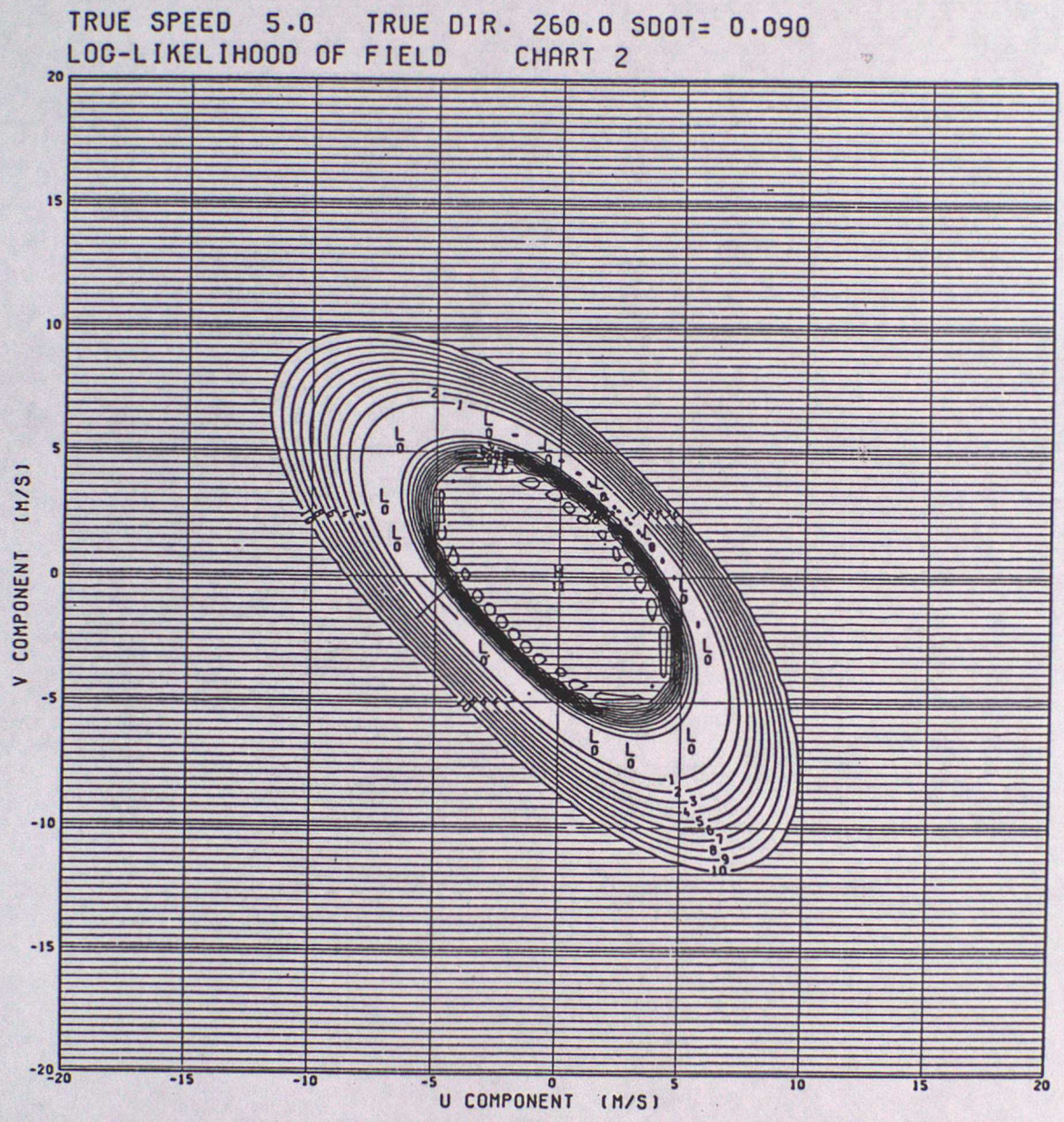
TRUE SPEED 5.0 TRUE DIR. 260.0 SDOT= 0.090
LOG-LIKELIHOOD OF FIELD CHART 2
V COMPONENT (M/S)
U COMPONENT (M/S)
20
15
10
5
0
-5
-10
-15
-20

FIGURE 2.2

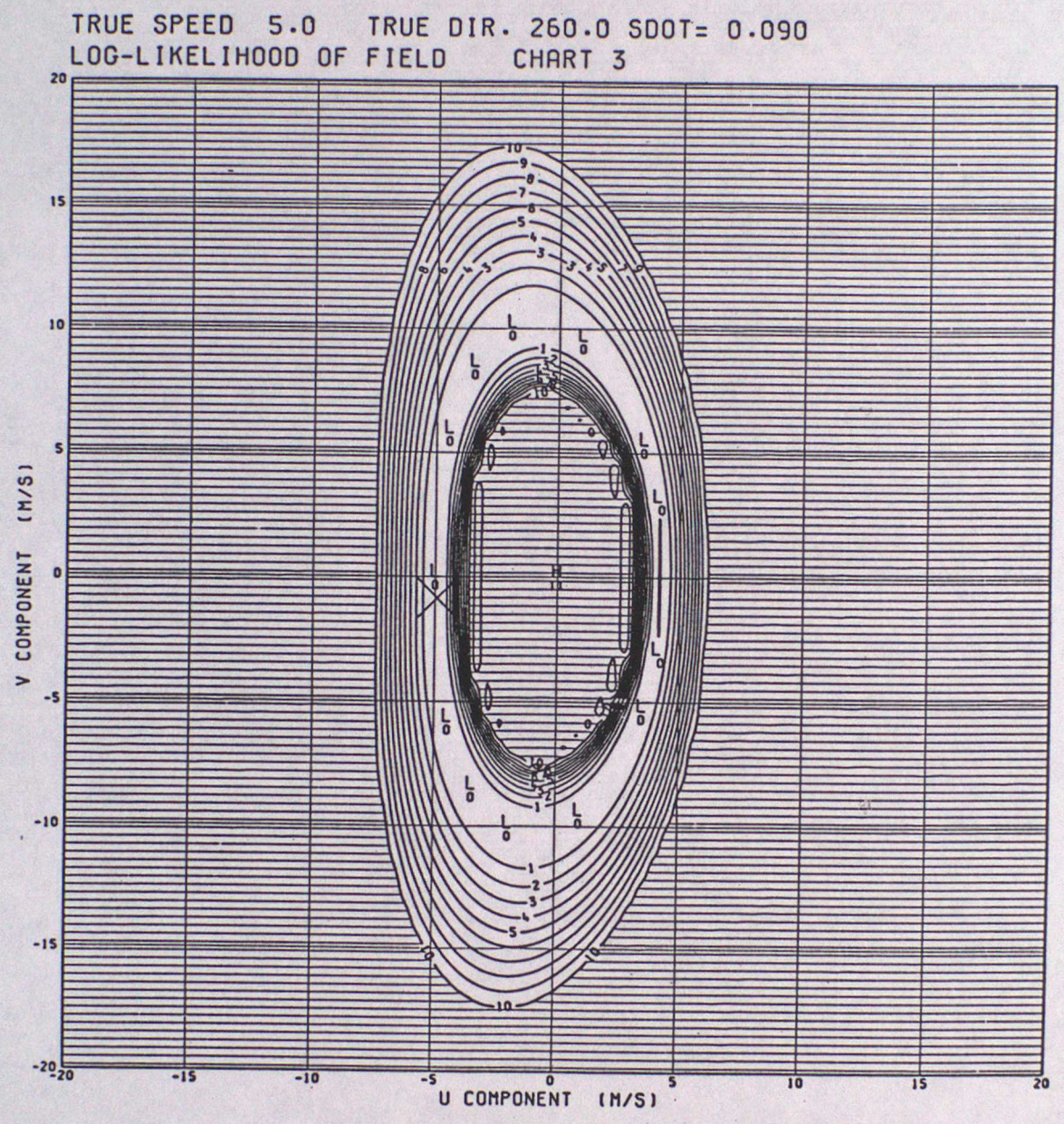
TRUE SPEED 5.0 TRUE DIR. 260.0 SDOT= 0.090
LOG-LIKELIHOOD OF FIELD CHART 3
V COMPONENT (M/S)
U COMPONENT (M/S)
20
15
10
5
0
-5
-10
-15
-20

FIGURE 2.3

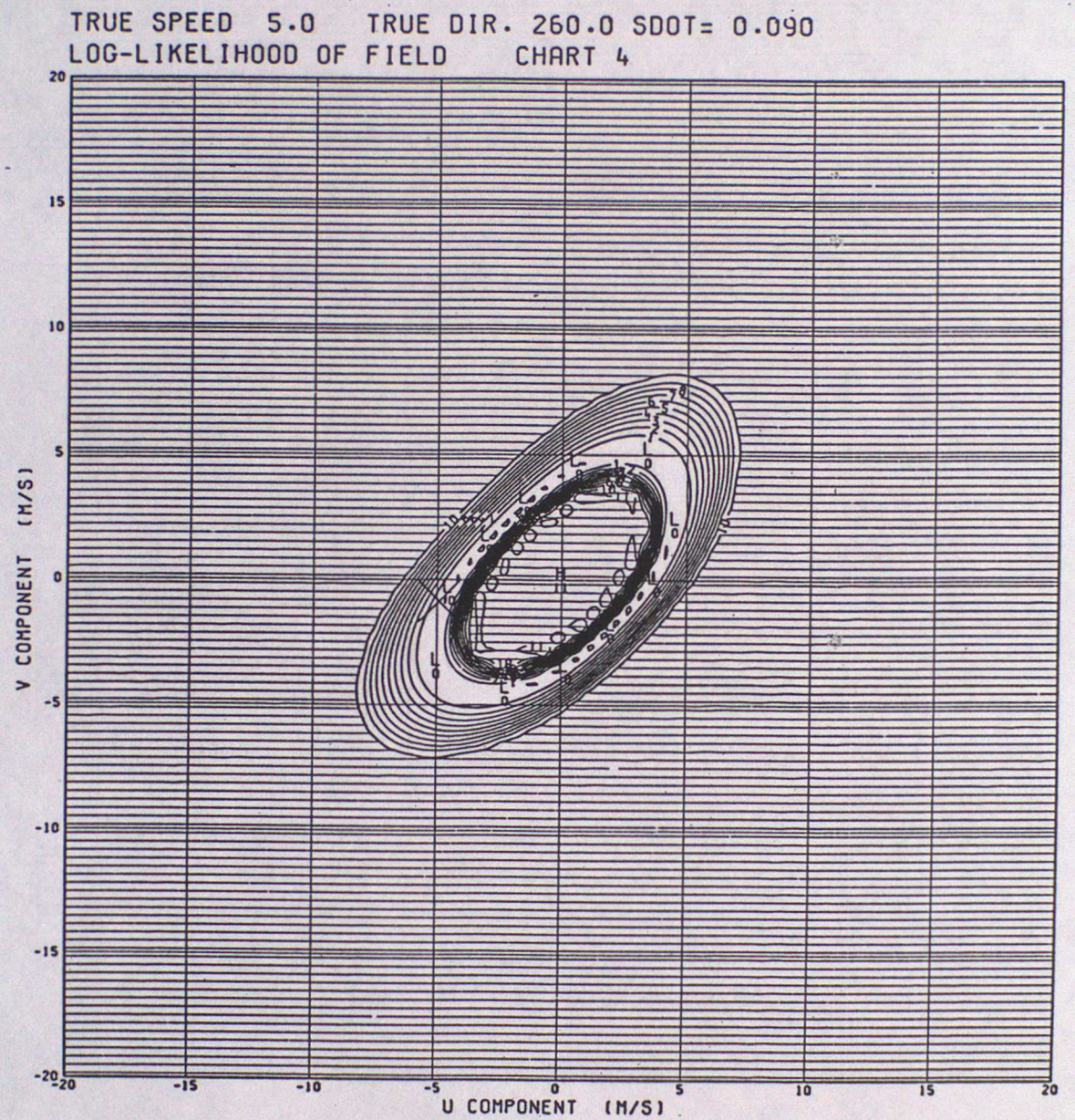
TRUE SPEED 5.0 TRUE DIR. 260.0 SDOT= 0.090
LOG-LIKELIHOOD OF FIELD CHART 4
V COMPONENT (M/S)
U COMPONENT (M/S)
20
15
10
5
0
-5
-10
-15
-20

FIGURE 2-4

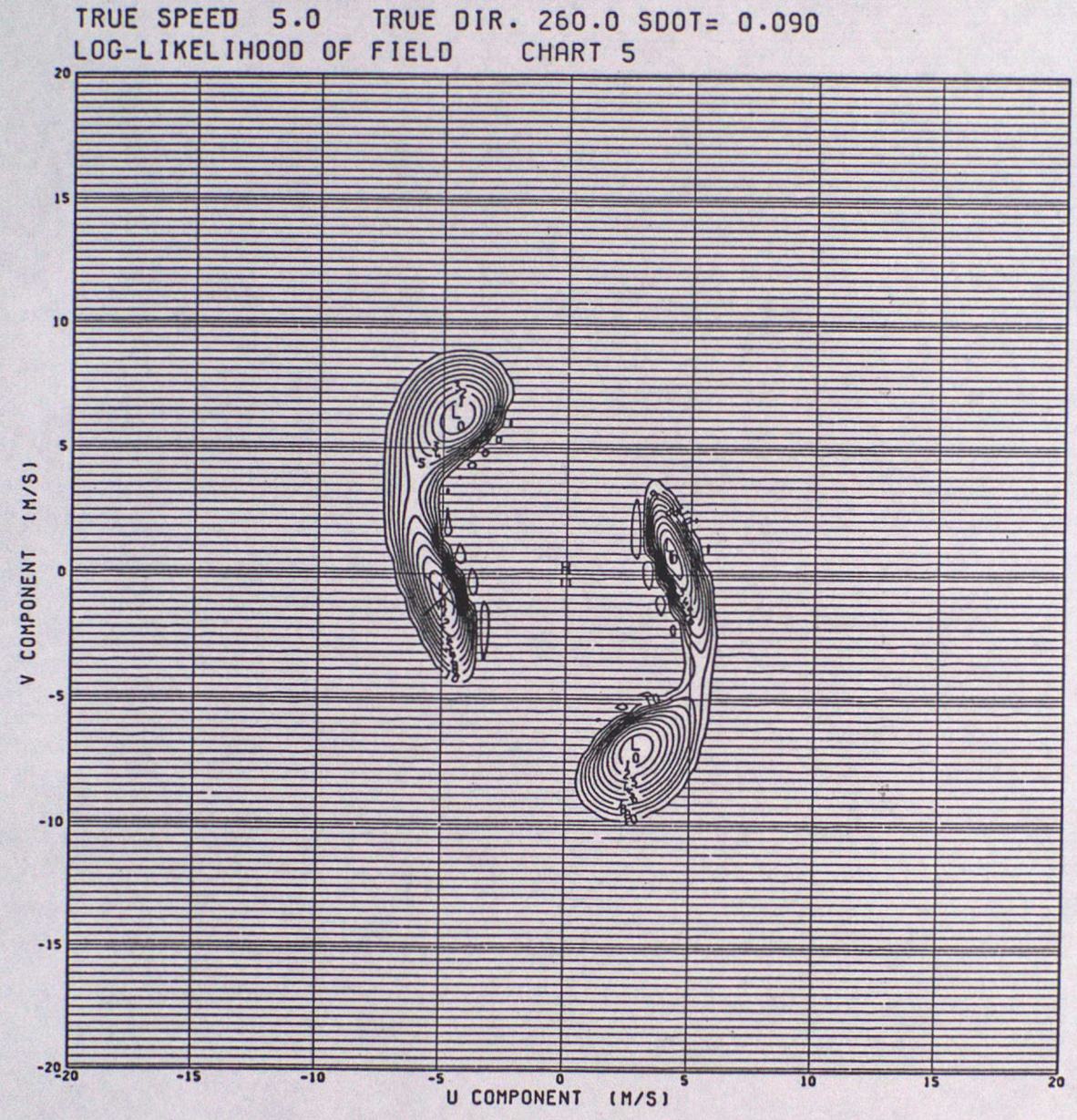
TRUE SPEED 5.0 TRUE DIR. 260.0 SDOT= 0.090
LOG-LIKELIHOOD OF FIELD CHART 5
V COMPONENT (M/S)
U COMPONENT (M/S)
20
15
10
5
0
-5
-10
-15
-20

Figure 2.5

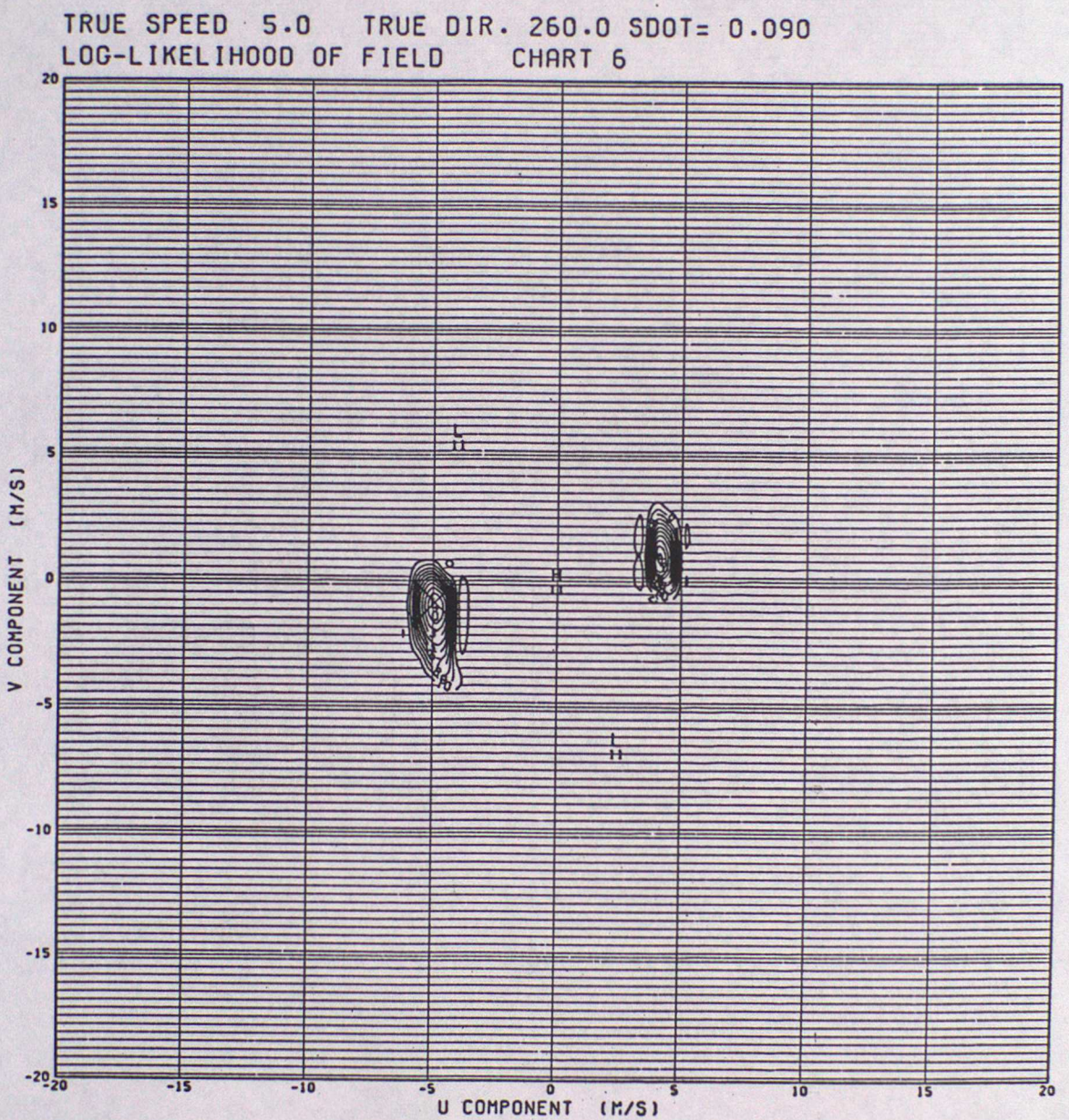
TRUE SPEED 5.0 TRUE DIR. 260.0 SDOT= 0.090
LOG-LIKELIHOOD OF FIELD CHART 6
V COMPONENT (M/S)
U COMPONENT (M/S)
20
15
10
5
0
-5
-10
-15
-20

FIGURE 2.6

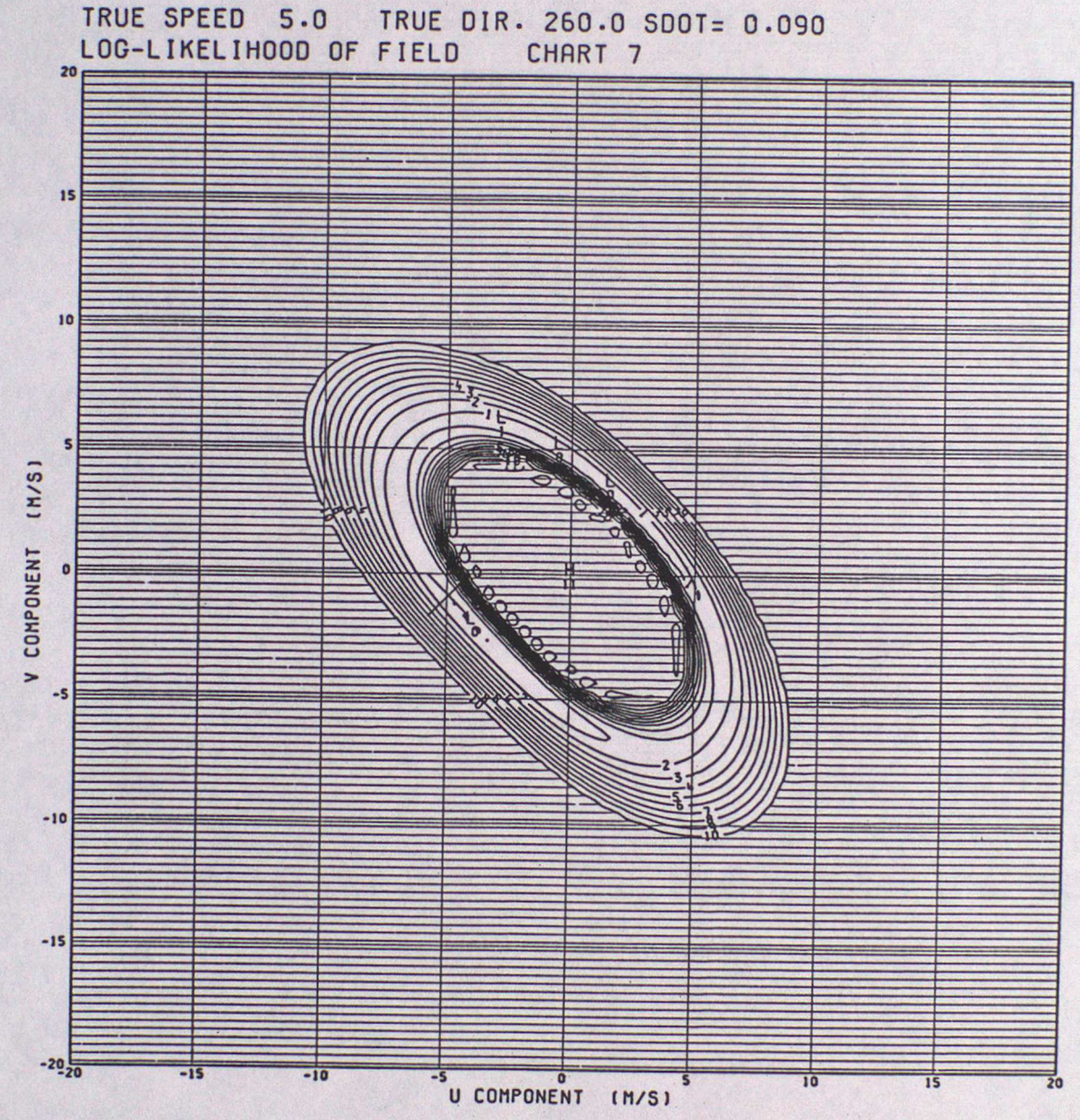
TRUE SPEED 5.0 TRUE DIR. 260.0 SDOT= 0.090
LOG-LIKELIHOOD OF FIELD CHART 7
V COMPONENT (M/S)
U COMPONENT (M/S)
20
15
10
5
0
-5
-10
-15
-20

FIGURE 2.7

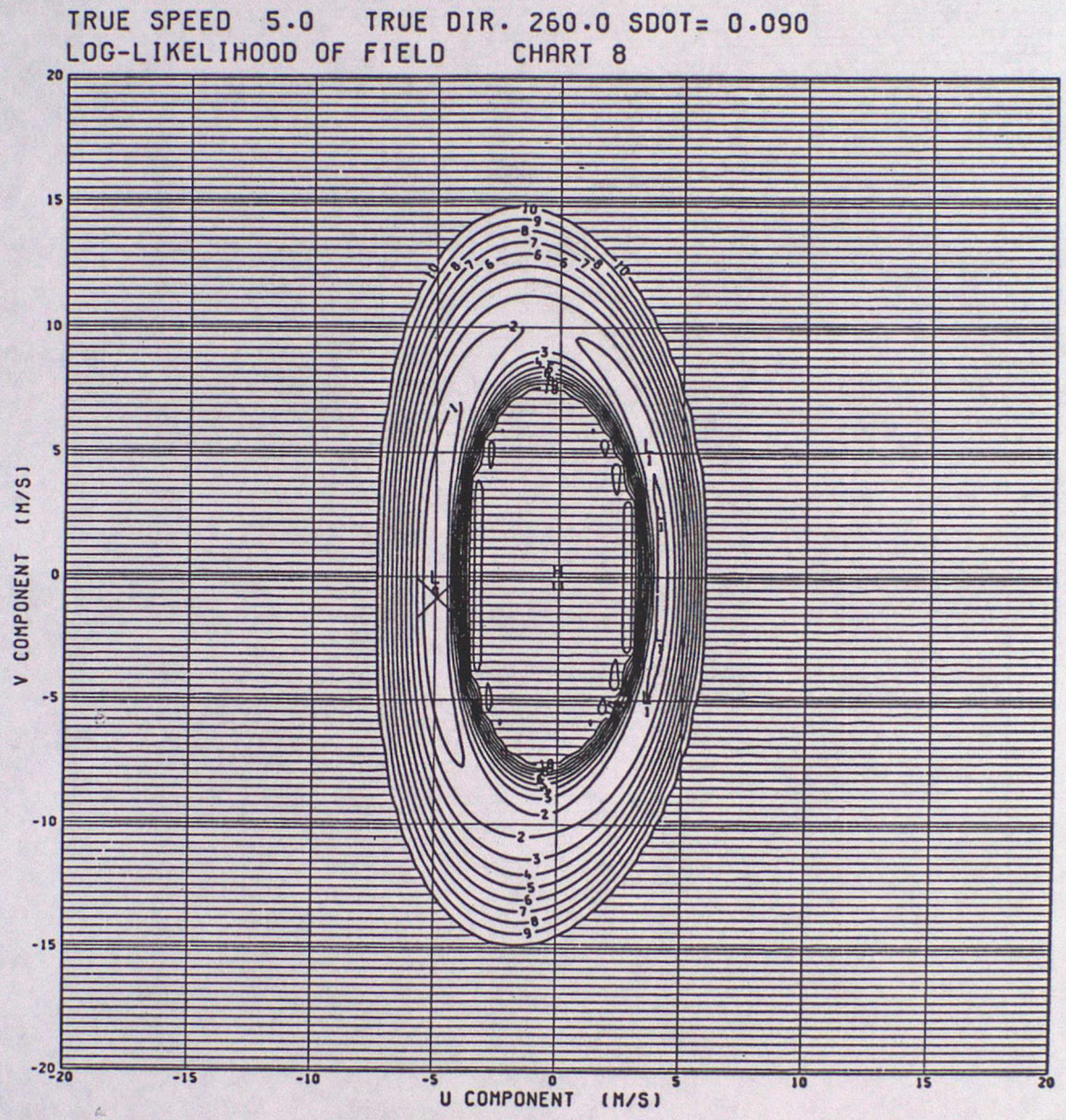
TRUE SPEED 5.0 TRUE DIR. 260.0 SDOT= 0.090
LOG-LIKELIHOOD OF FIELD CHART 8
V COMPONENT (M/S)
U COMPONENT (M/S)
20
15
10
5
0
-5
-10
-15
-20

FIGURE 2.8

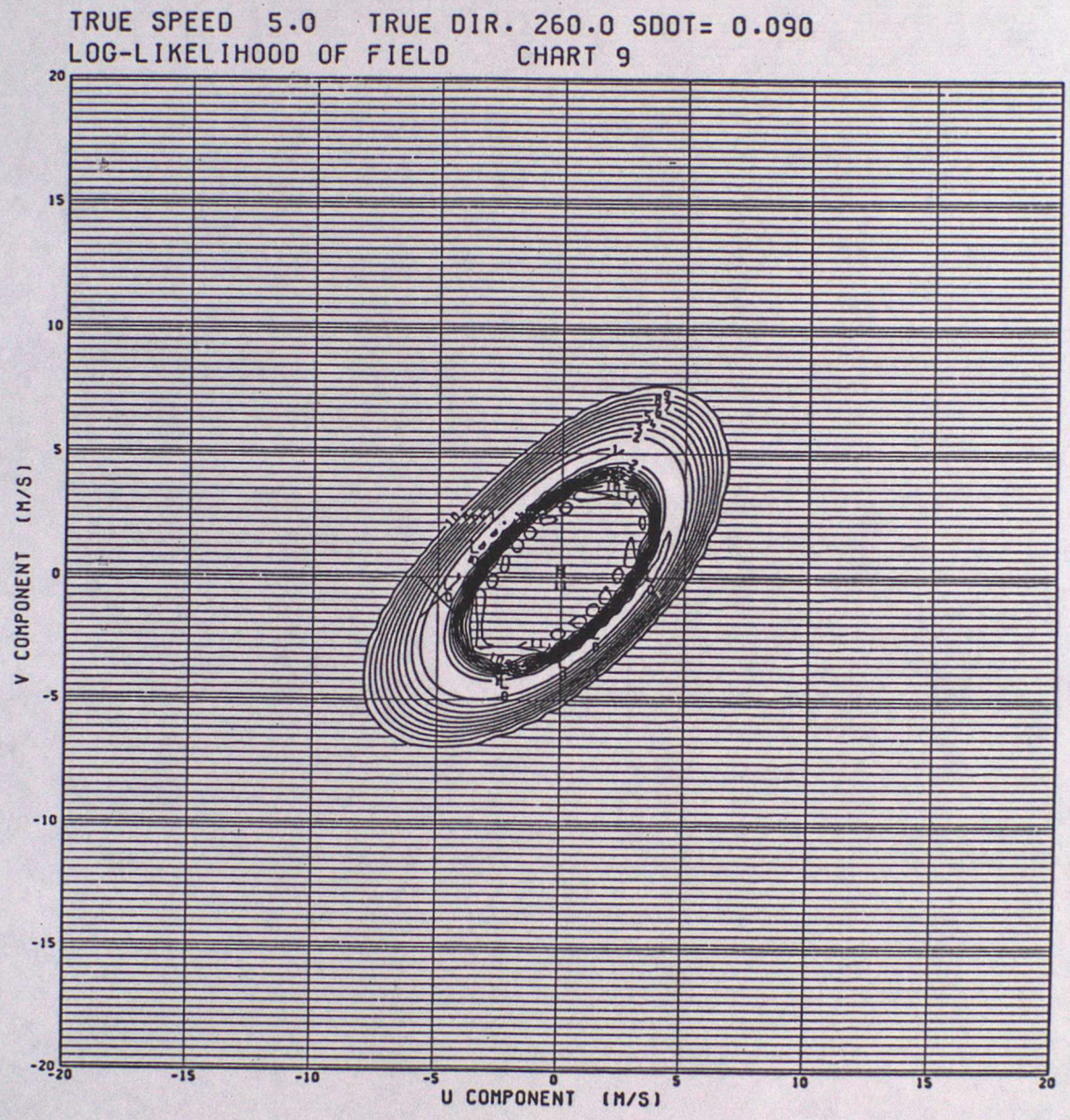
TRUE SPEED 5.0 TRUE DIR. 260.0 SDOT= 0.090
LOG-LIKELIHOOD OF FIELD CHART 9
V COMPONENT (M/S)
U COMPONENT (M/S)
20
15
10
5
0
-5
-10
-15
-20

FIGURE 2.9

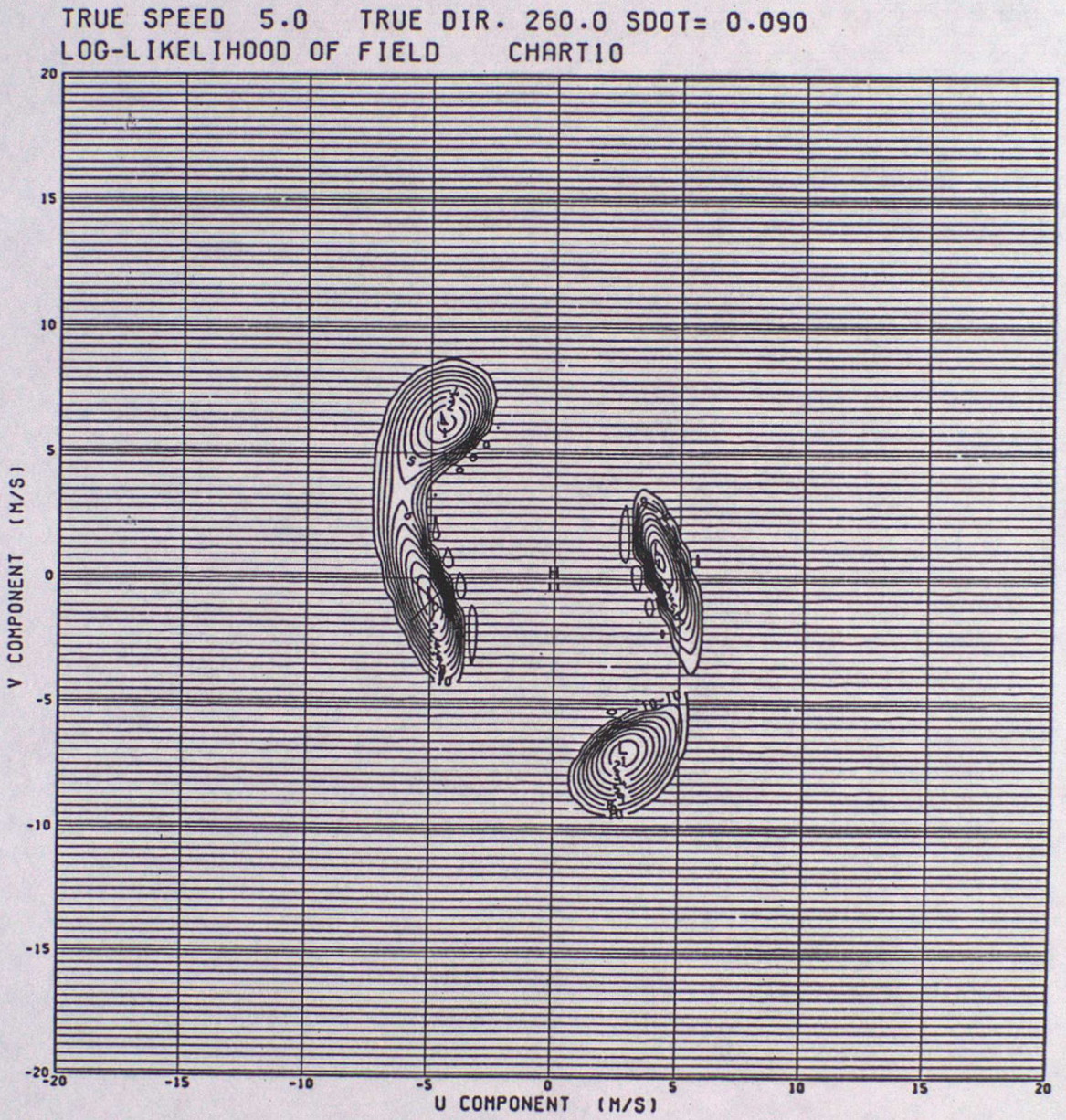
TRUE SPEED 5.0 TRUE DIR. 260.0 SDOT= 0.090
LOG-LIKELIHOOD OF FIELD CHART10
V COMPONENT (M/S)
U COMPONENT (M/S)
20
15
10
5
0
-5
-10
-15
-20

FIGURE 2.10

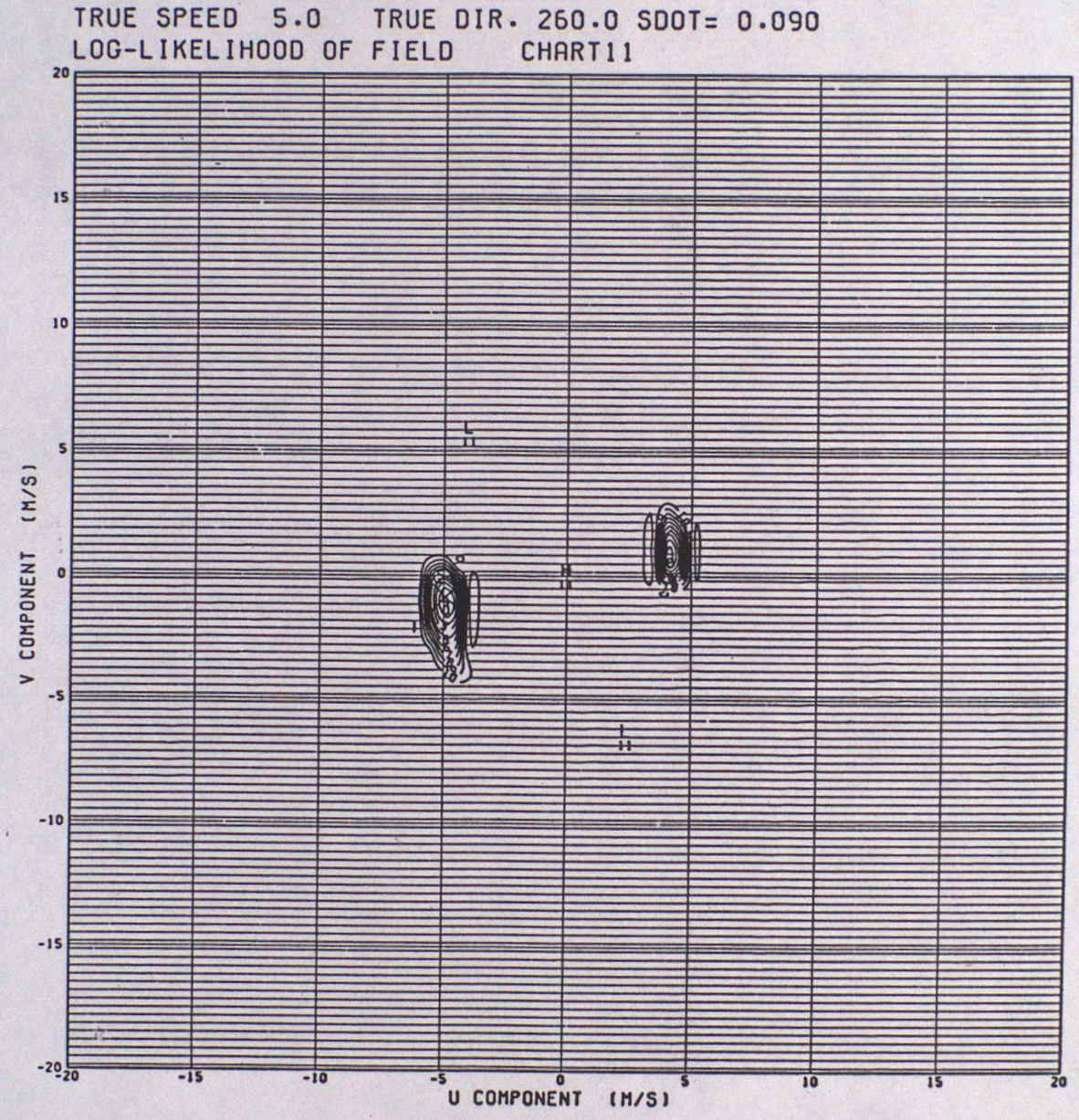
TRUE SPEED 5.0 TRUE DIR. 260.0 SDOT= 0.090
LOG-LIKELIHOOD OF FIELD CHART11
V COMPONENT (M/S)
U COMPONENT (M/S)
20
15
10
5
0
-5
-10
-15
-20
-20
-15
-10
-5
0
5
10
15
20

FIGURE 2.11

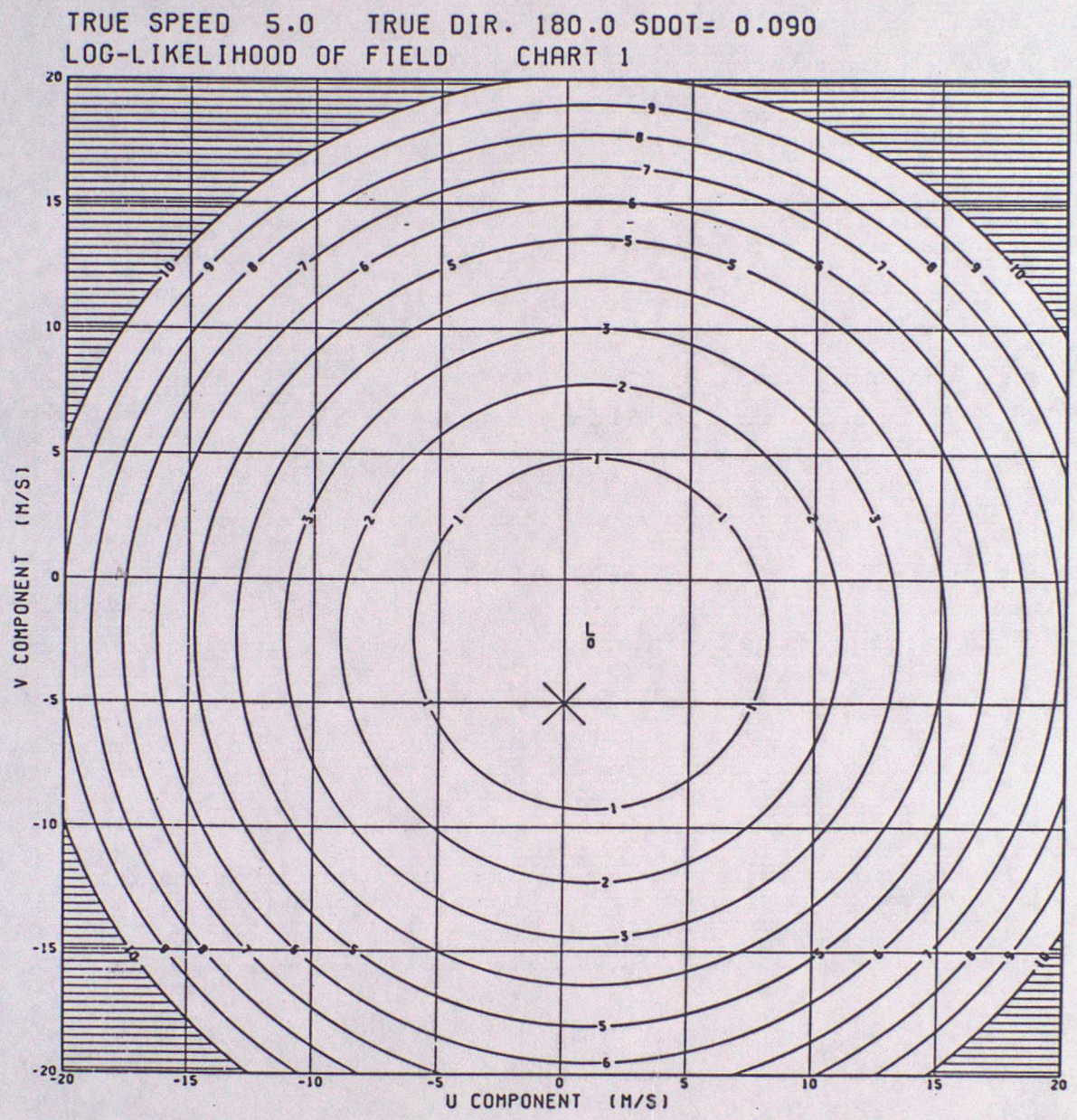
TRUE SPEED 5.0 TRUE DIR. 180.0 SDOT= 0.090
LOG-LIKELIHOOD OF FIELD CHART 1
V COMPONENT (M/S)
U COMPONENT (M/S)
LO
20
15
10
5
0
-5
-10
-15
-20

FIGURE 3.1

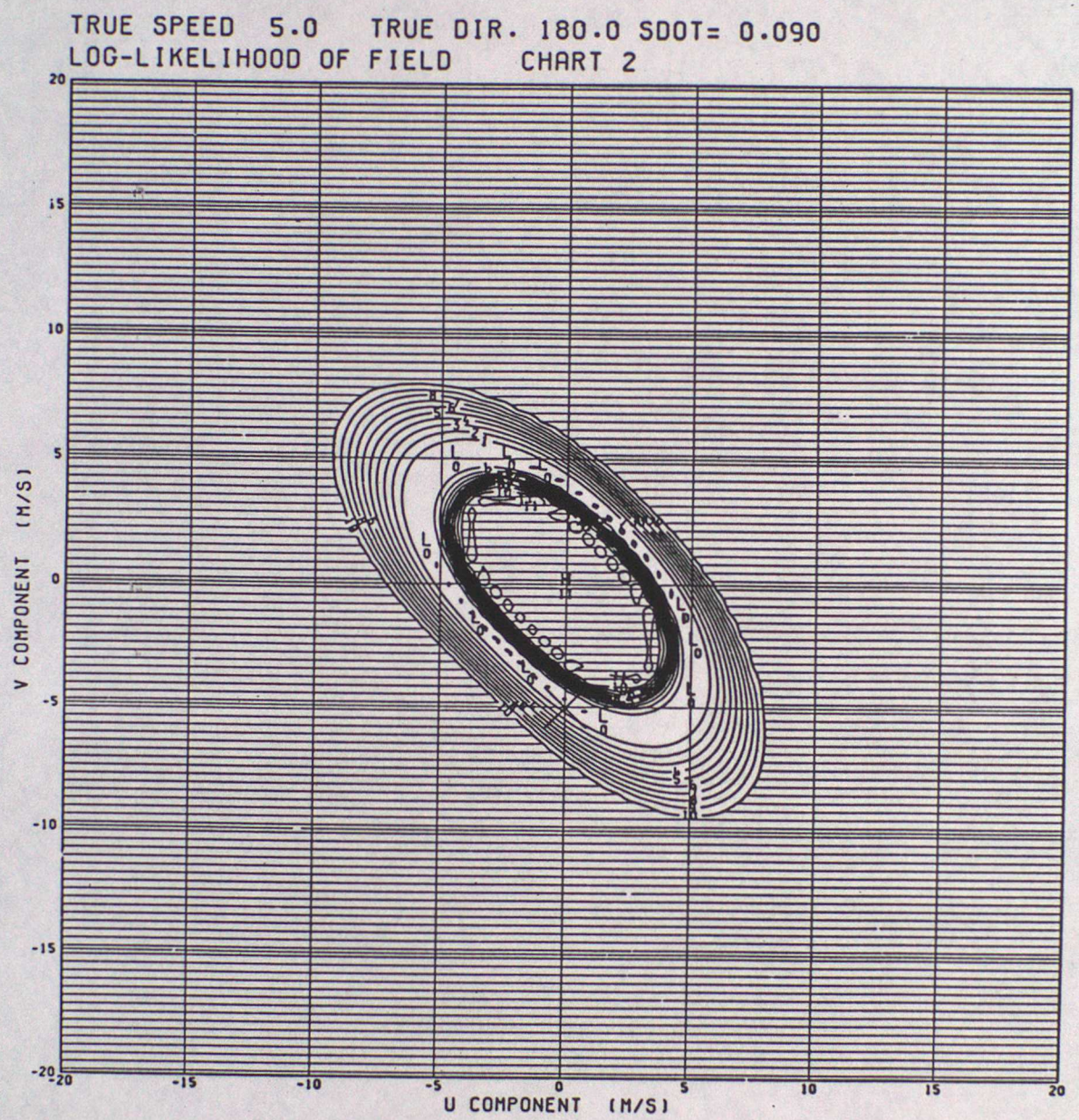
TRUE SPEED 5.0 TRUE DIR. 180.0 SDOT= 0.090
LOG-LIKELIHOOD OF FIELD CHART 2
V COMPONENT (M/S)
U COMPONENT (M/S)
20
15
10
5
0
-5
-10
-15
-20

FIGURE 3.2

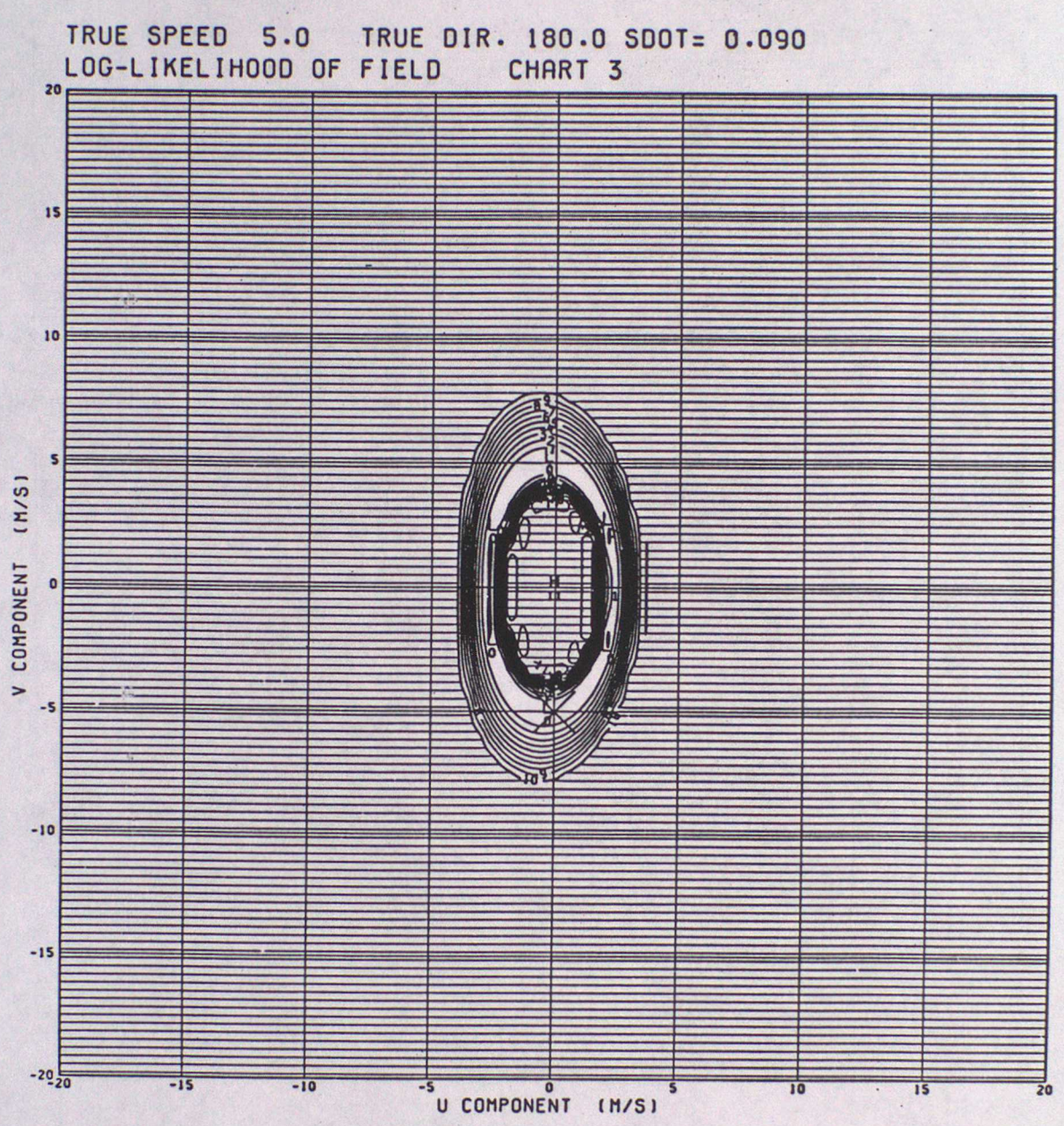
TRUE SPEED 5.0 TRUE DIR. 180.0 SDOT= 0.090
LOG-LIKELIHOOD OF FIELD CHART 3
V COMPONENT (M/S)
U COMPONENT (M/S)
20
15
10
5
0
-5
-10
-15
-20

FIGURE 3.3

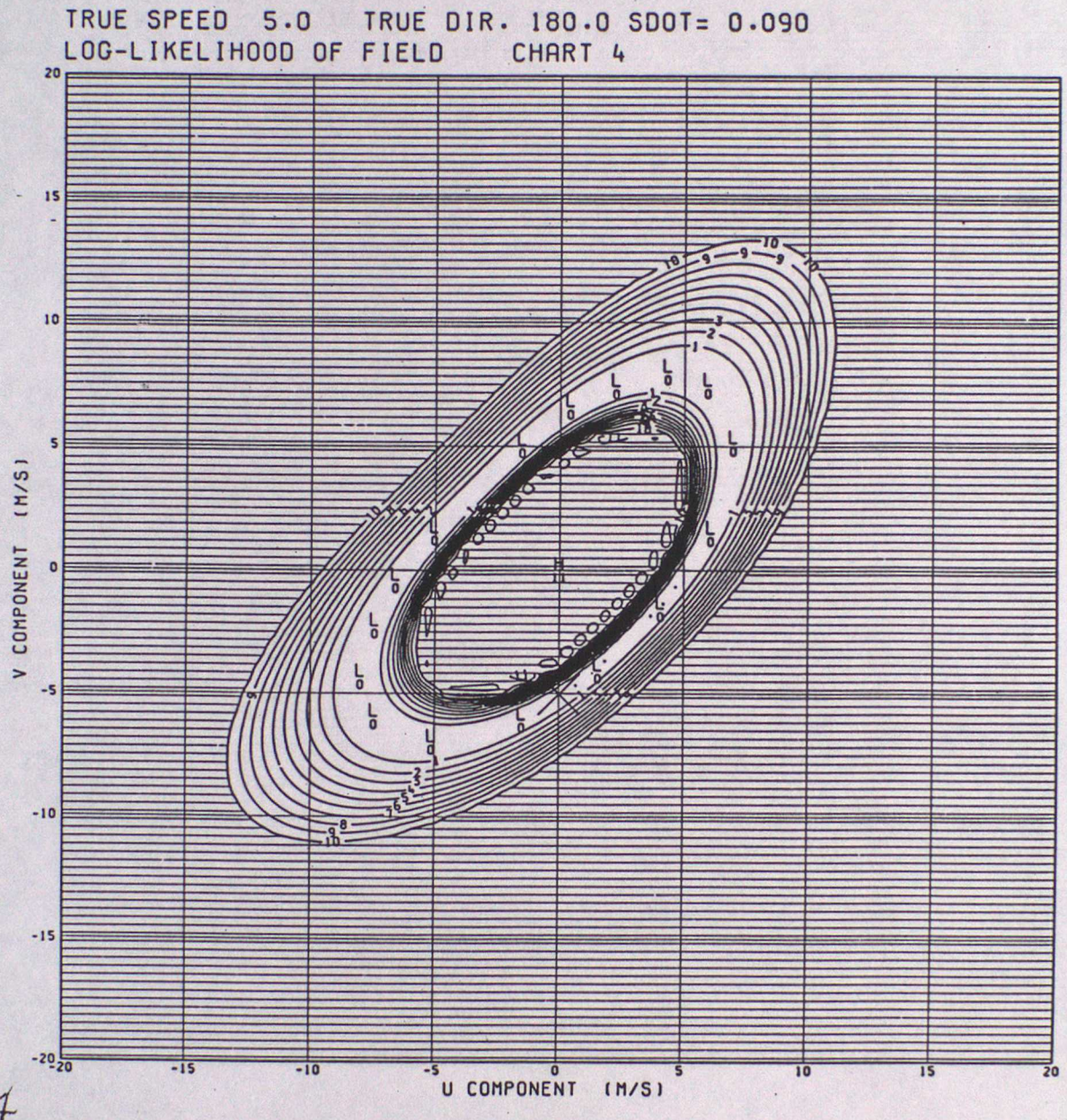
TRUE SPEED 5.0 TRUE DIR. 180.0 SDOT= 0.090
LOG-LIKELIHOOD OF FIELD CHART 4
V COMPONENT (M/S)
U COMPONENT (M/S)
20
15
10
5
0
-5
-10
-15
-20

FIGURE 3.4

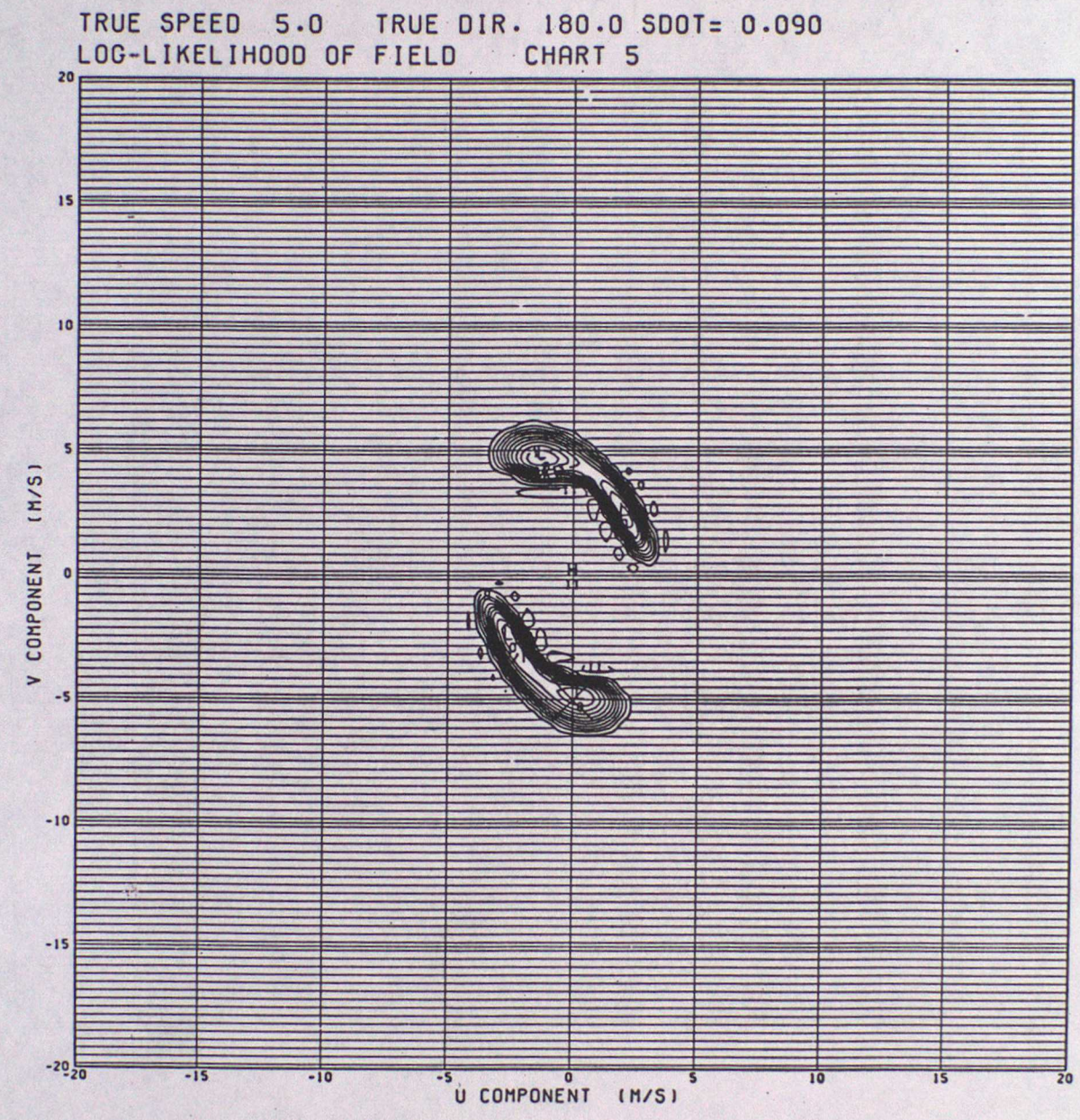
TRUE SPEED 5.0 TRUE DIR. 180.0 SDOT= 0.090
LOG-LIKELIHOOD OF FIELD CHART 5
V COMPONENT (M/S)
U COMPONENT (M/S)
20
15
10
5
0
-5
-10
-15
-20

FIGURE 3.5

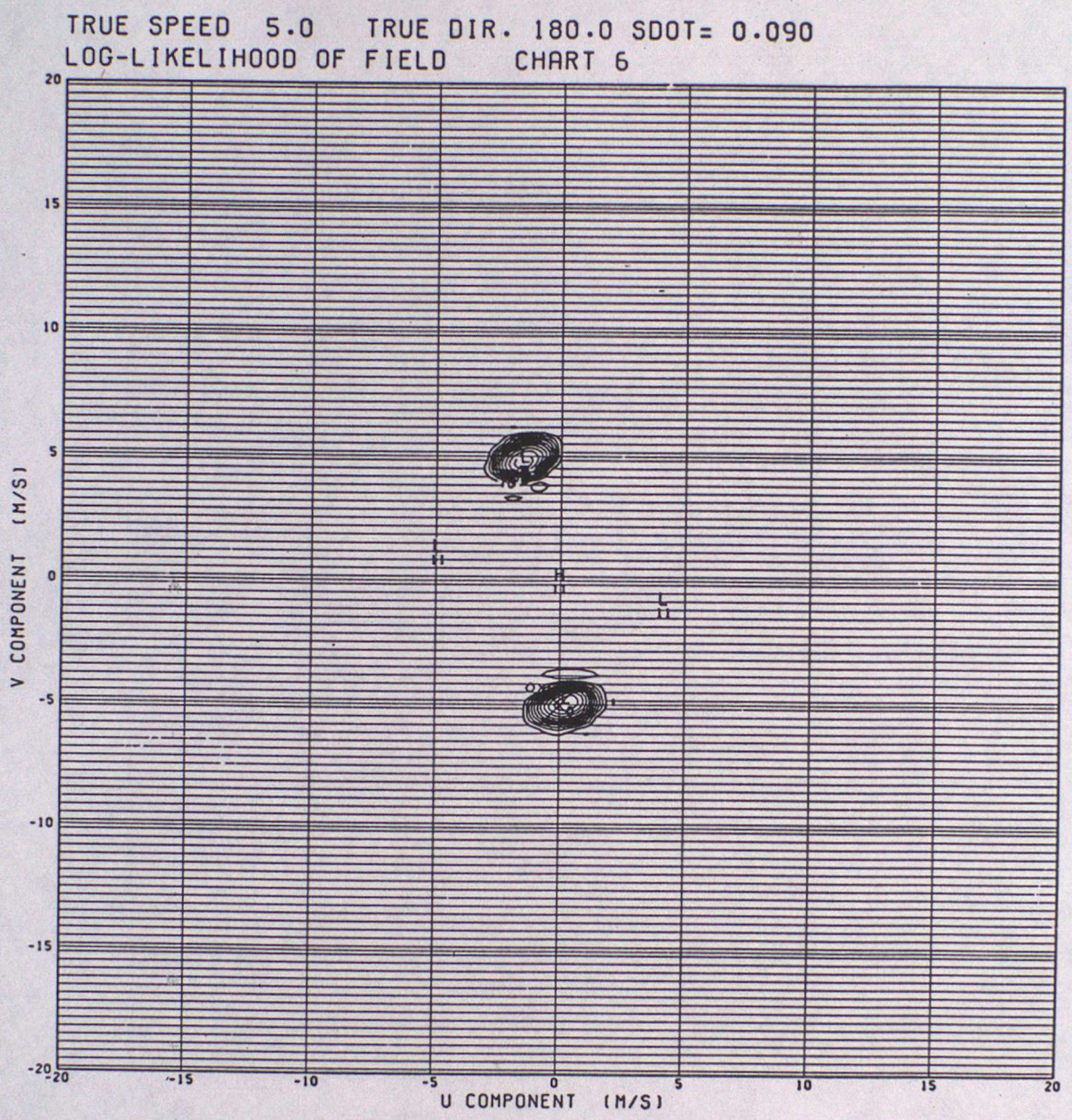
TRUE SPEED 5.0 TRUE DIR. 180.0 SDOT= 0.090
LOG-LIKELIHOOD OF FIELD CHART 6
V COMPONENT (M/S)
U COMPONENT (M/S)
20
15
10
5
0
-5
-10
-15
-20
-20
-15
-10
-5
0
5
10
15
20
L
H
H
L

FIGURE 3.6

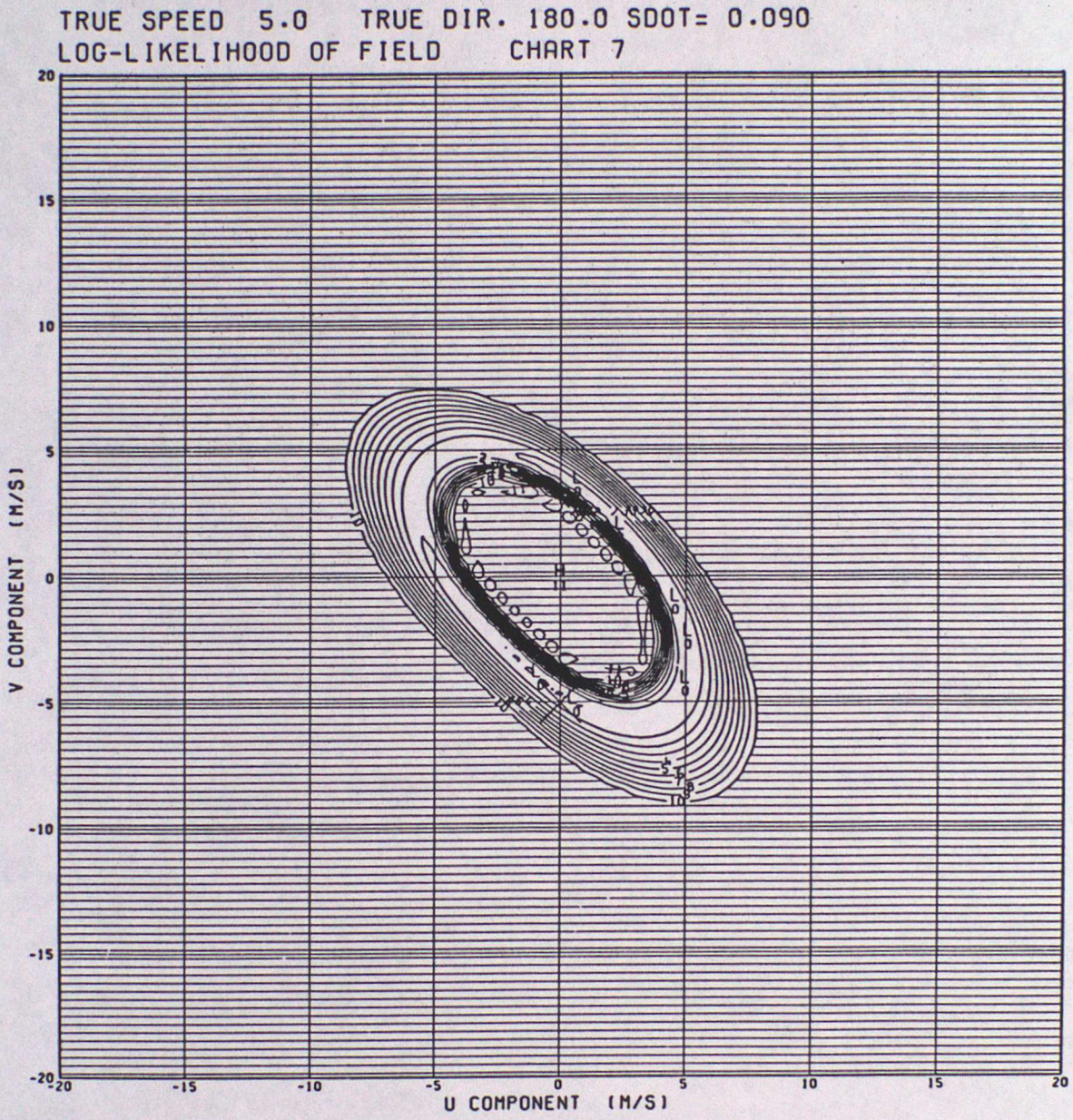
TRUE SPEED 5.0 TRUE DIR. 180.0 SDOT= 0.090
LOG-LIKELIHOOD OF FIELD CHART 7
V COMPONENT (M/S)
U COMPONENT (M/S)
20
15
10
5
0
-5
-10
-15
-20

FIGURE 3.7

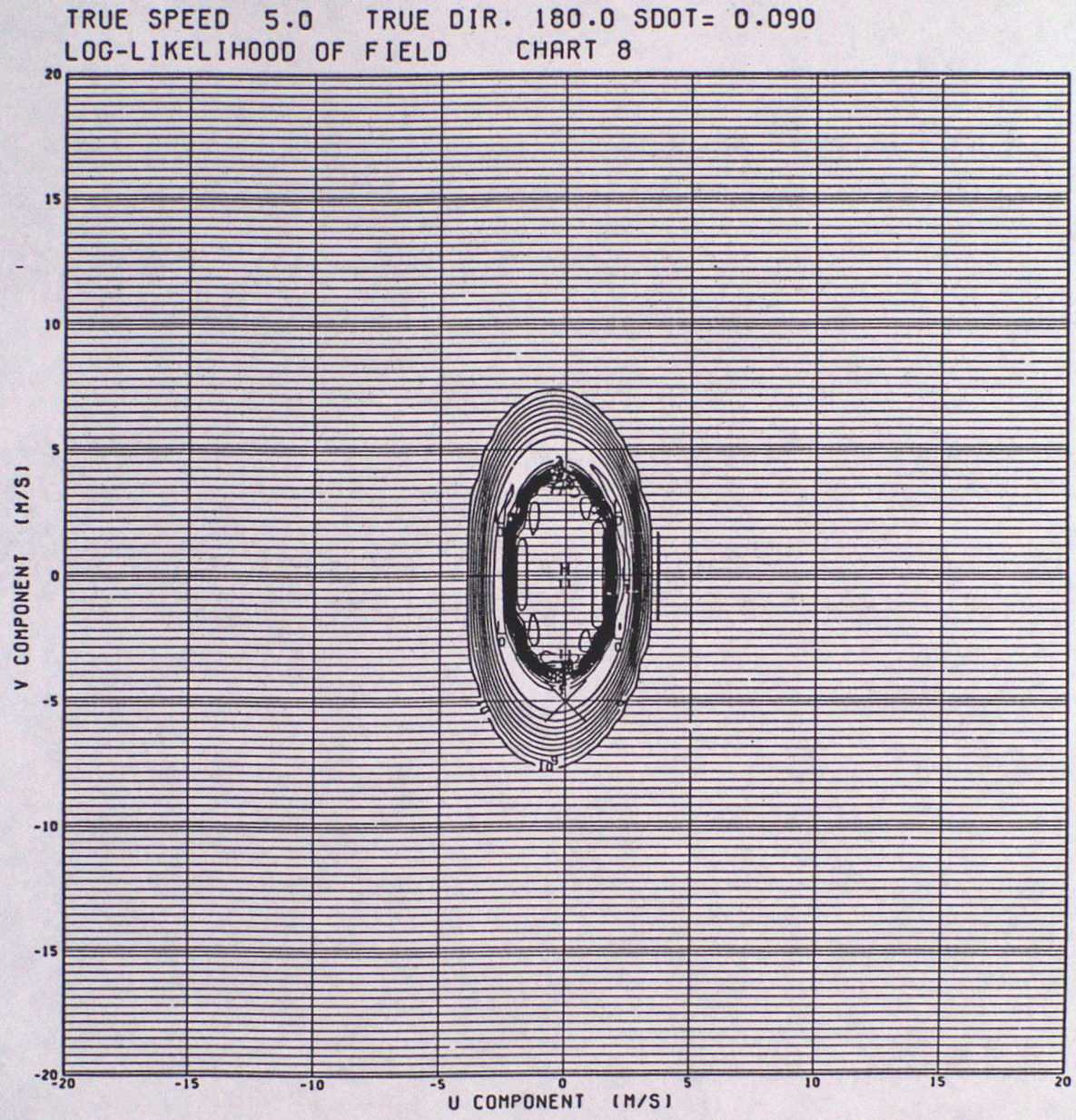
TRUE SPEED 5.0 TRUE DIR. 180.0 SDOT= 0.090
LOG-LIKELIHOOD OF FIELD CHART 8
V COMPONENT (M/S)
U COMPONENT (M/S)
20
15
10
5
0
-5
-10
-15
-20

FIGURE 3.8

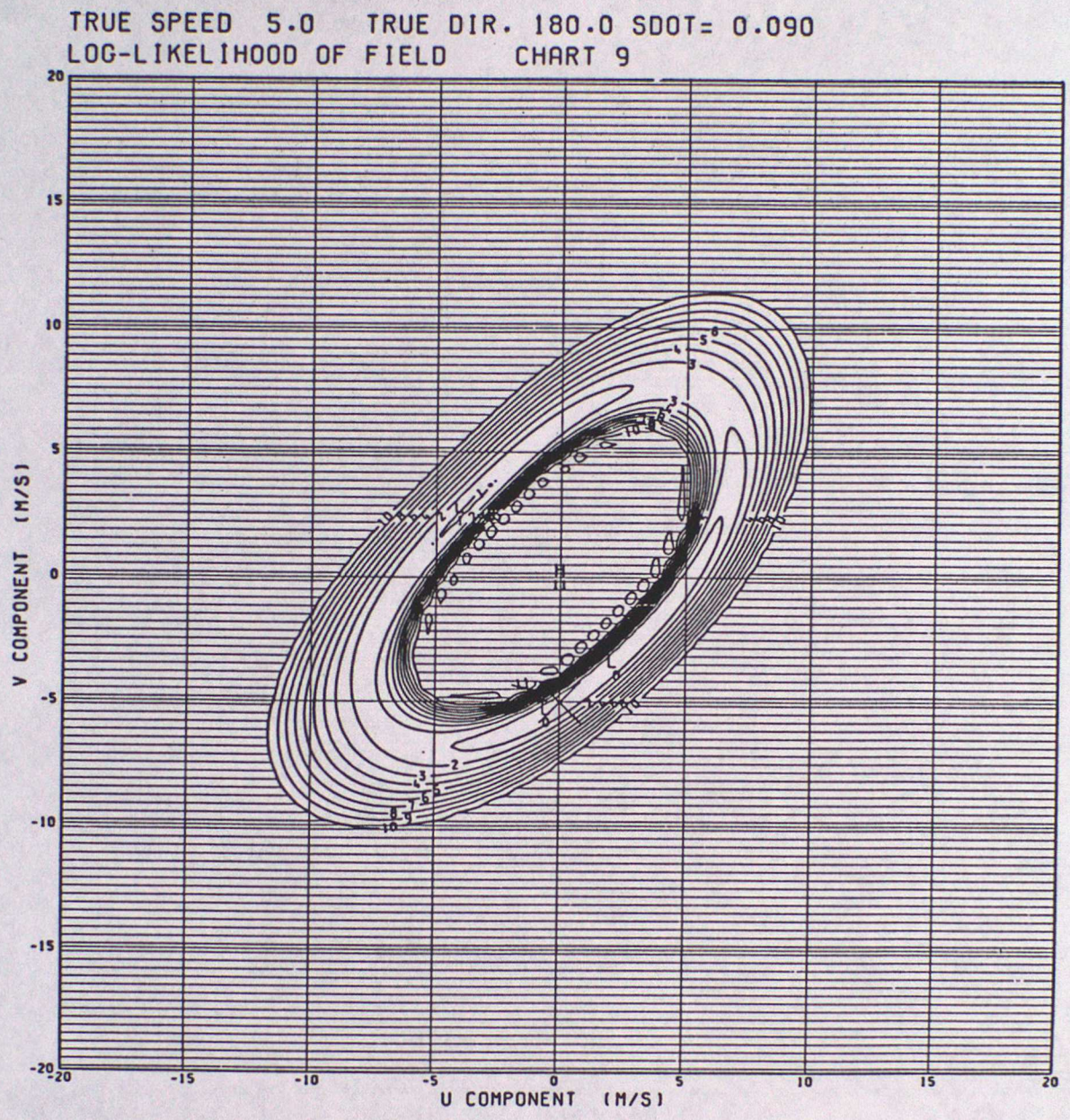
TRUE SPEED 5.0 TRUE DIR. 180.0 SDOT= 0.090
LOG-LIKELIHOOD OF FIELD CHART 9
V COMPONENT (M/S)
U COMPONENT (M/S)
20
15
10
5
0
-5
-10
-15
-20

FIGURE 3.9

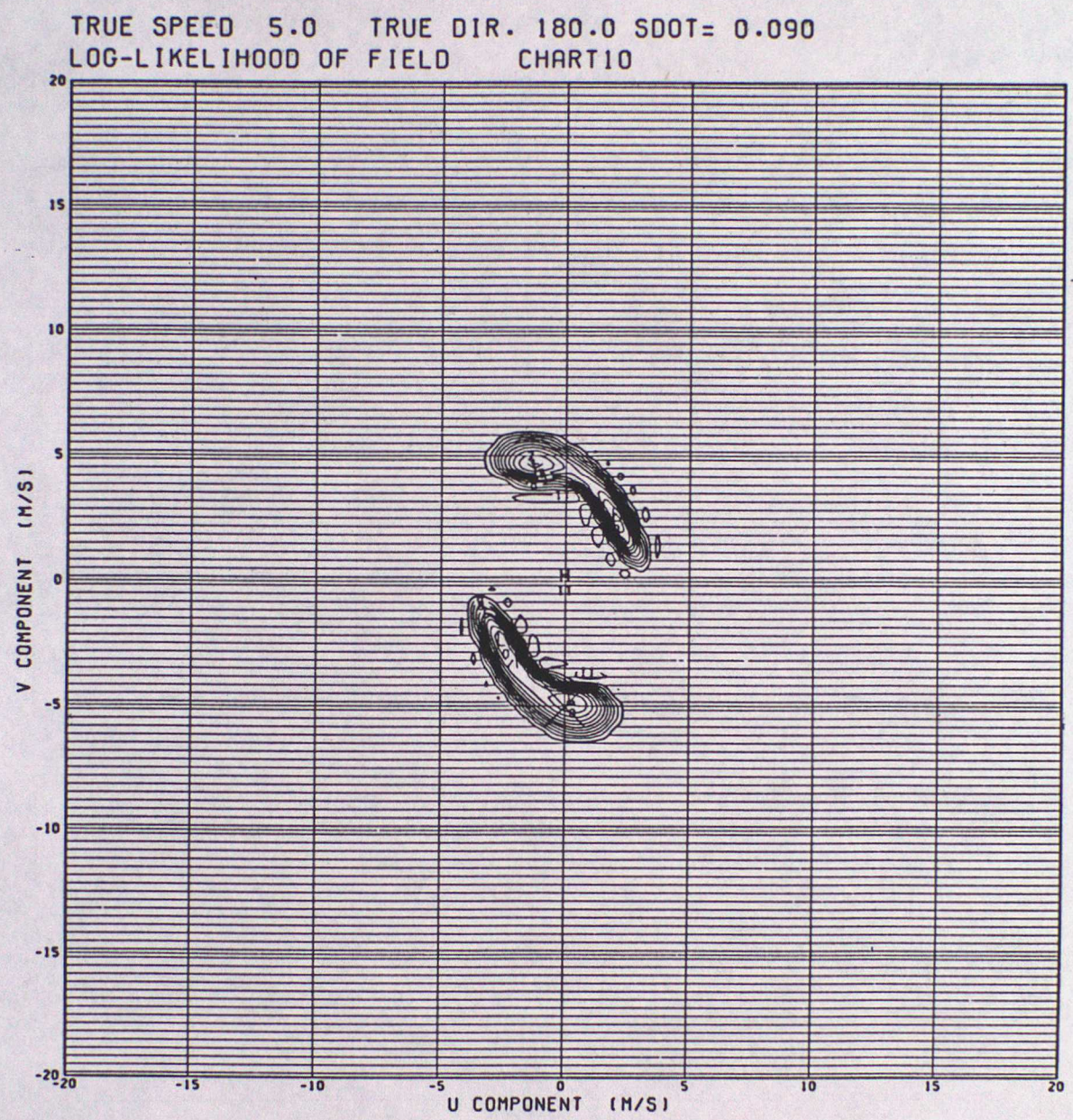
TRUE SPEED 5.0 TRUE DIR. 180.0 SDOT= 0.090
LOG-LIKELIHOOD OF FIELD CHART10
V COMPONENT (M/S)
U COMPONENT (M/S)
20
15
10
5
0
-5
-10
-15
-20
-20
-15
-10
-5
0
5
10
15
20

FIGURE 3.10

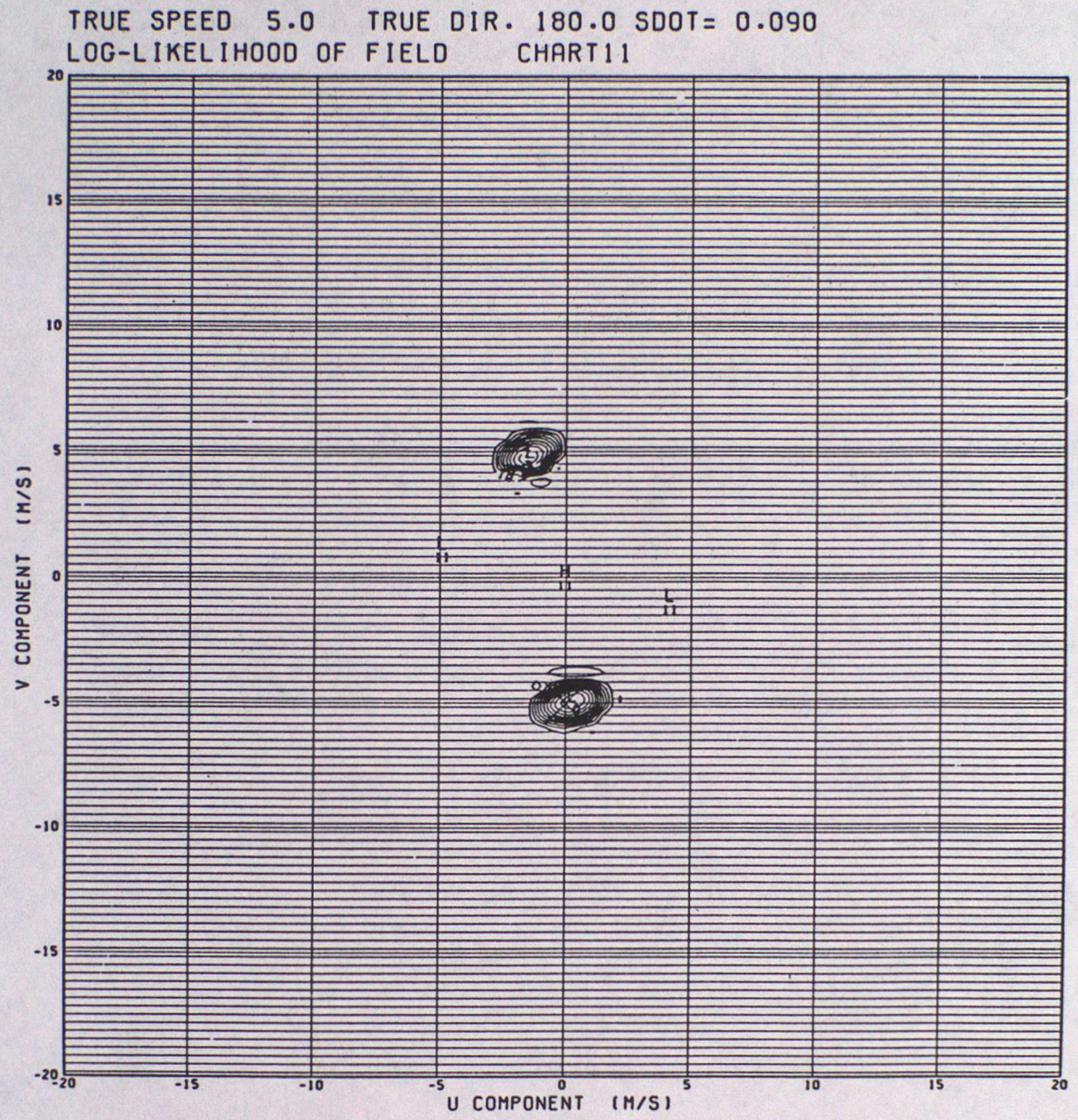
TRUE SPEED 5.0 TRUE DIR. 180.0 SDOT= 0.090
LOG-LIKELIHOOD OF FIELD CHART11
V COMPONENT (M/S)
U COMPONENT (M/S)
20
15
10
5
0
-5
-10
-15
-20
H
L

FIGURE 3.11

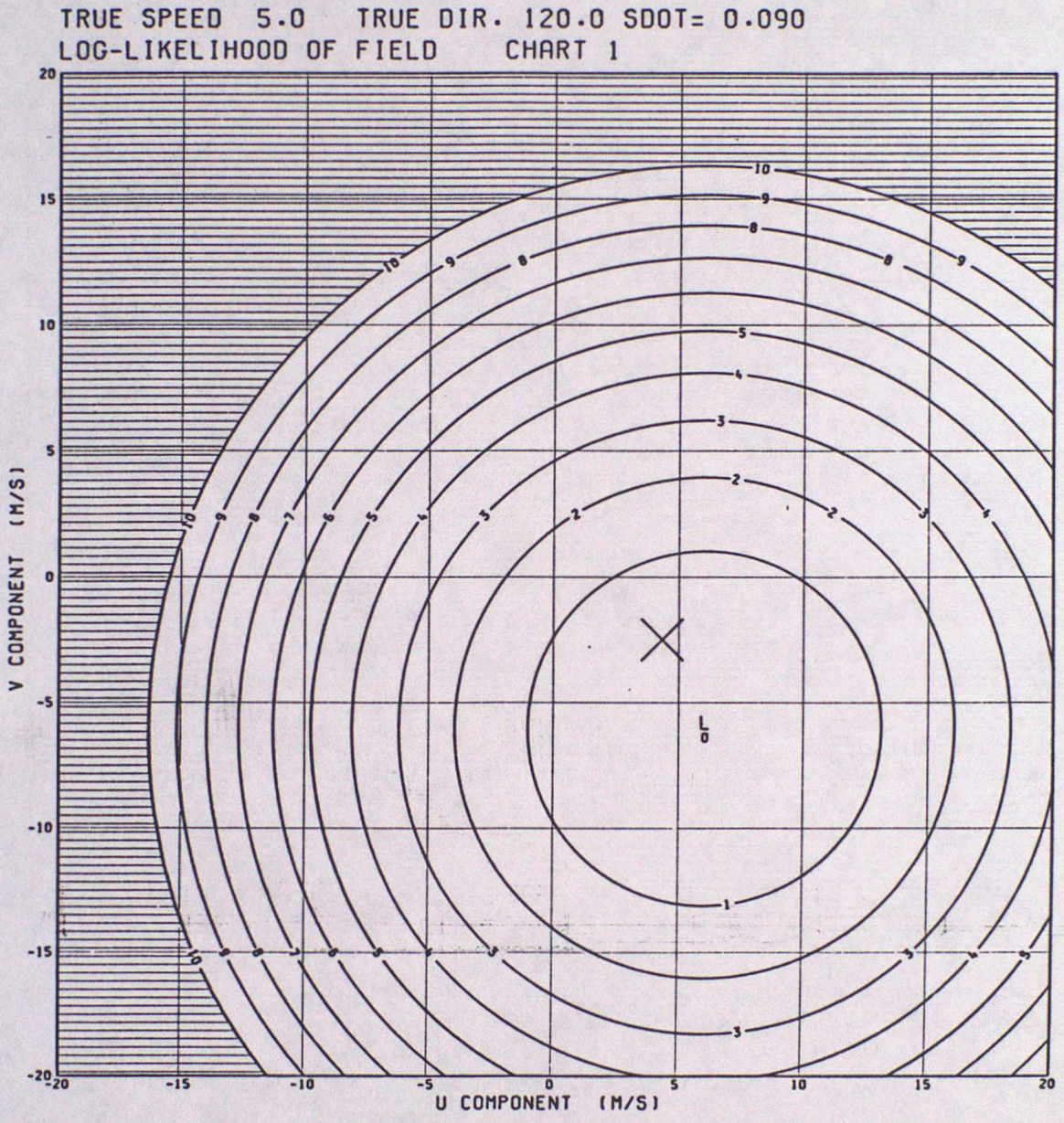
TRUE SPEED 5.0 TRUE DIR. 120.0 SDOT= 0.090
LOG-LIKELIHOOD OF FIELD CHART 1
V COMPONENT (M/S)
U COMPONENT (M/S)
20
15
10
5
0
-5
-10
-15
-20
-20
-15
-10
-5
0
5
10
15
20

FIGURE 4.1

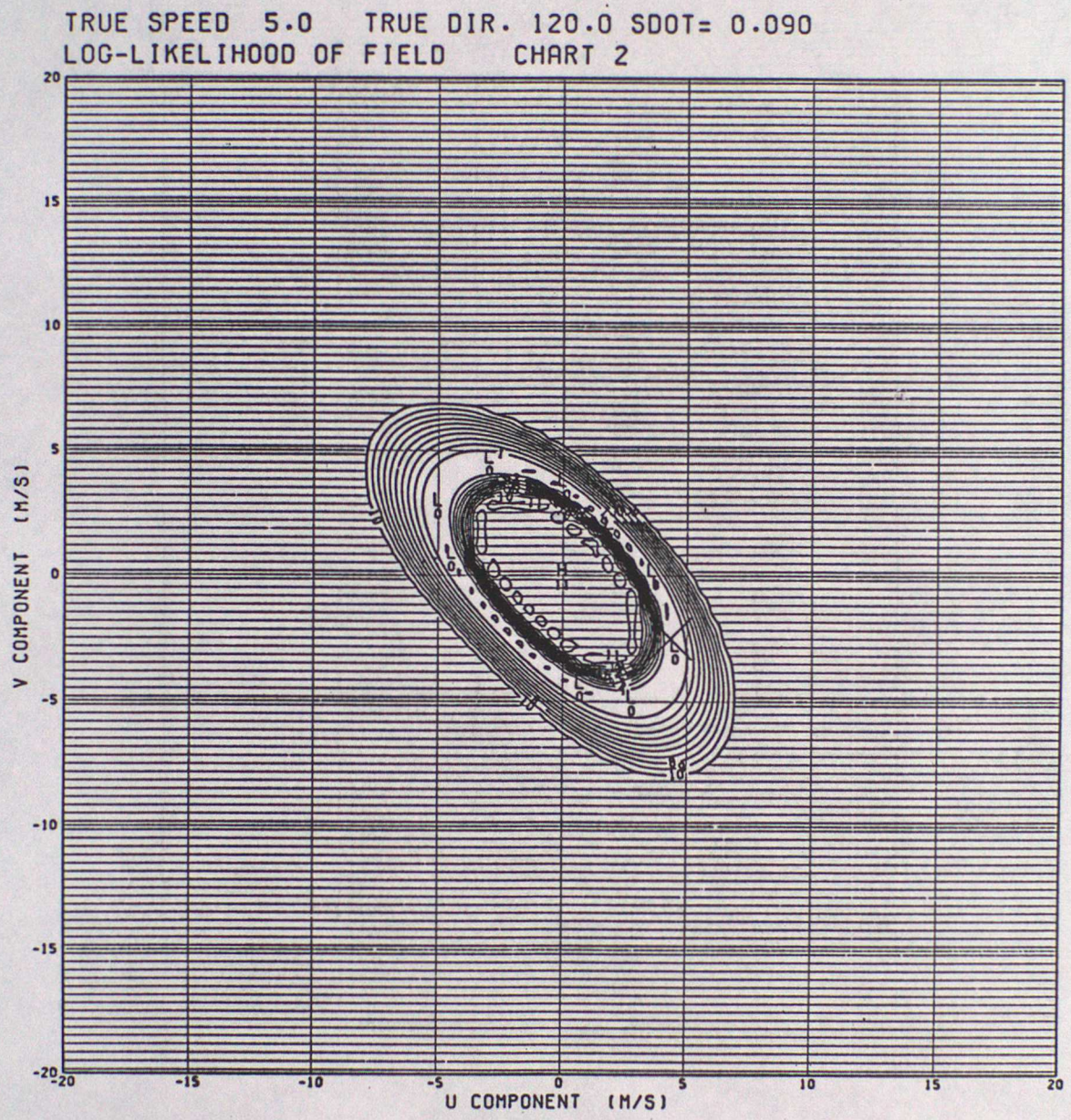
TRUE SPEED 5.0 TRUE DIR. 120.0 SDOT= 0.090
LOG-LIKELIHOOD OF FIELD CHART 2
V COMPONENT (M/S)
U COMPONENT (M/S)
20
15
10
5
0
-5
-10
-15
-20

FIGURE 4.2

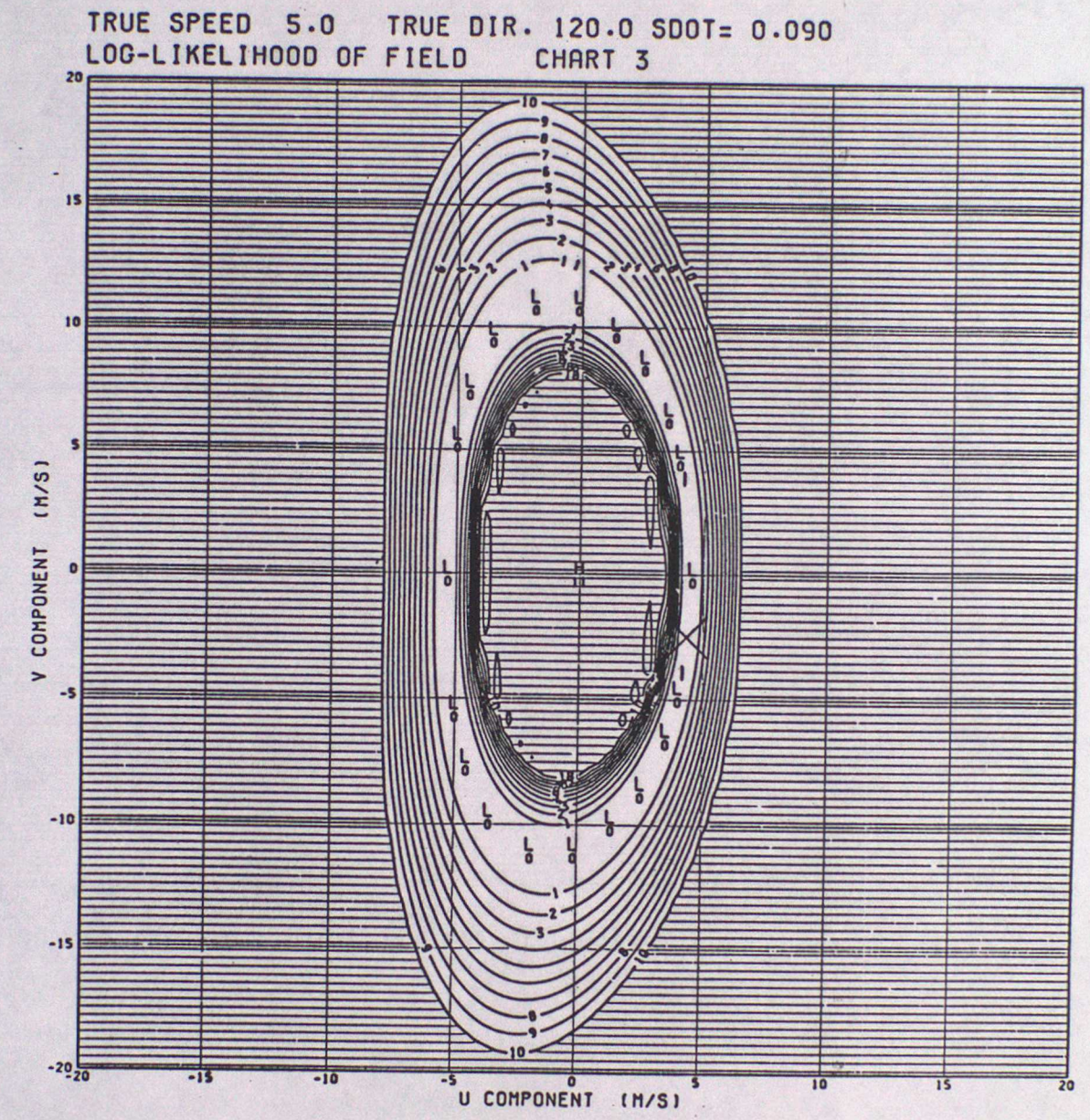
TRUE SPEED 5.0 TRUE DIR. 120.0 SDOT= 0.090
LOG-LIKELIHOOD OF FIELD CHART 3
V COMPONENT (M/S)
U COMPONENT (M/S)
20
15
10
5
0
-5
-10
-15
-20

FIGURE 4.3

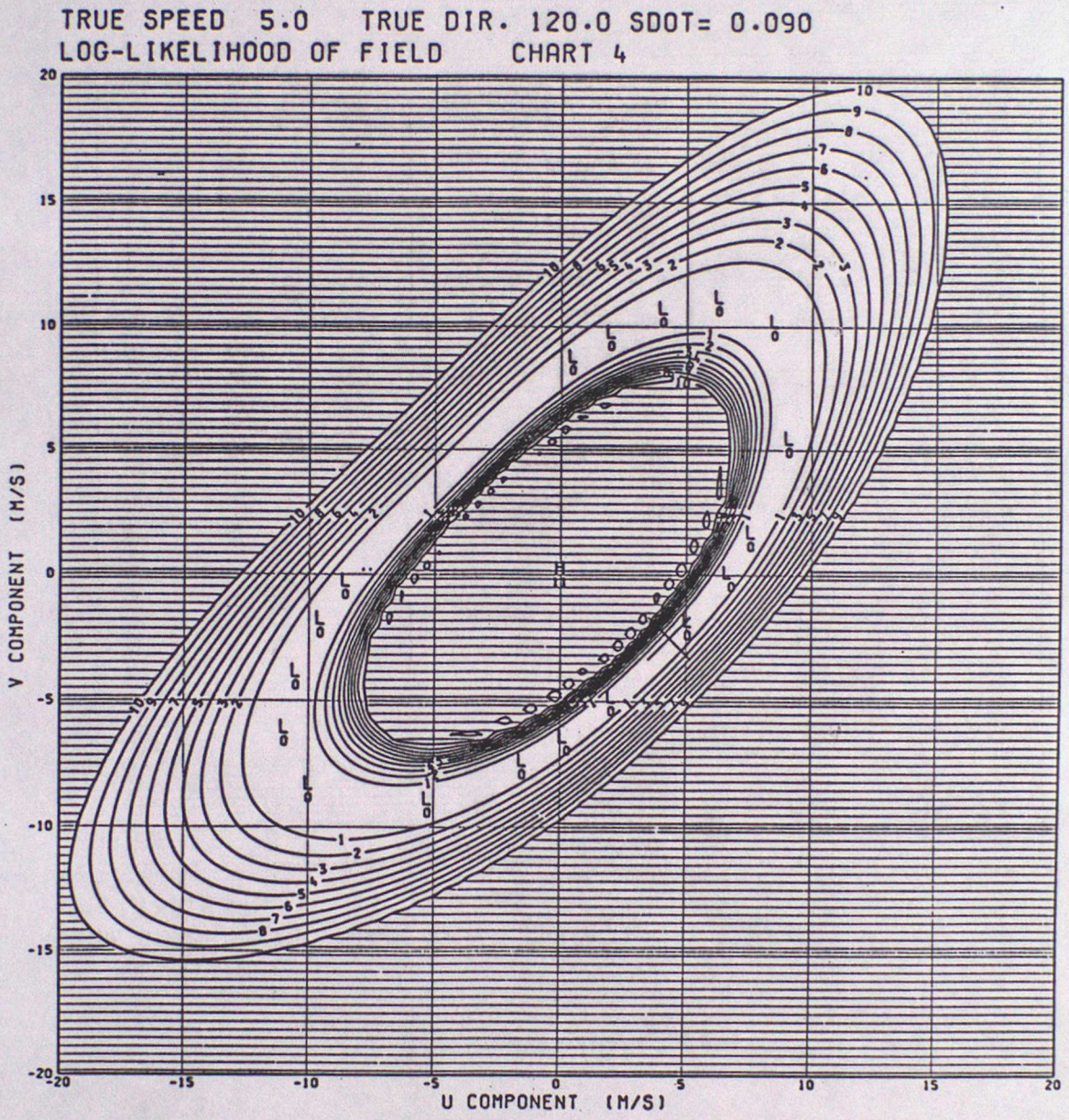
TRUE SPEED 5.0 TRUE DIR. 120.0 SDOT= 0.090
LOG-LIKELIHOOD OF FIELD CHART 4
V COMPONENT (M/S)
U COMPONENT (M/S)
20
15
10
5
0
-5
-10
-15
-20

FIGURE 4.4

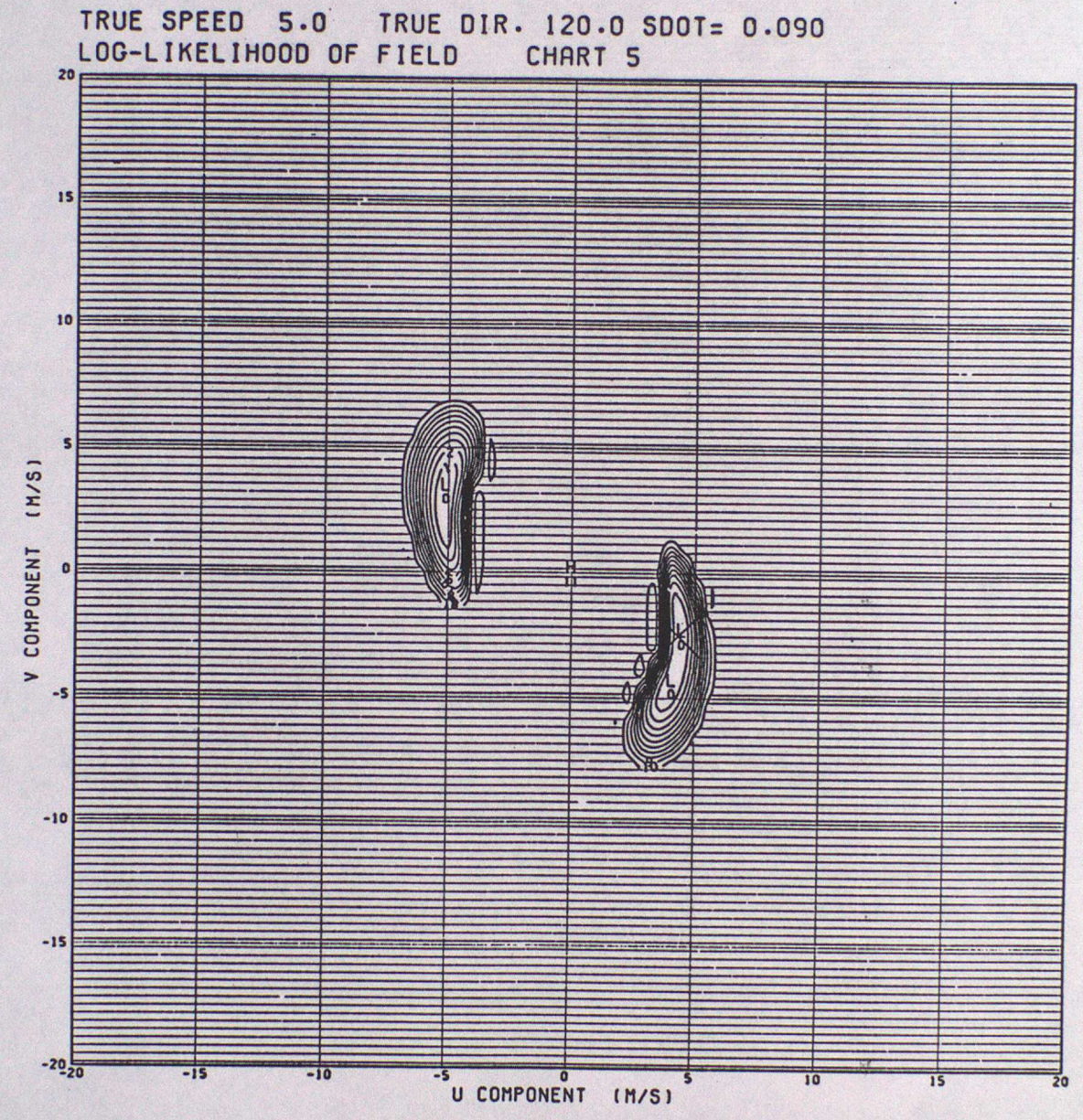
TRUE SPEED 5.0 TRUE DIR. 120.0 SDOT= 0.090
LOG-LIKELIHOOD OF FIELD CHART 5
V COMPONENT (M/S)
U COMPONENT (M/S)
20
15
10
5
0
-5
-10
-15
-20
-20
-15
-10
-5
0
5
10
15
20

FIGURE 4.5

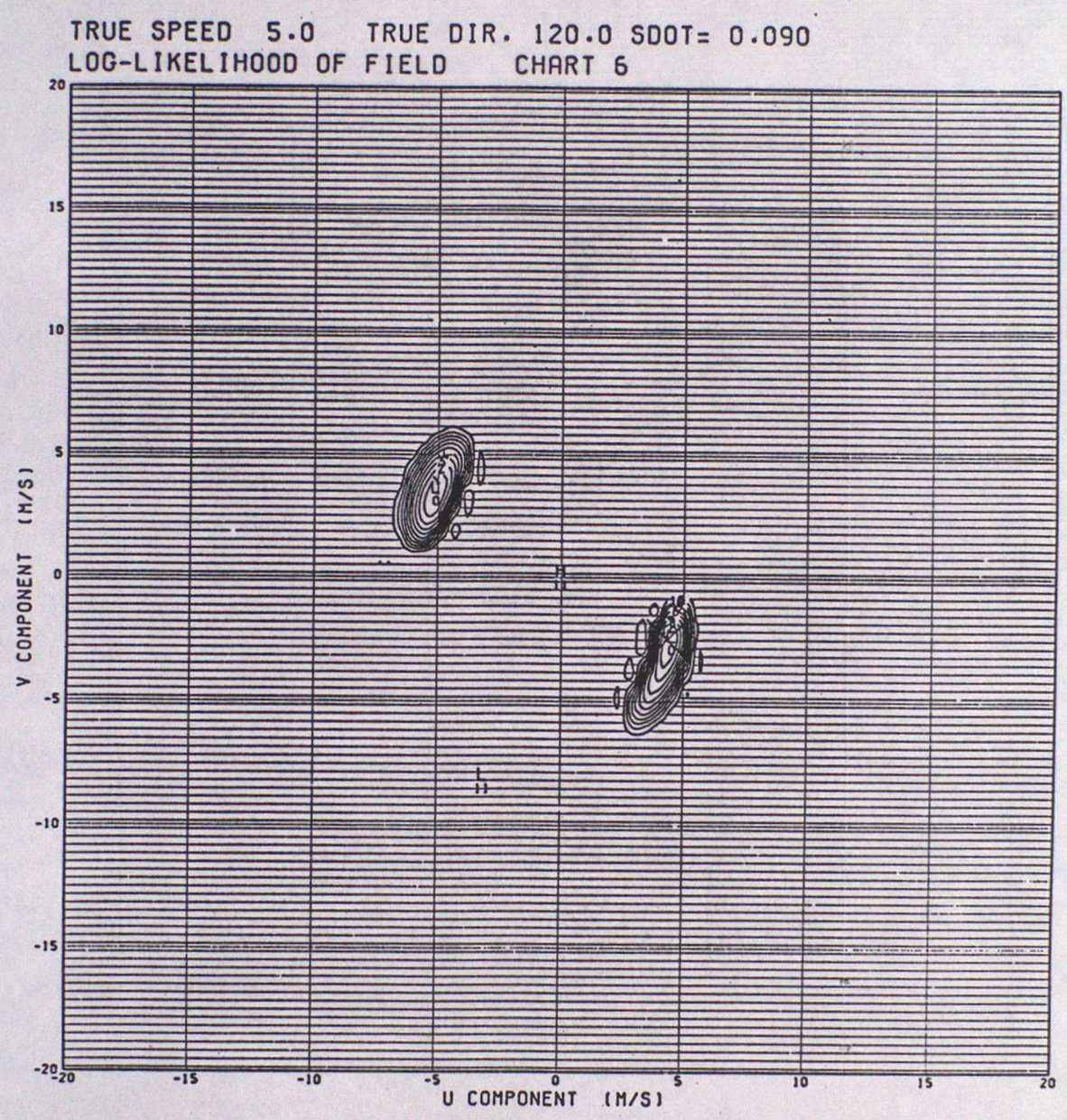
TRUE SPEED 5.0 TRUE DIR. 120.0 SDOT= 0.090
LOG-LIKELIHOOD OF FIELD CHART 6
V COMPONENT (M/S)
U COMPONENT (M/S)
20
15
10
5
0
-5
-10
-15
-20

FIGURE 4-6

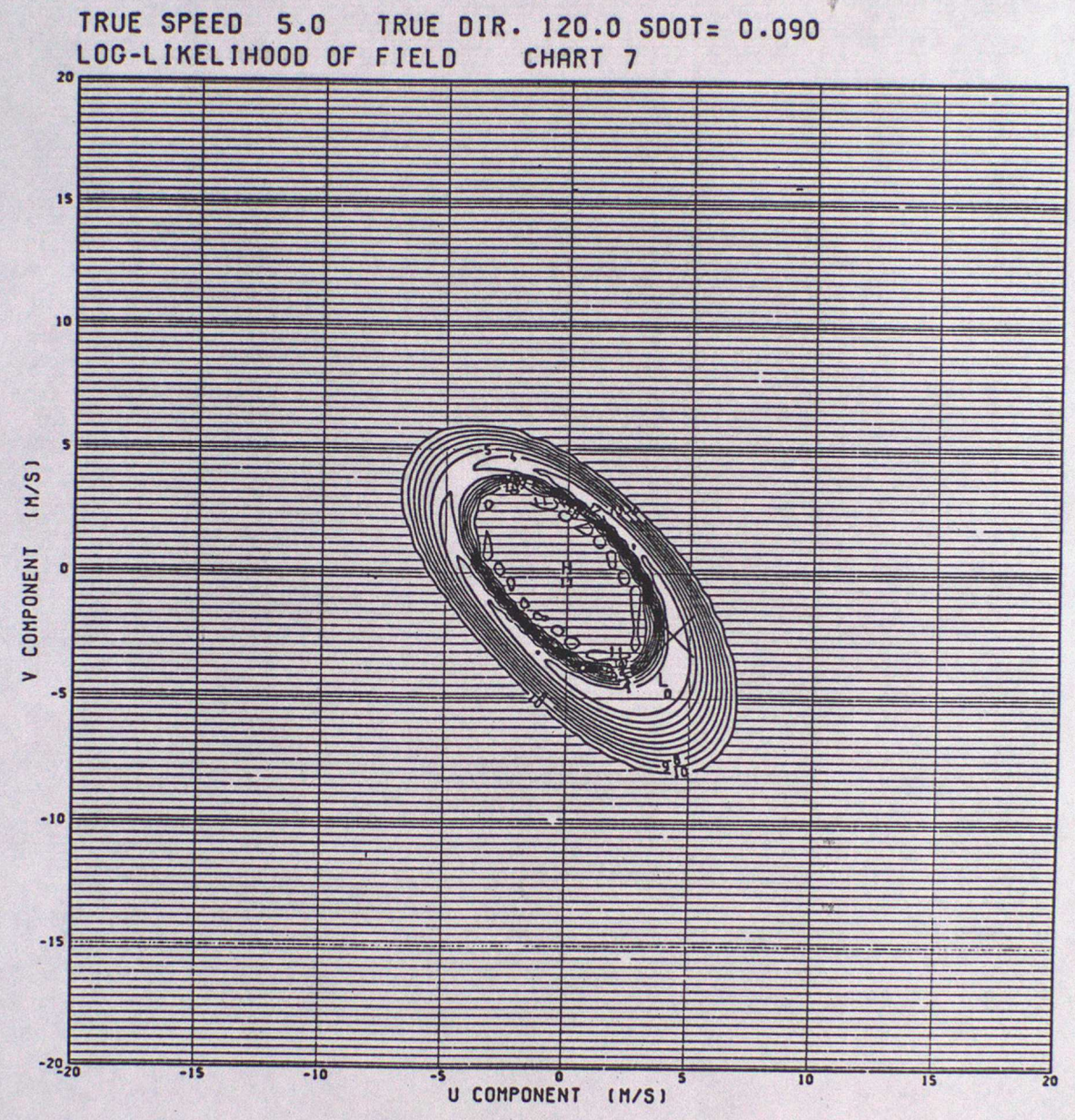
TRUE SPEED 5.0 TRUE DIR. 120.0 SDOT= 0.090
LOG-LIKELIHOOD OF FIELD CHART 7
V COMPONENT (M/S)
U COMPONENT (M/S)
20
15
10
5
0
-5
-10
-15
-20

Fig. 4-7

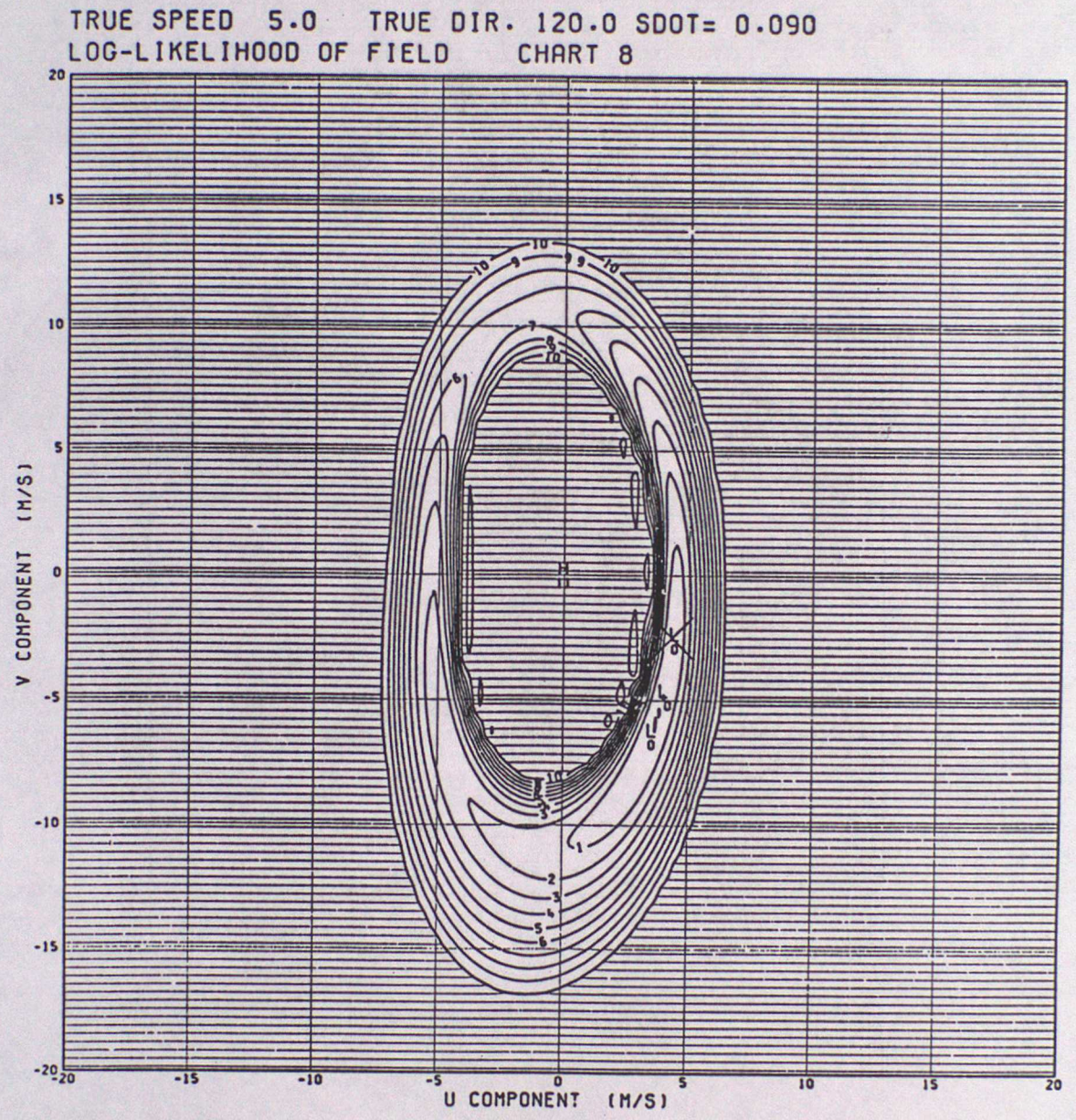
TRUE SPEED 5.0 TRUE DIR. 120.0 SDOT= 0.090
LOG-LIKELIHOOD OF FIELD CHART 8
V COMPONENT (M/S)
U COMPONENT (M/S)
20
15
10
5
0
-5
-10
-15
-20

FIGURE 4-8

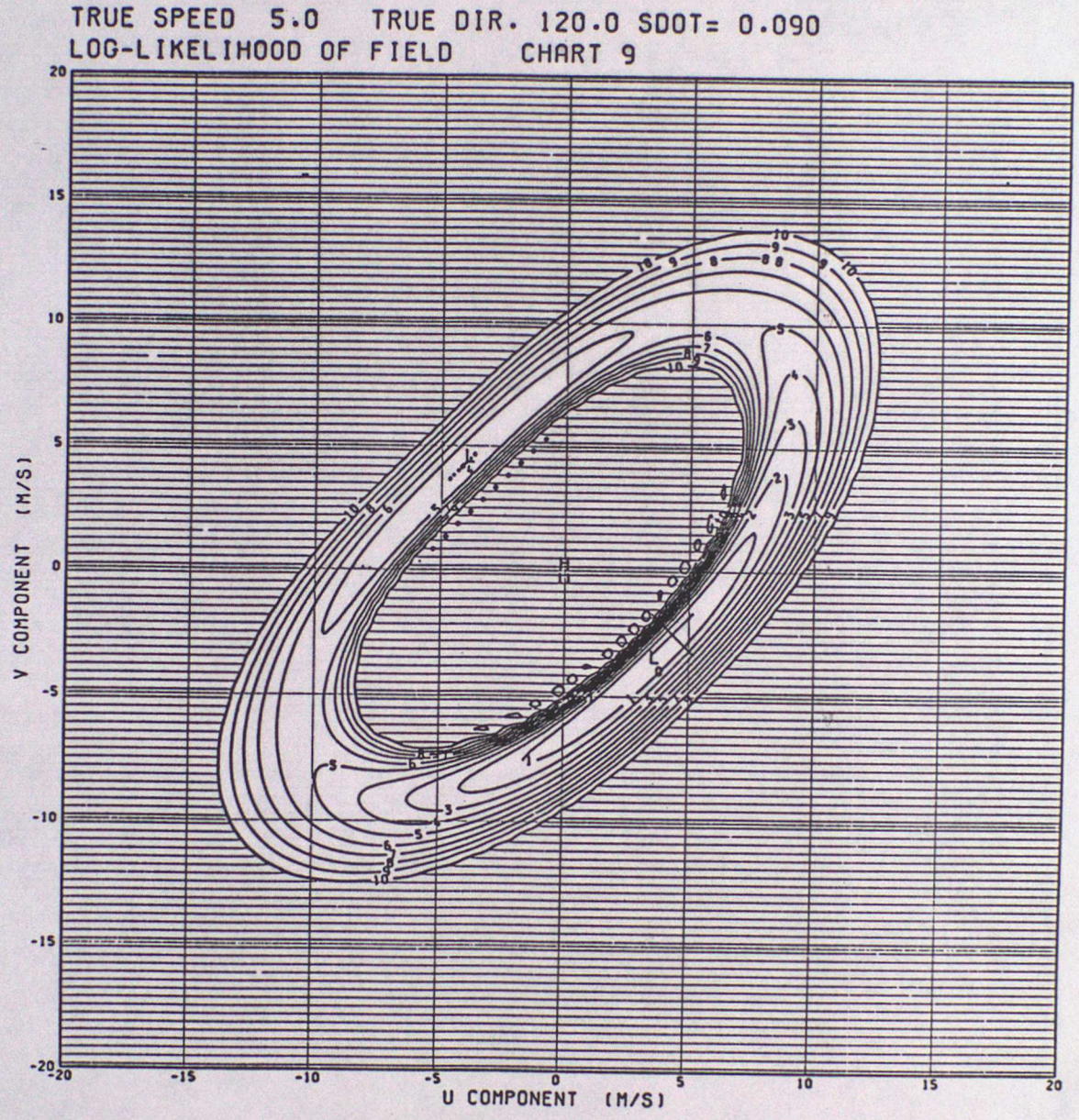
TRUE SPEED 5.0 TRUE DIR. 120.0 SDOT= 0.090
LOG-LIKELIHOOD OF FIELD CHART 9
V COMPONENT (M/S)
U COMPONENT (M/S)
20
15
10
5
0
-5
-10
-15
-20

FIGURE 4.9

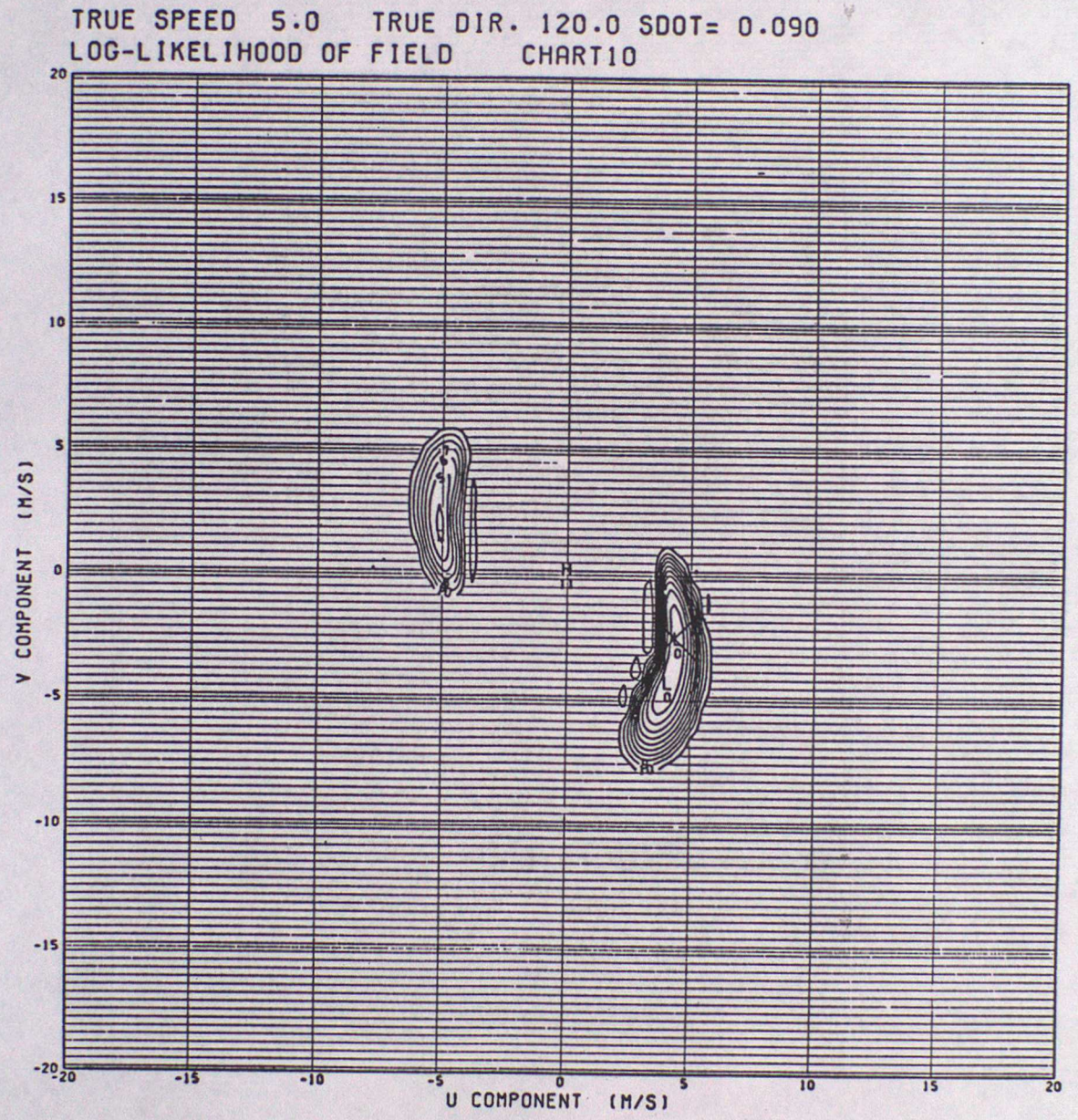
TRUE SPEED 5.0 TRUE DIR. 120.0 SDOT= 0.090
LOG-LIKELIHOOD OF FIELD CHART10
V COMPONENT (M/S)
U COMPONENT (M/S)
20
15
10
5
0
-5
-10
-15
-20

FIGURE 4.10

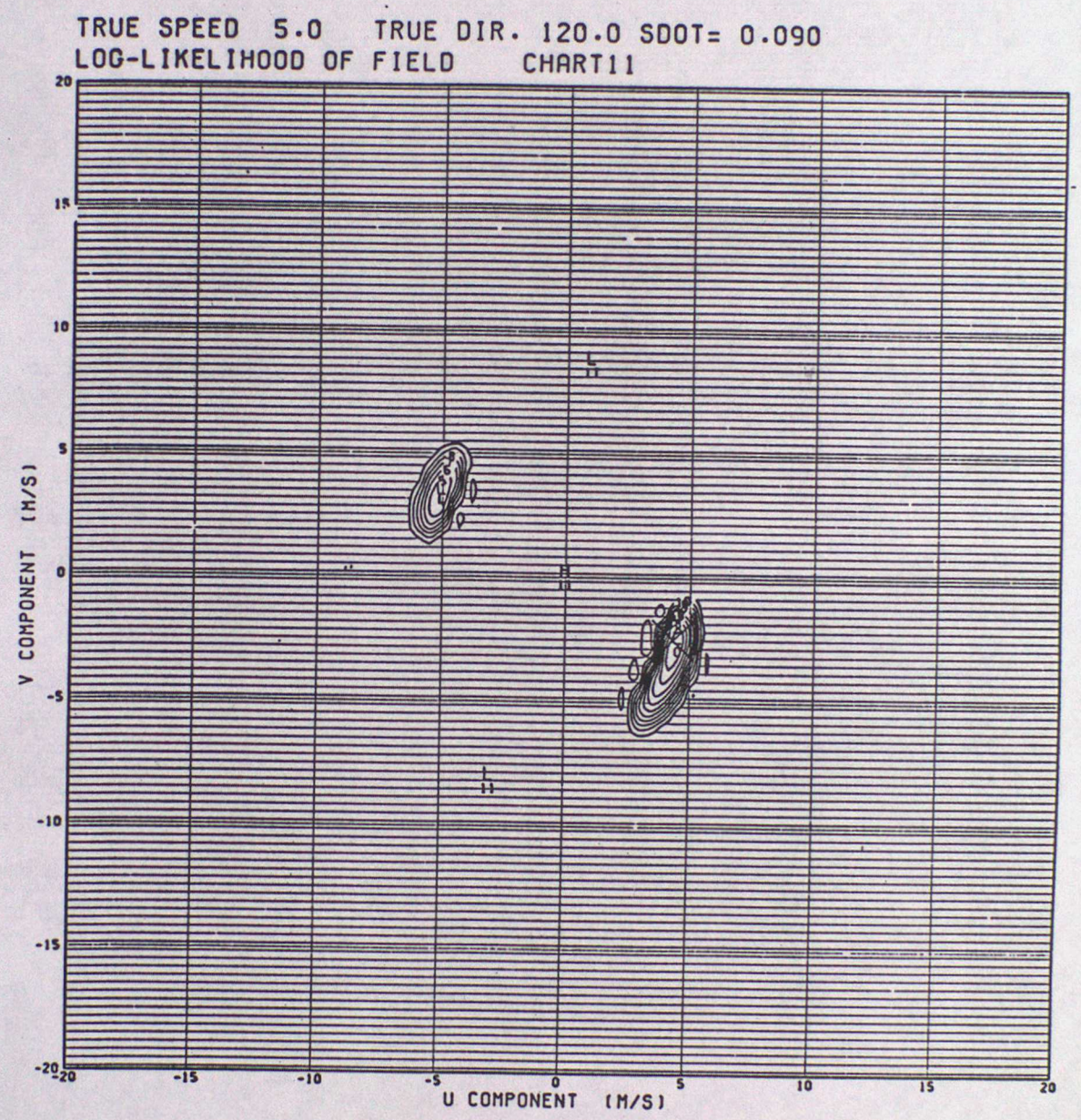
TRUE SPEED 5.0 TRUE DIR. 120.0 SDOT= 0.090
LOG-LIKELIHOOD OF FIELD CHART11
V COMPONENT (M/S)
U COMPONENT (M/S)
20
15
10
5
0
-5
-10
-15
-20

FIGURE 4.11

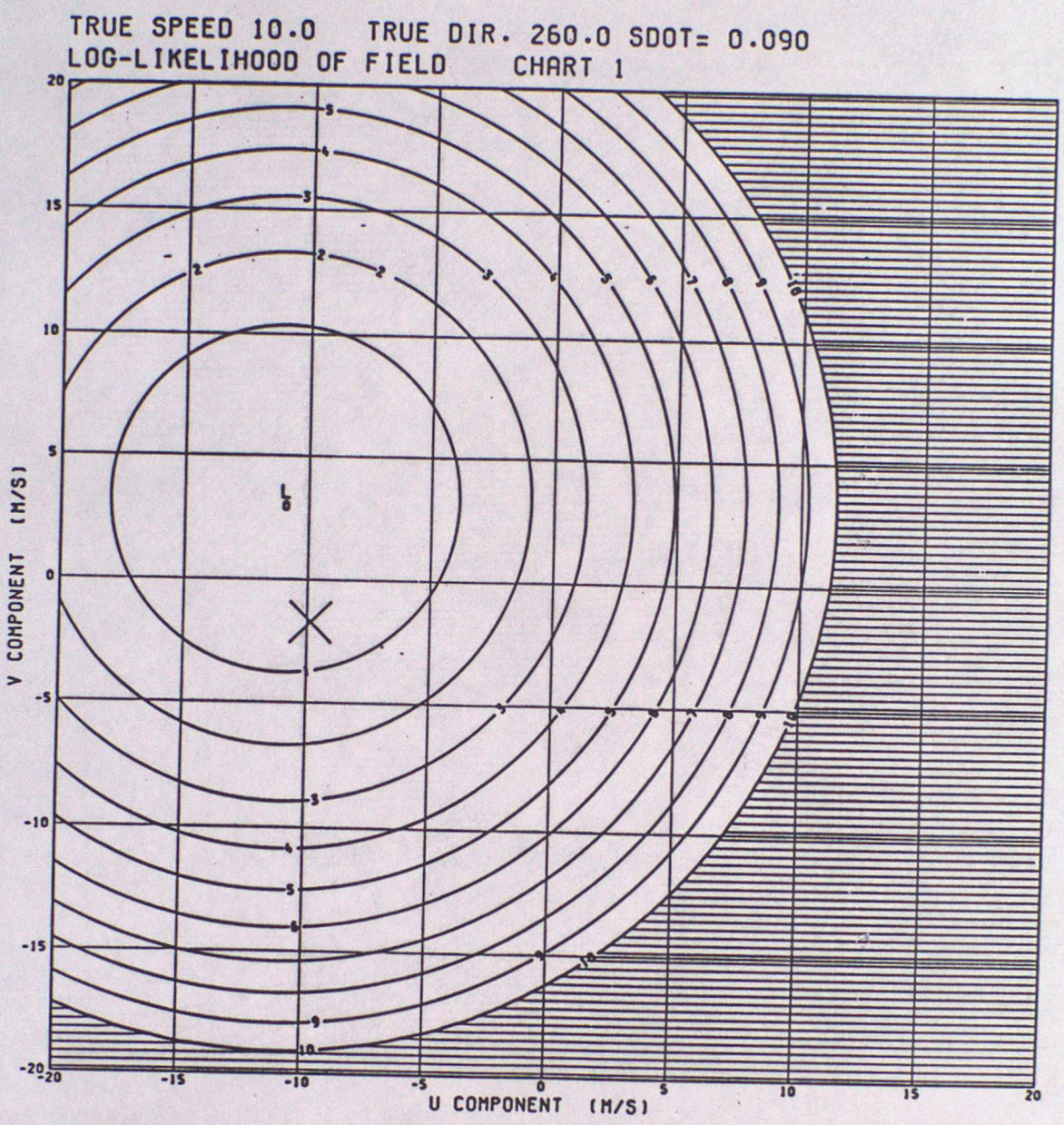
TRUE SPEED 10.0 TRUE DIR. 260.0 SDOT= 0.090
LOG-LIKELIHOOD OF FIELD CHART 1
V COMPONENT (M/S)
U COMPONENT (M/S)
20
15
10
5
0
-5
-10
-15
-20
-20
-15
-10
-5
0
5
10
15
20

FIGURE 5.1

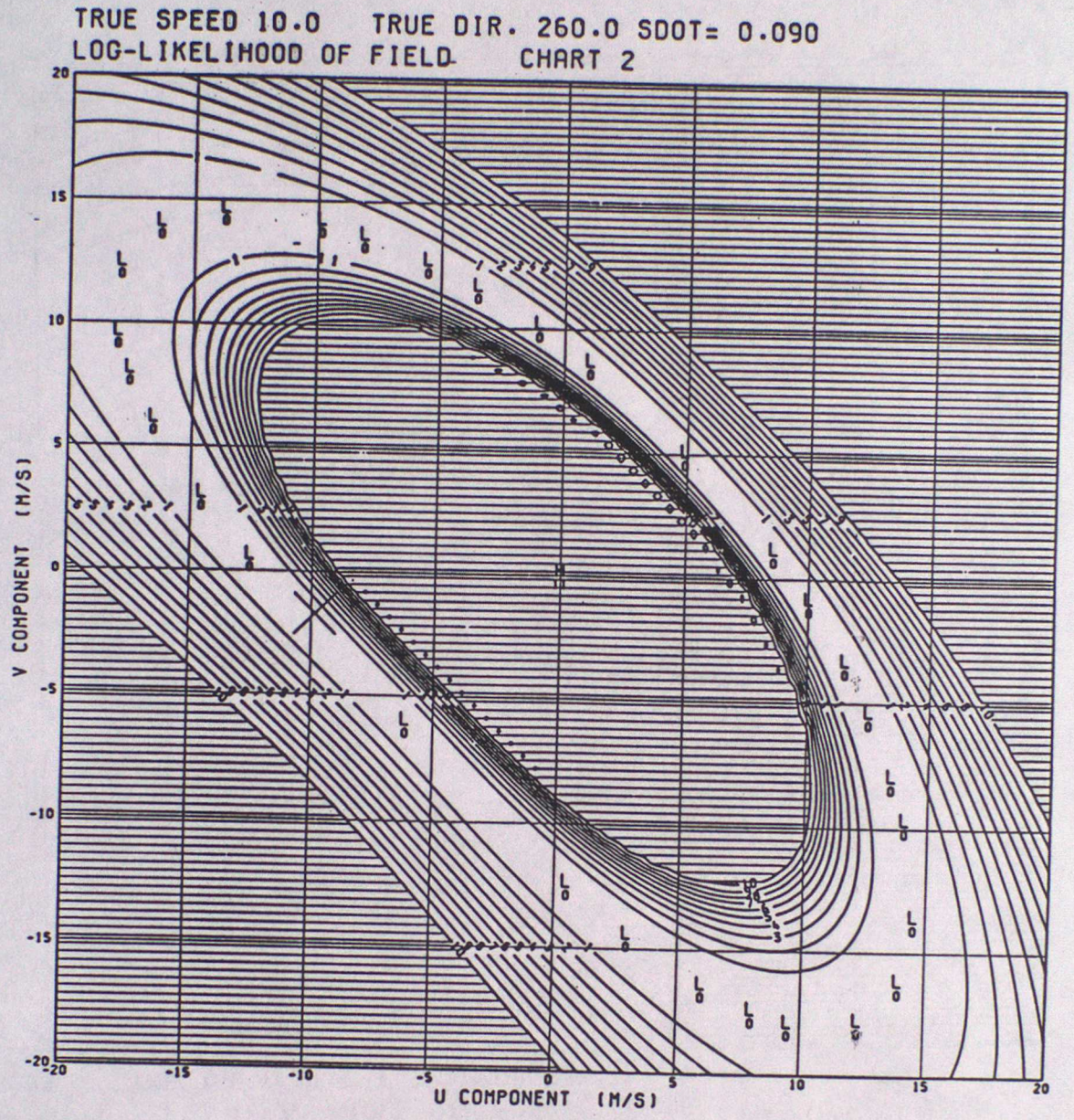
TRUE SPEED 10.0 TRUE DIR. 260.0 SDOT= 0.090
LOG-LIKELIHOOD OF FIELD CHART 2
V COMPONENT (M/S)
U COMPONENT (M/S)
20
15
10
5
0
-5
-10
-15
-20

FIGURE 5.2

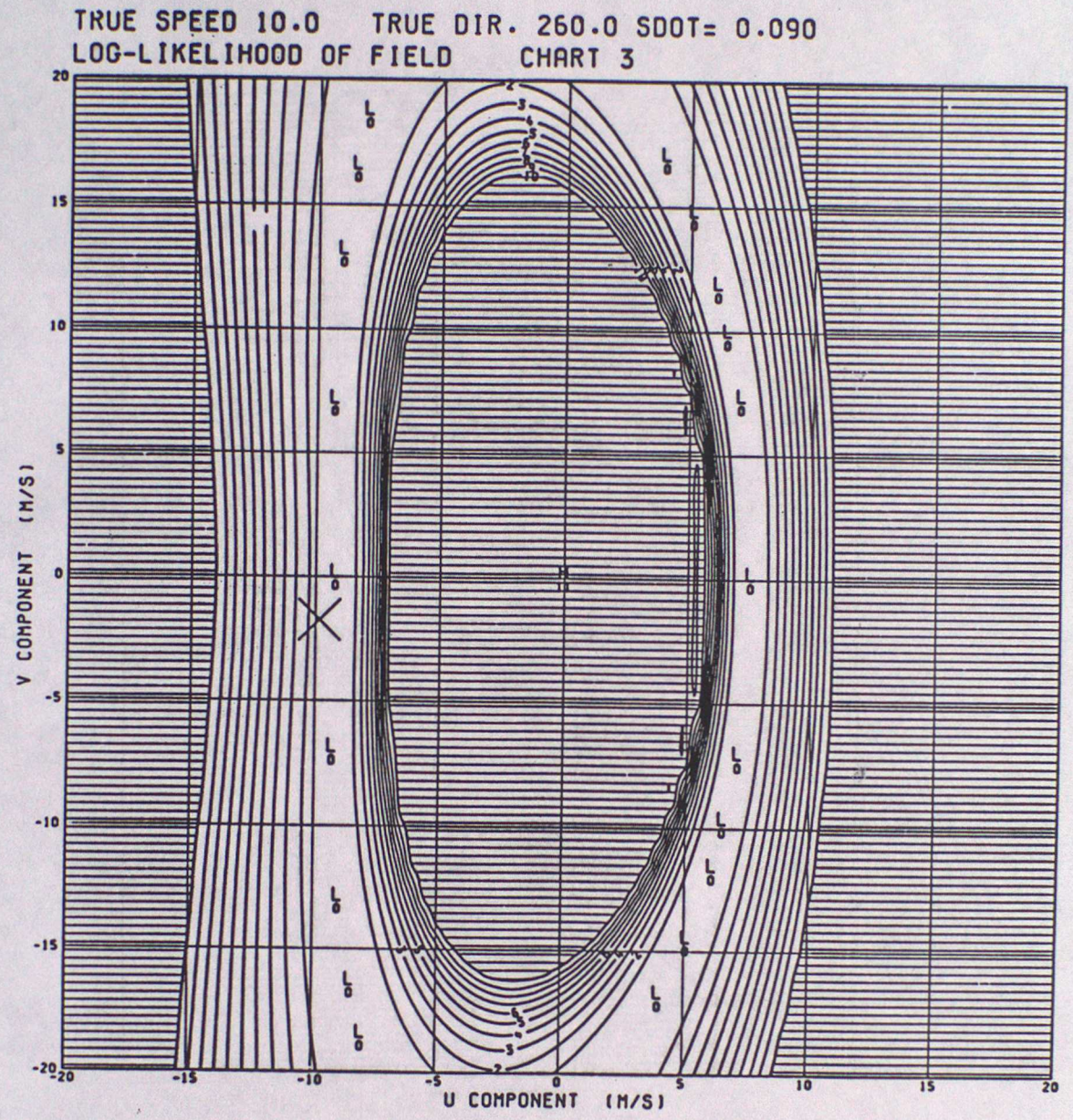
TRUE SPEED 10.0 TRUE DIR. 260.0 SDOT= 0.090
LOG-LIKELIHOOD OF FIELD CHART 3
V COMPONENT (M/S)
U COMPONENT (M/S)
20
15
10
5
0
-5
-10
-15
-20

FIGURE 5.3

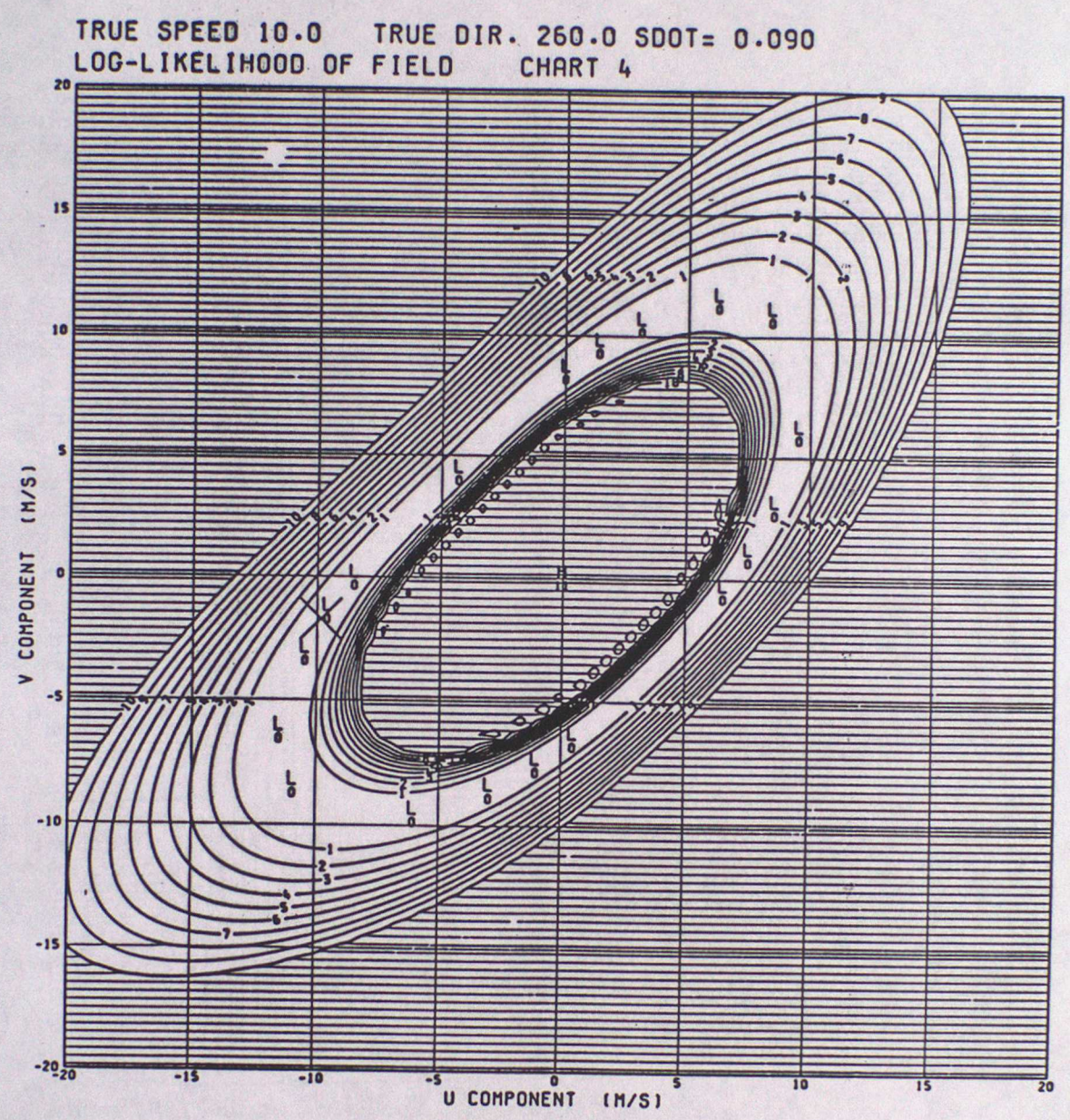
TRUE SPEED 10.0 TRUE DIR. 260.0 SDOT= 0.090
LOG-LIKELIHOOD OF FIELD CHART 4
V COMPONENT (M/S)
U COMPONENT (M/S)
20
15
10
5
0
-5
-10
-15
-20

FIGURE 5-4

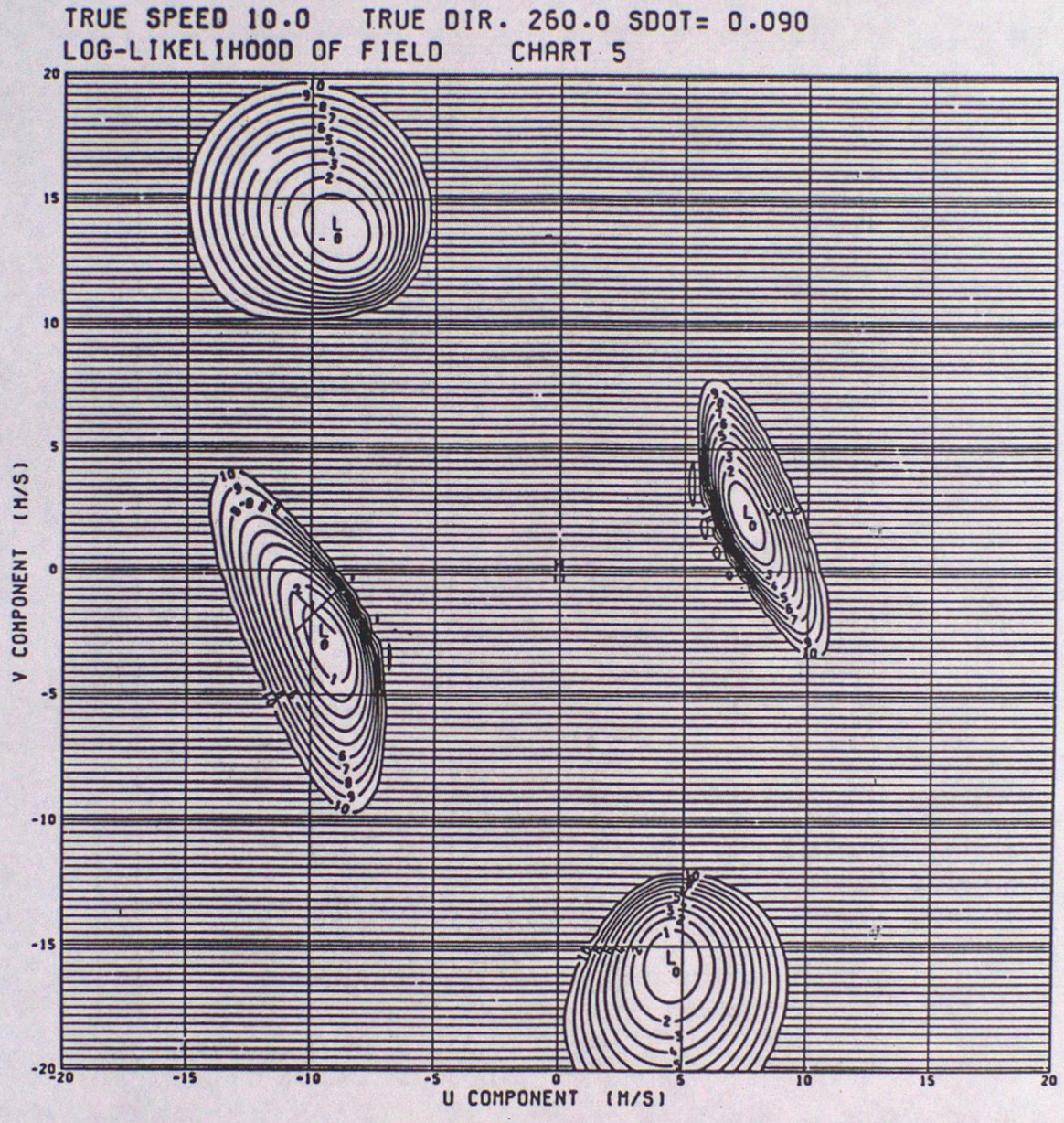
TRUE SPEED 10.0 TRUE DIR. 260.0 SDOT= 0.090
LOG-LIKELIHOOD OF FIELD CHART 5
V COMPONENT (M/S)
U COMPONENT (M/S)
20
15
10
5
0
-5
-10
-15
-20

FIGURE 5-5

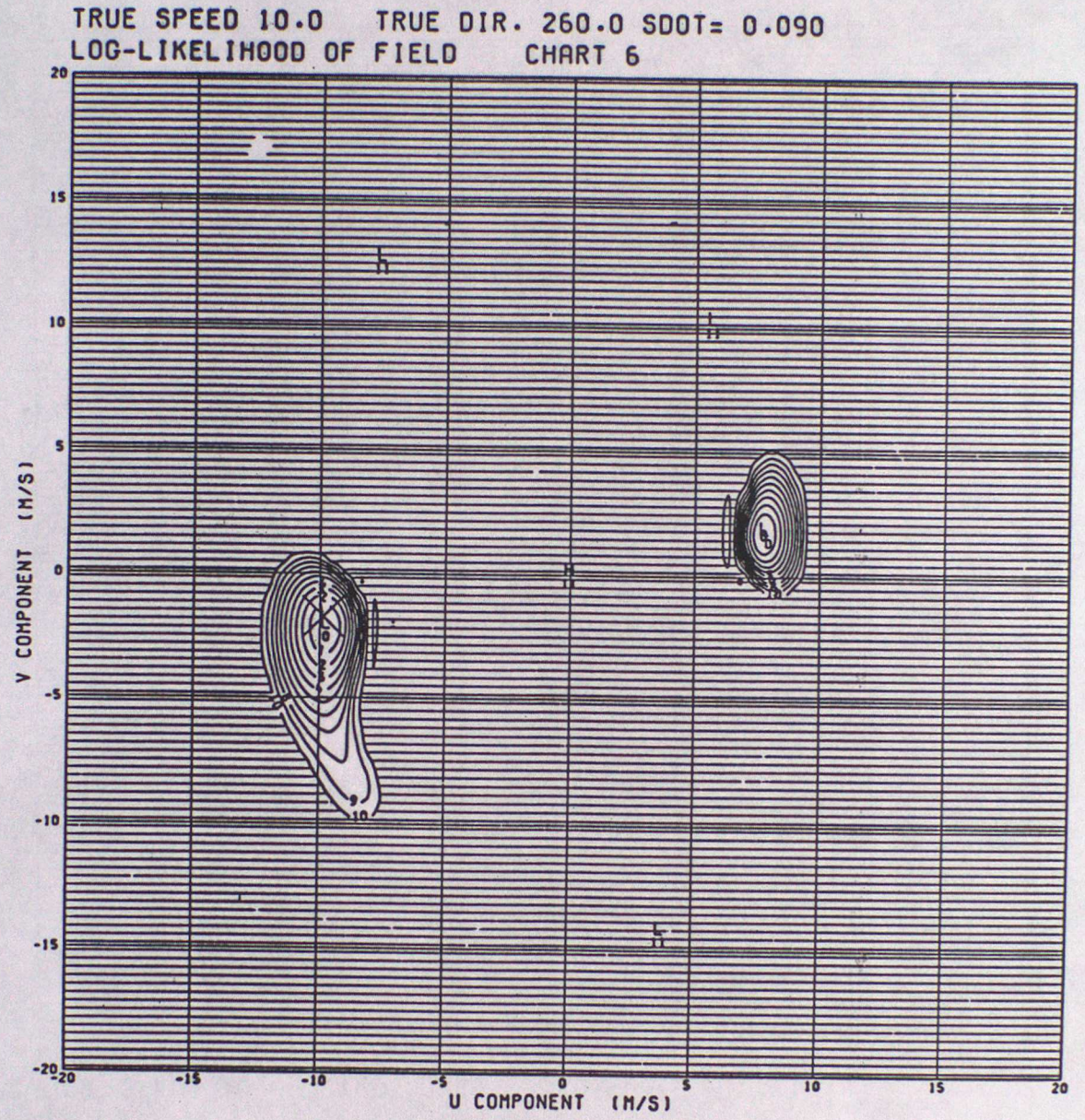
TRUE SPEED 10.0 TRUE DIR. 260.0 SDOT= 0.090
LOG-LIKELIHOOD OF FIELD CHART 6
V COMPONENT (M/S)
U COMPONENT (M/S)
20
15
10
5
0
-5
-10
-15
-20

FIGURE 5.6

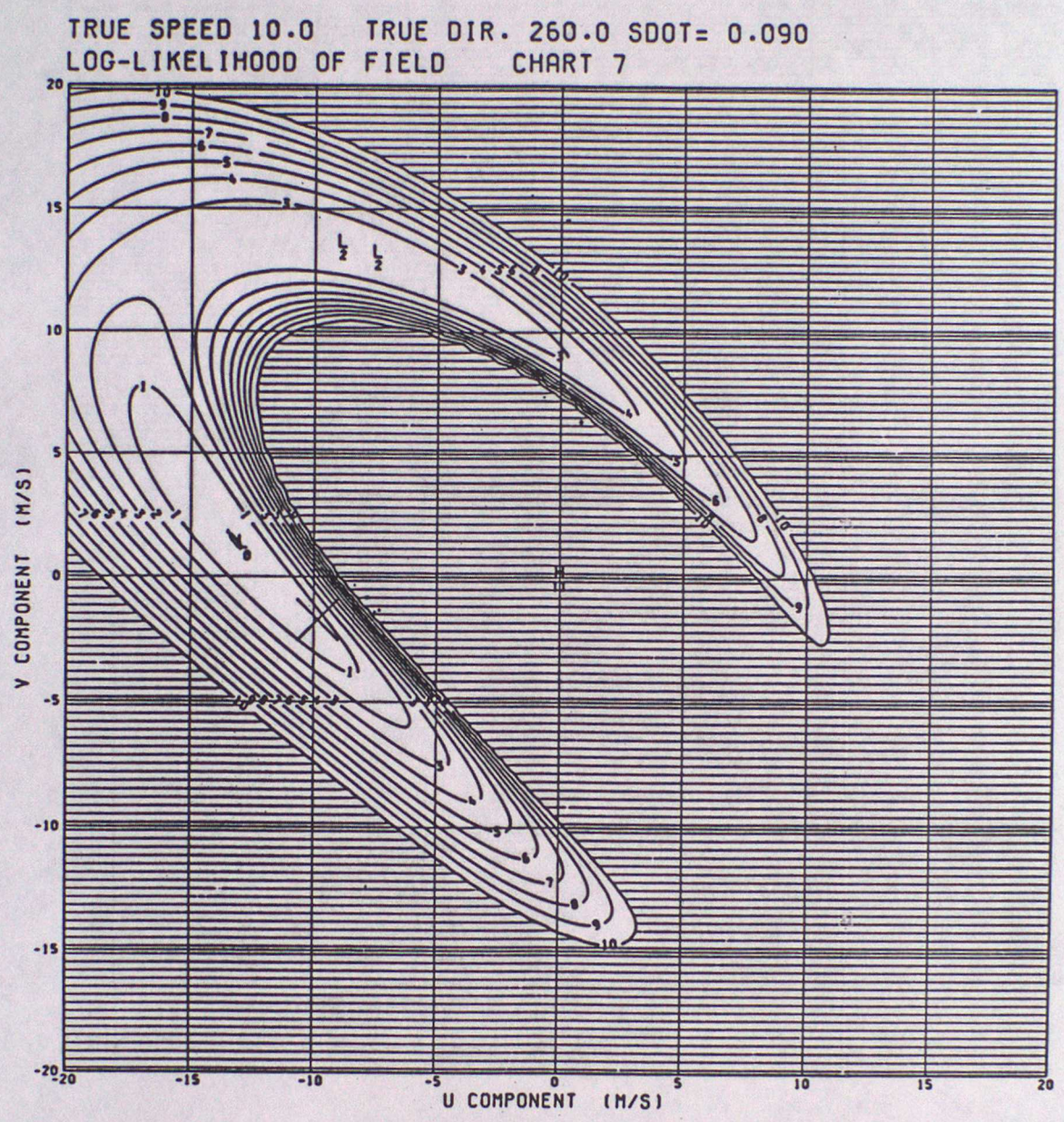
TRUE SPEED 10.0 TRUE DIR. 260.0 SDOT= 0.090
LOG-LIKELIHOOD OF FIELD CHART 7
V COMPONENT (M/S)
U COMPONENT (M/S)
20
15
10
5
0
-5
-10
-15
-20

FIGURE 5-7

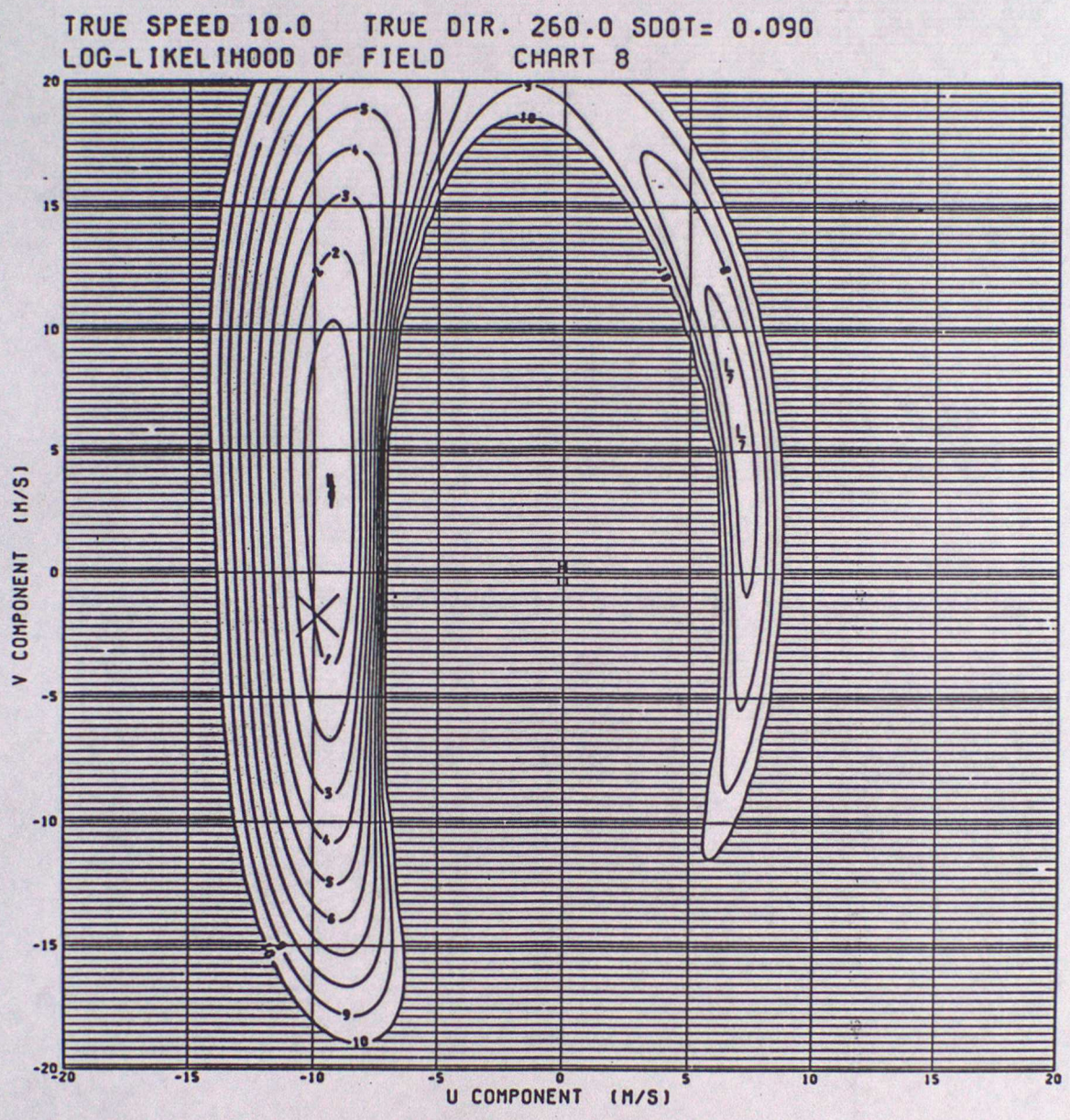
TRUE SPEED 10.0 TRUE DIR. 260.0 SDOT= 0.090
LOG-LIKELIHOOD OF FIELD CHART 8
V COMPONENT (M/S)
U COMPONENT (M/S)
20
15
10
5
0
-5
-10
-15
-20

FIGURE 5-8

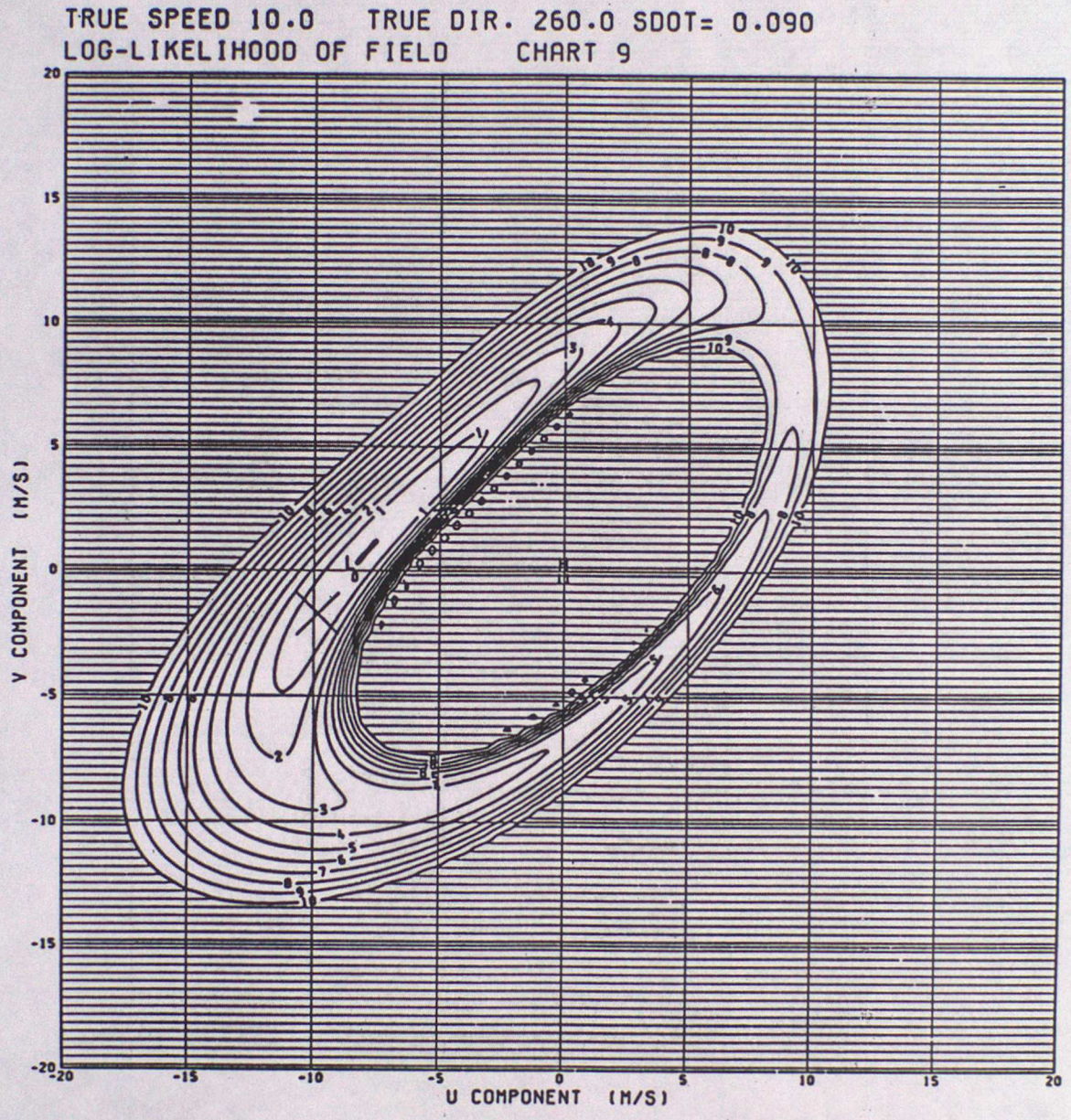
TRUE SPEED 10.0 TRUE DIR. 260.0 SDOT= 0.090
LOG-LIKELIHOOD OF FIELD CHART 9
V COMPONENT (M/S)
U COMPONENT (M/S)
20
15
10
5
0
-5
-10
-15
-20

FIGURE 5.9

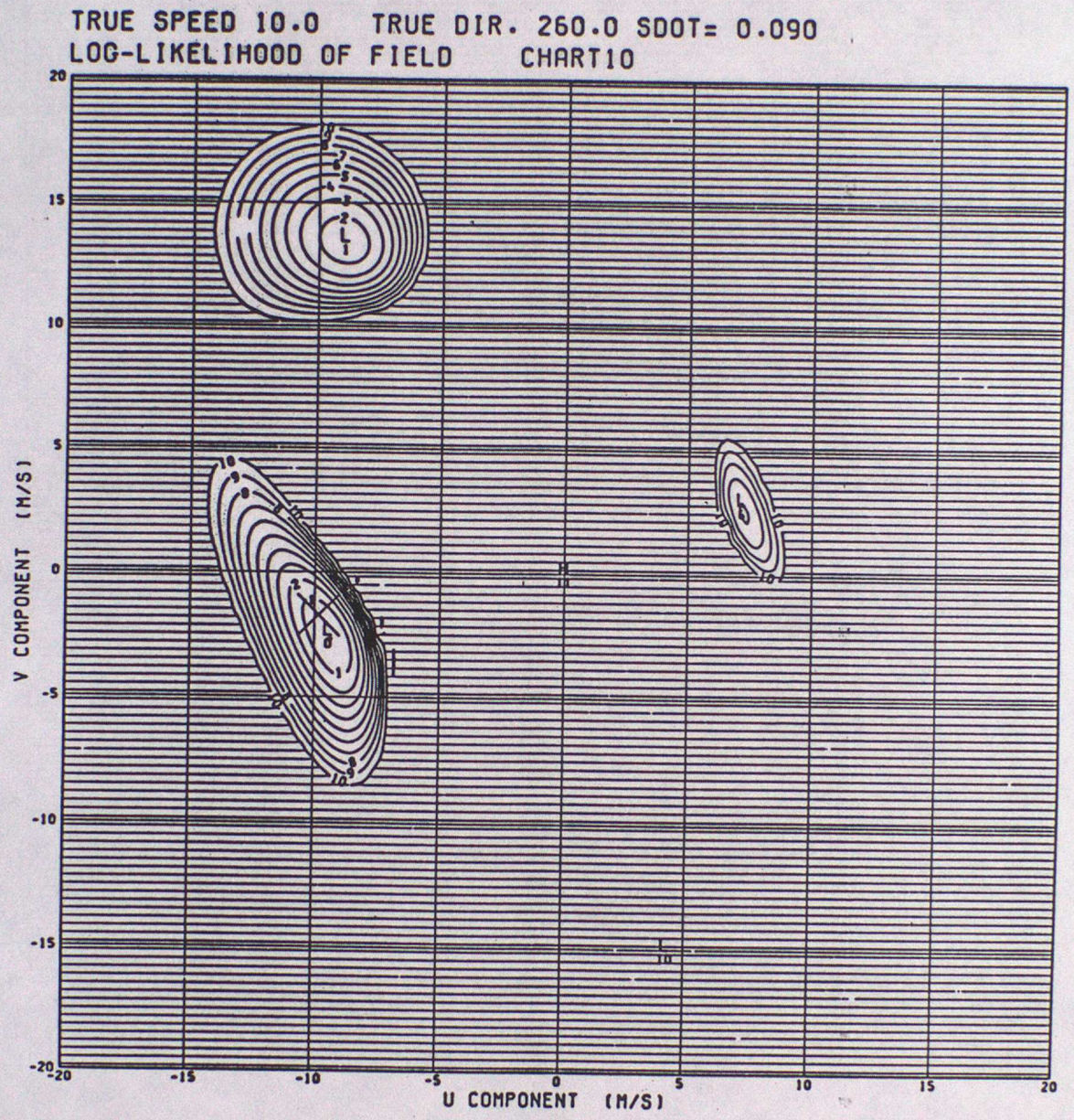
TRUE SPEED 10.0 TRUE DIR. 260.0 SDOT= 0.090
LOG-LIKELIHOOD OF FIELD CHART10
V COMPONENT (M/S)
U COMPONENT (M/S)
20
15
10
5
0
-5
-10
-15
-20

FIGURE 5.10

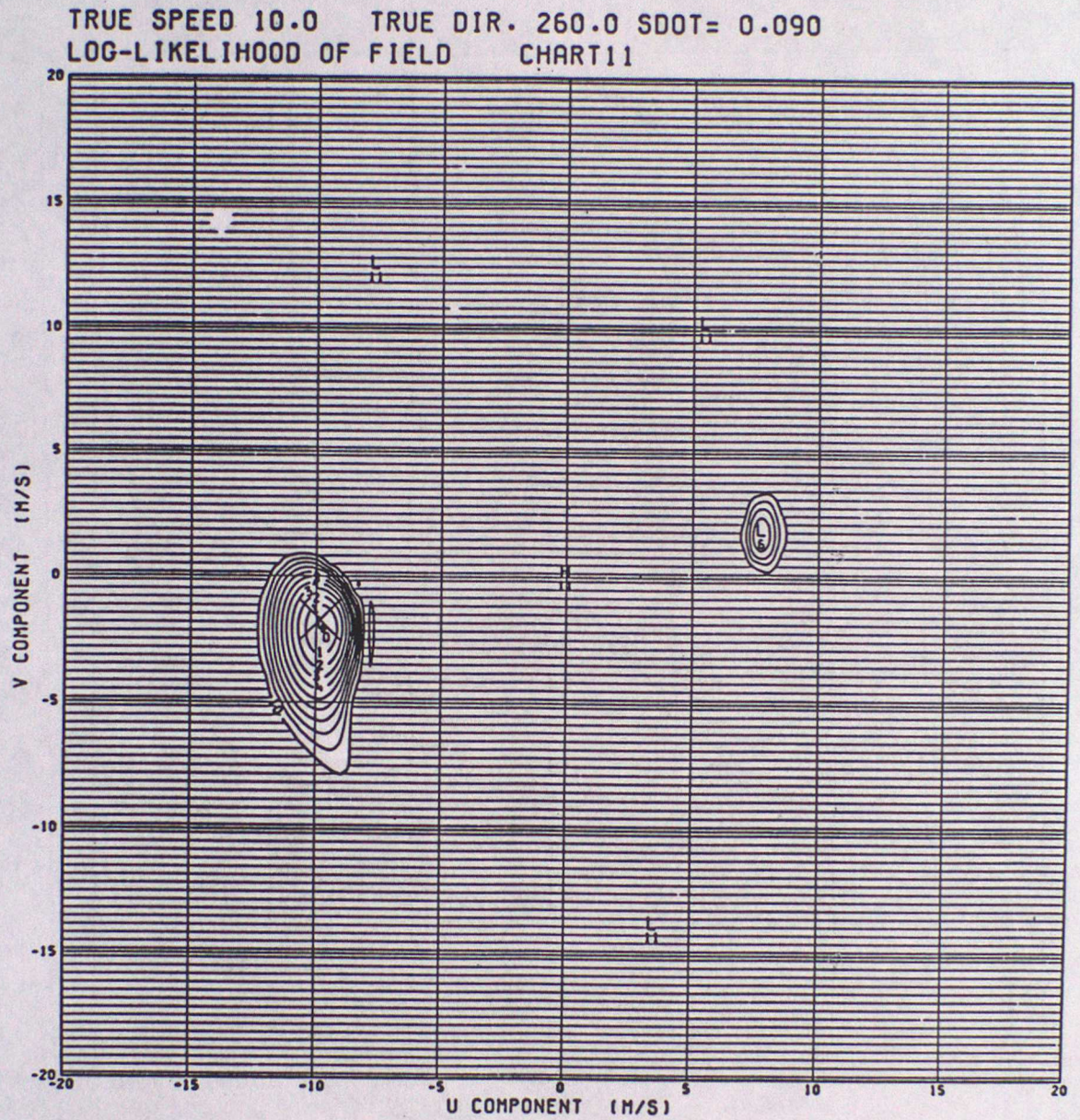
TRUE SPEED 10.0 TRUE DIR. 260.0 SDOT= 0.090
LOG-LIKELIHOOD OF FIELD CHART11
V COMPONENT (M/S)
U COMPONENT (M/S)
20
15
10
5
0
-5
-10
-15
-20

FIGURE 5.11

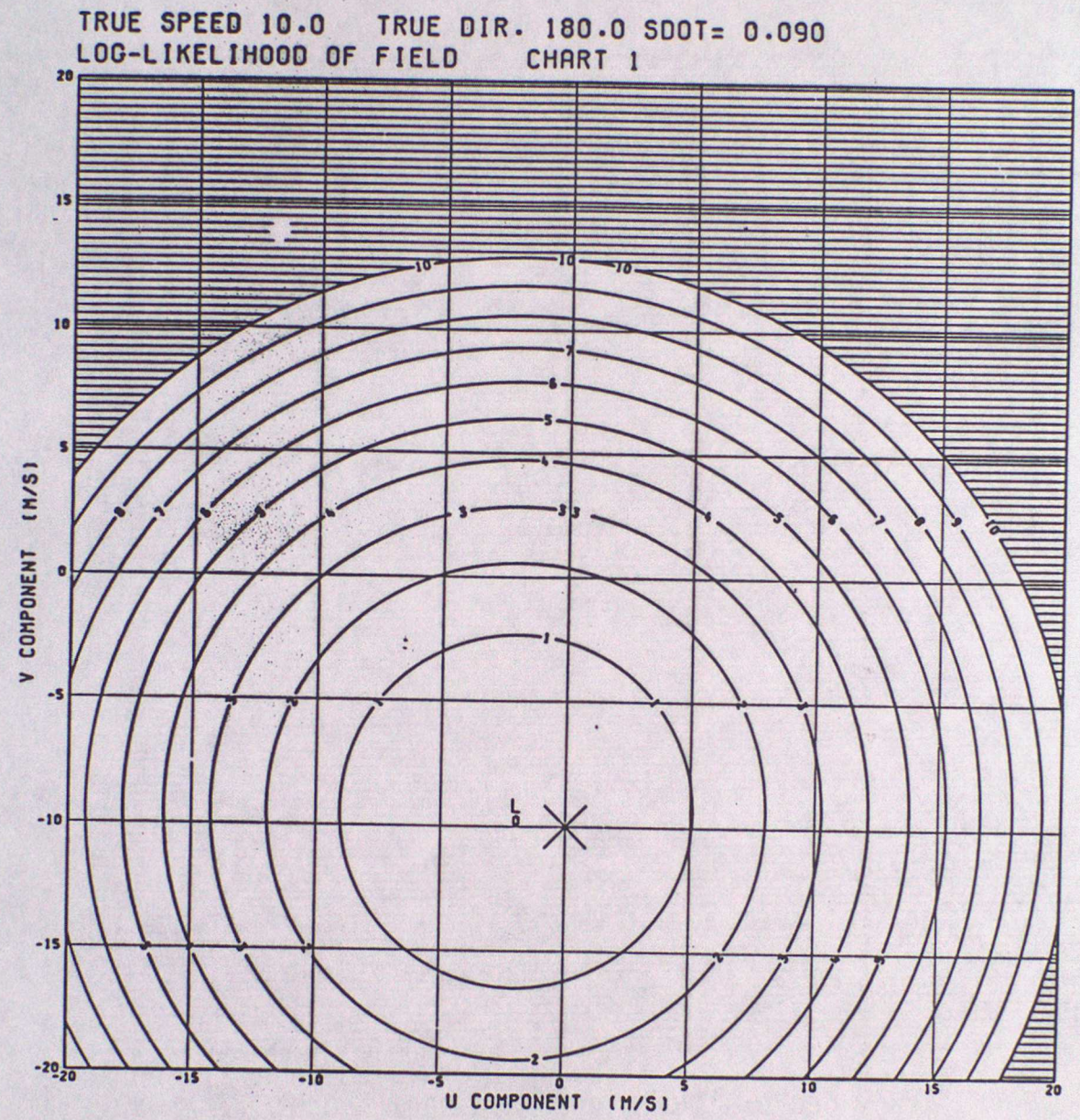
TRUE SPEED 10.0 TRUE DIR. 180.0 SDOT= 0.090
LOG-LIKELIHOOD OF FIELD CHART 1
V COMPONENT (M/S)
U COMPONENT (M/S)
20
15
10
5
0
-5
-10
-15
-20
-20
-15
-10
-5
0
5
10
15
20

FIGURE 6.1

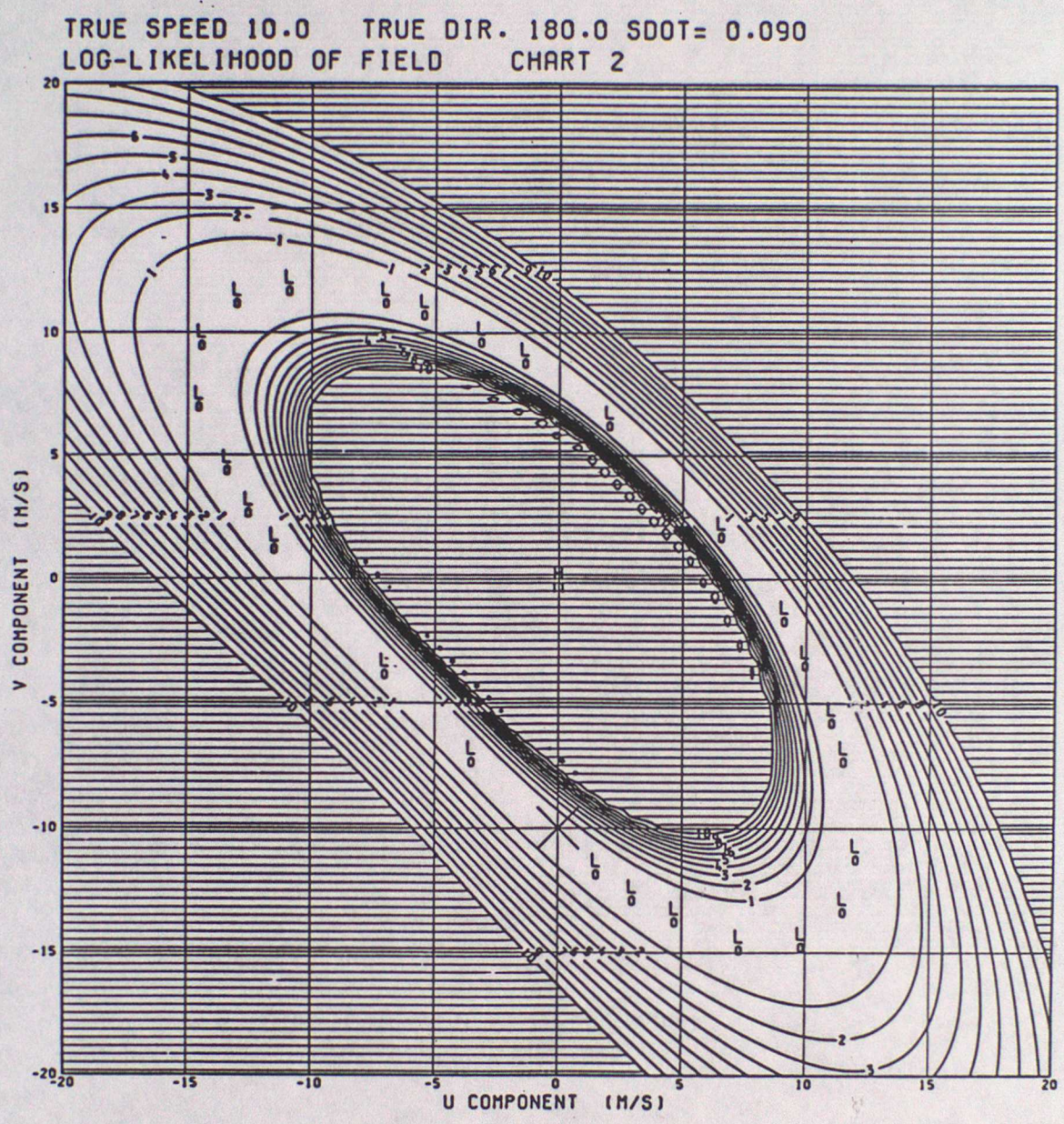
TRUE SPEED 10.0 TRUE DIR. 180.0 SDOT= 0.090
LOG-LIKELIHOOD OF FIELD CHART 2
V COMPONENT (M/S)
U COMPONENT (M/S)
20
15
10
5
0
-5
-10
-15
-20

Fig. 6.2

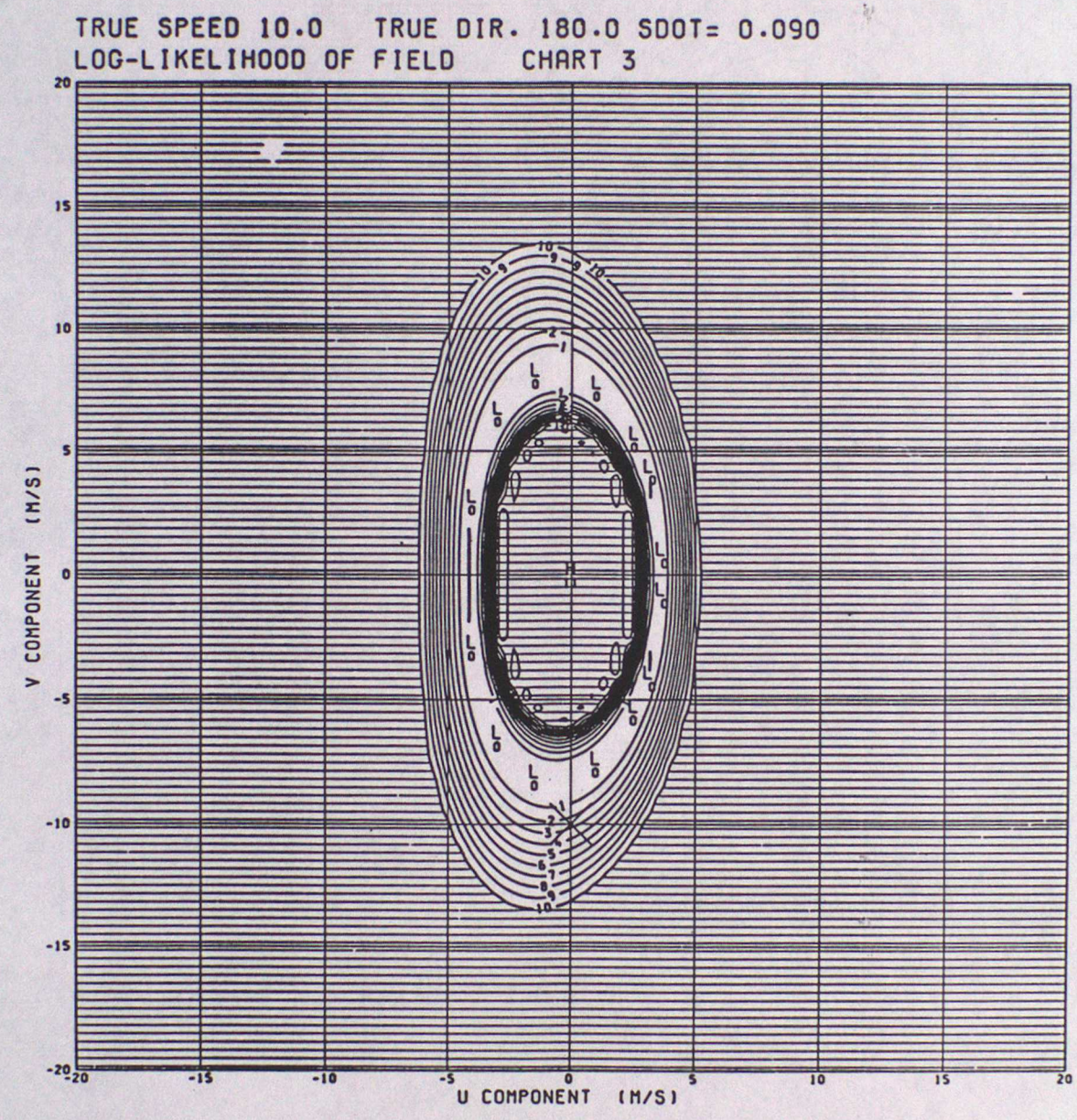
TRUE SPEED 10.0 TRUE DIR. 180.0 SDOT= 0.090
LOG-LIKELIHOOD OF FIELD CHART 3
V COMPONENT (M/S)
U COMPONENT (M/S)
20
15
10
5
0
-5
-10
-15
-20

F 5-3

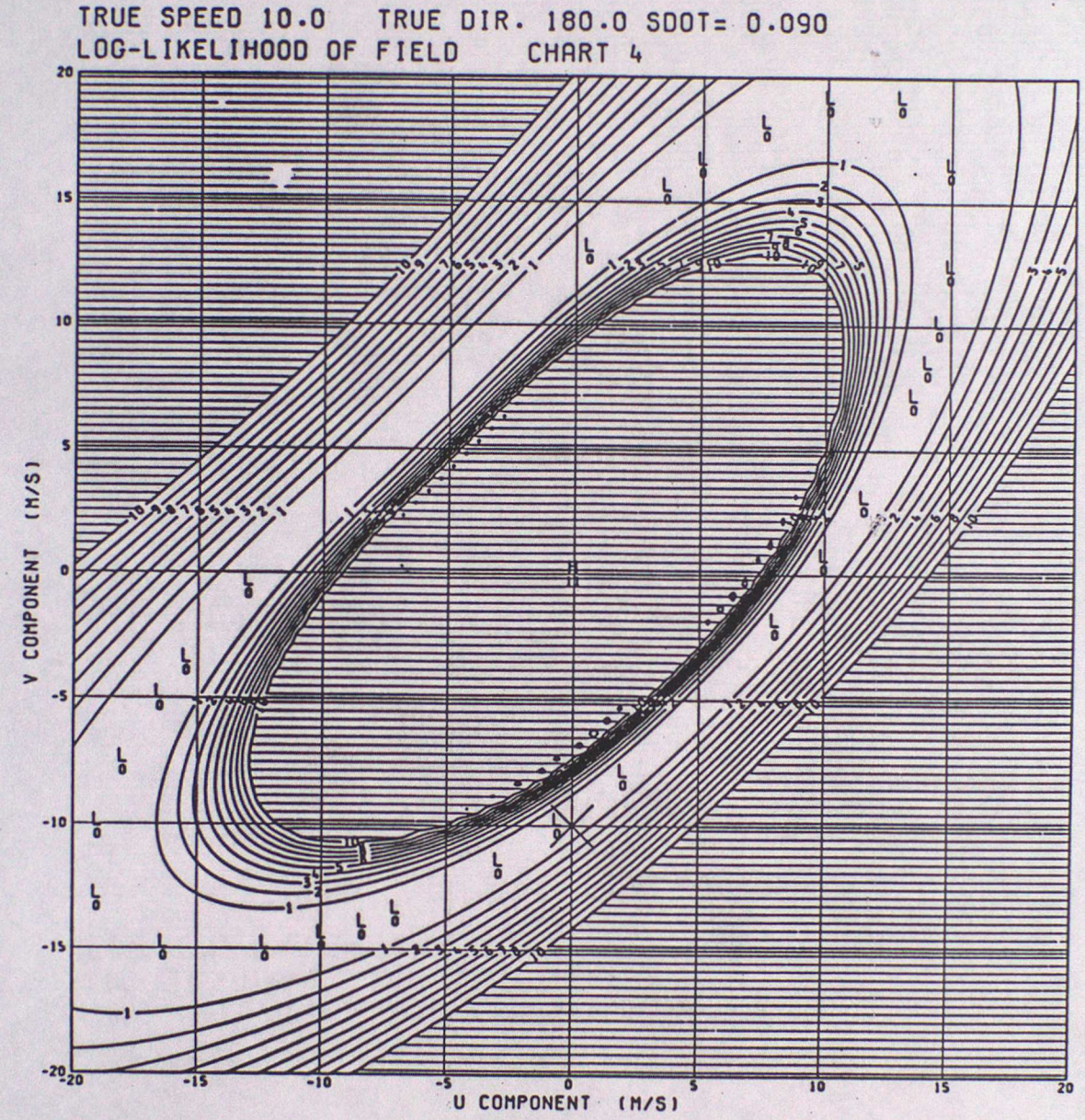
TRUE SPEED 10.0 TRUE DIR. 180.0 SDOT= 0.090
LOG-LIKELIHOOD OF FIELD CHART 4
V COMPONENT (M/S)
U COMPONENT (M/S)
20
15
10
5
0
-5
-10
-15
-20

FIGURE 6.4

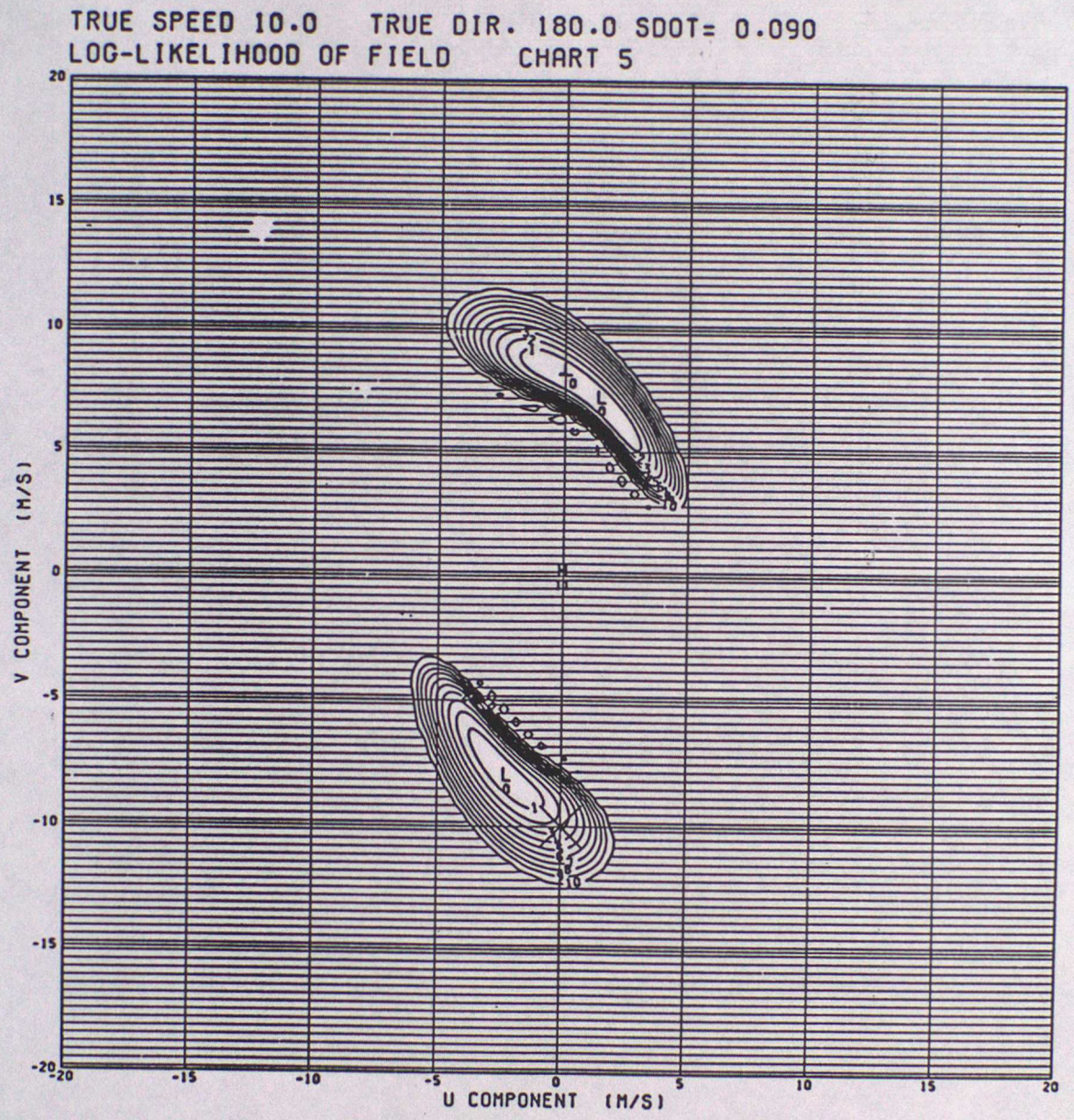
TRUE SPEED 10.0 TRUE DIR. 180.0 SDOT= 0.090
LOG-LIKELIHOOD OF FIELD CHART 5
V COMPONENT (M/S)
U COMPONENT (M/S)
20
15
10
5
0
-5
-10
-15
-20

Fig 6.5

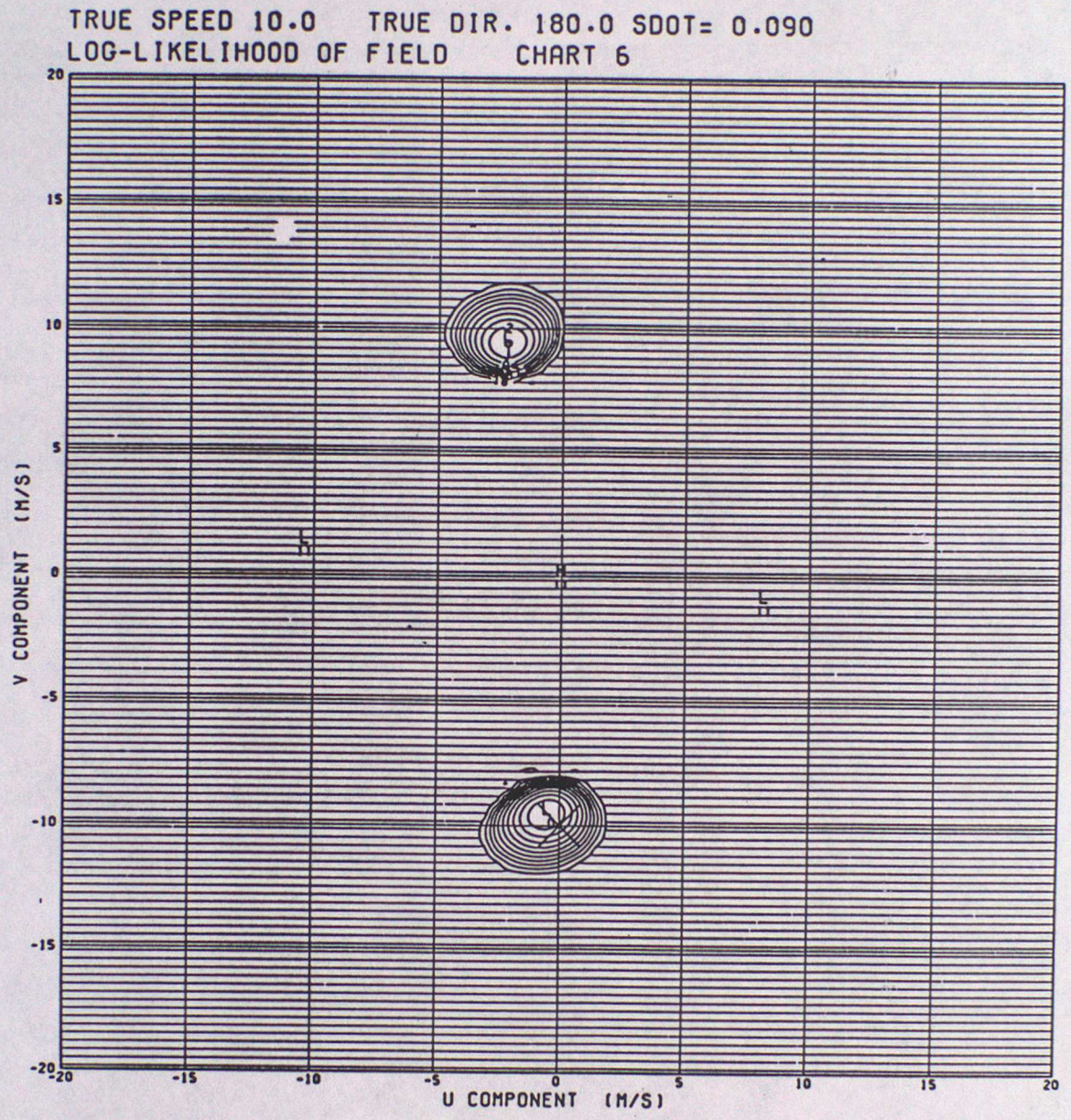
TRUE SPEED 10.0 TRUE DIR. 180.0 SDOT= 0.090
LOG-LIKELIHOOD OF FIELD CHART 6
V COMPONENT (M/S)
U COMPONENT (M/S)
20
15
10
5
0
-5
-10
-15
-20

Figure 6.6

TRUE SPEED 10.0 TRUE DIR. 180.0 SDOT= 0.090
LOG-LIKELIHOOD OF FIELD CHART 7

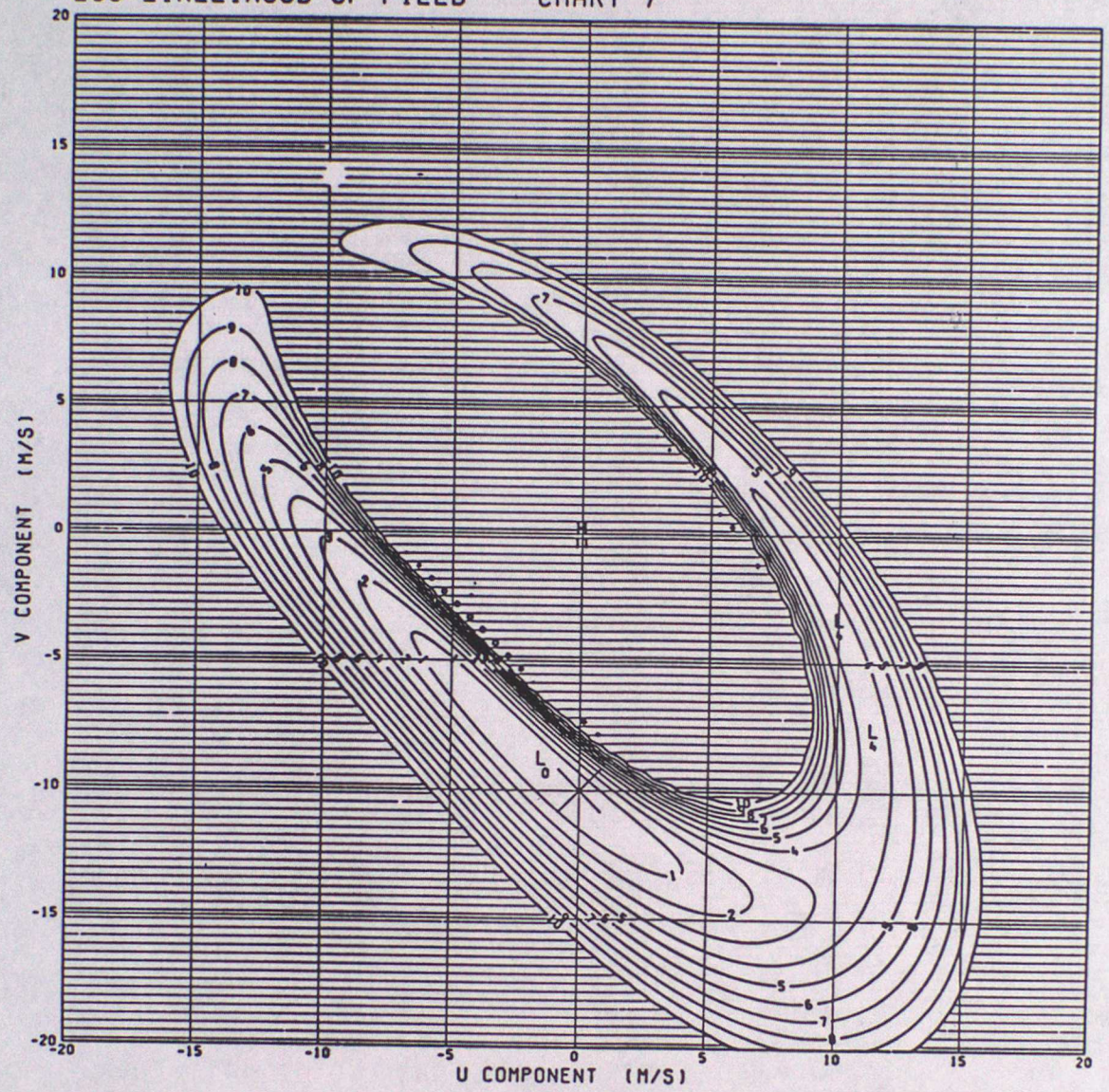

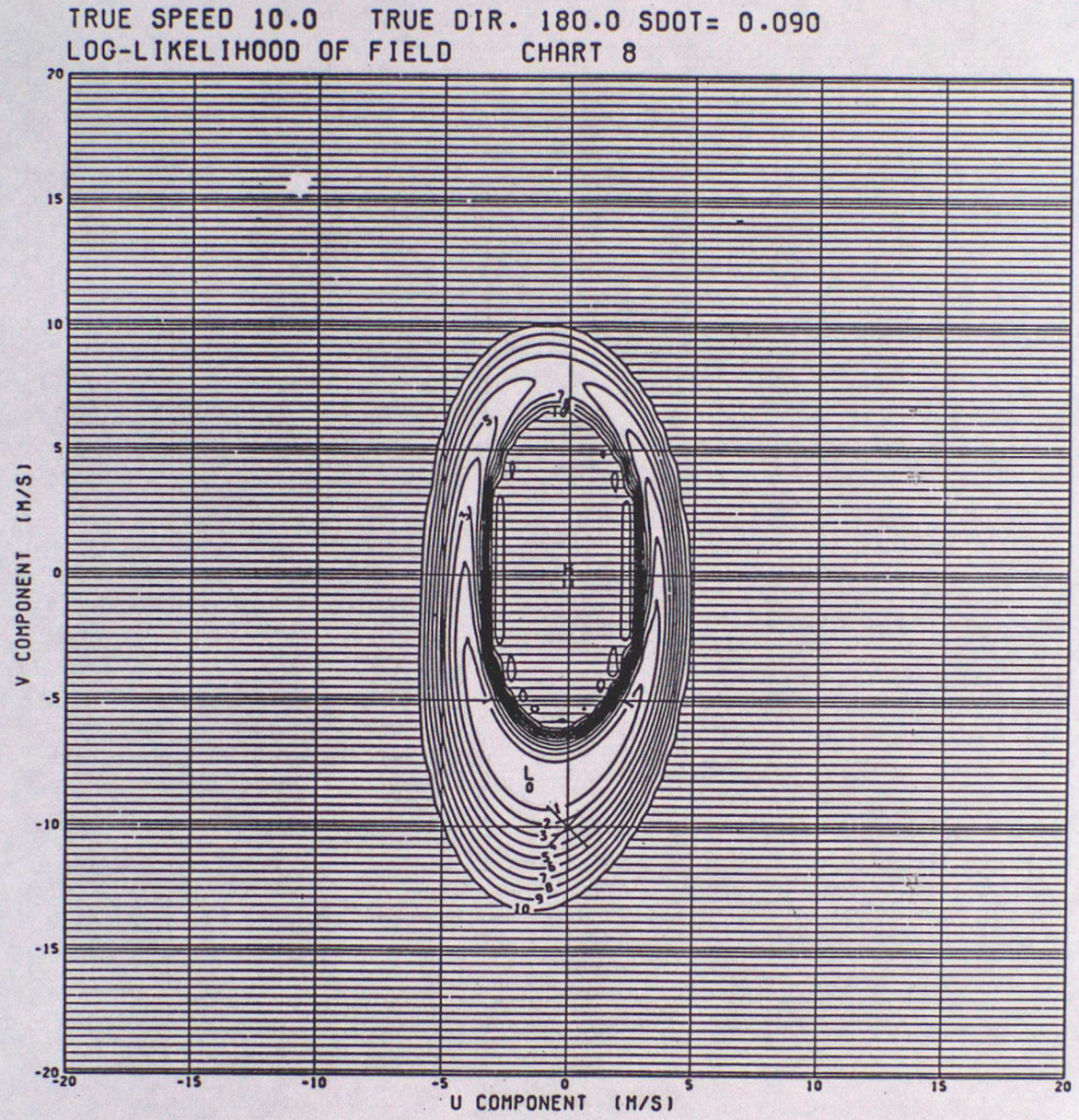
TRUE SPEED 10.0 TRUE DIR. 180.0 SDOT= 0.090
LOG-LIKELIHOOD OF FIELD CHART 8
V COMPONENT (M/S)
U COMPONENT (M/S)
20
15
10
5
0
-5
-10
-15
-20

FIGURE 6.8

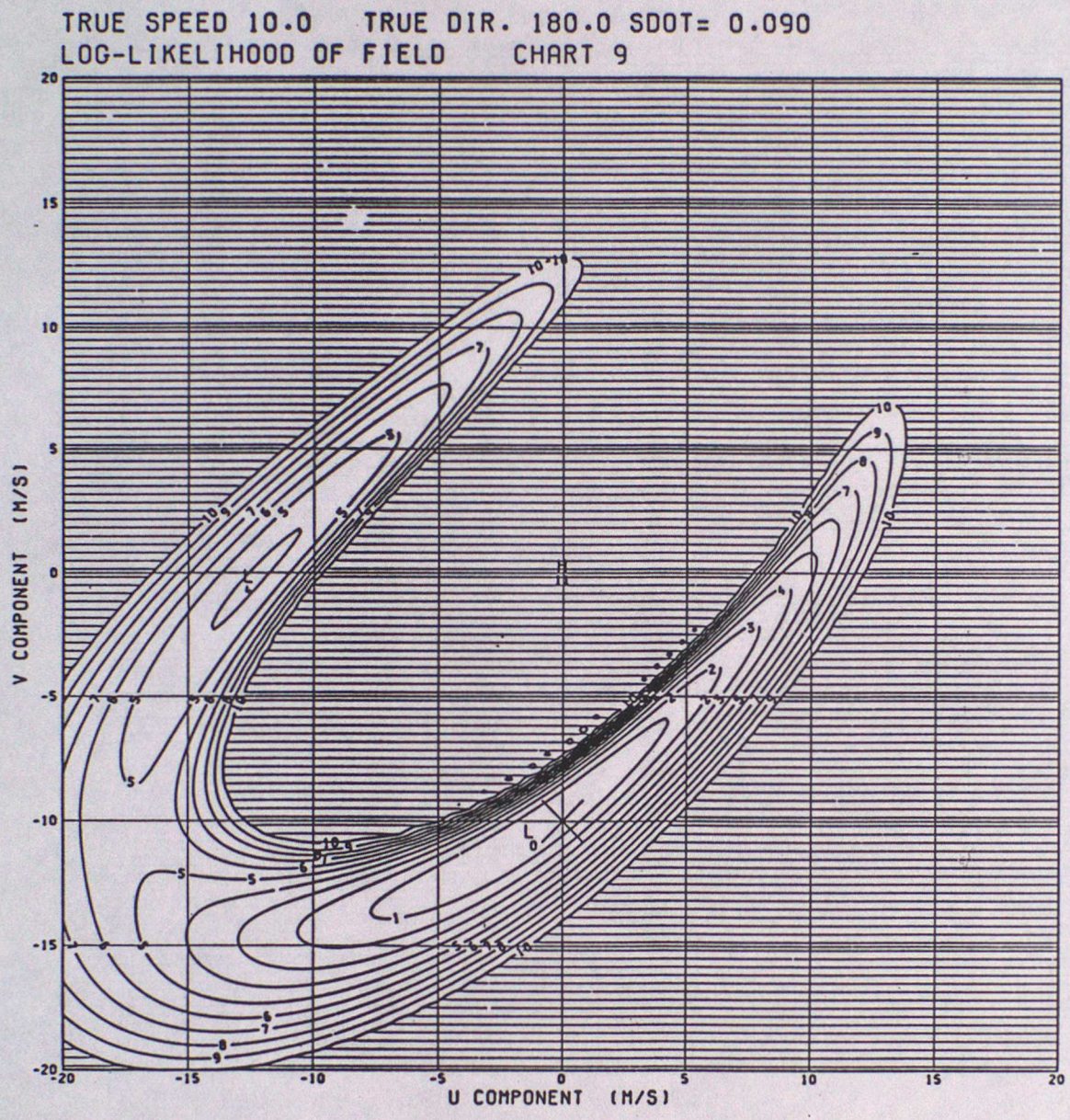
TRUE SPEED 10.0 TRUE DIR. 180.0 SDOT= 0.090
LOG-LIKELIHOOD OF FIELD CHART 9
V COMPONENT (M/S)
U COMPONENT (M/S)
20
15
10
5
0
-5
-10
-15
-20

FIGURE 6-9

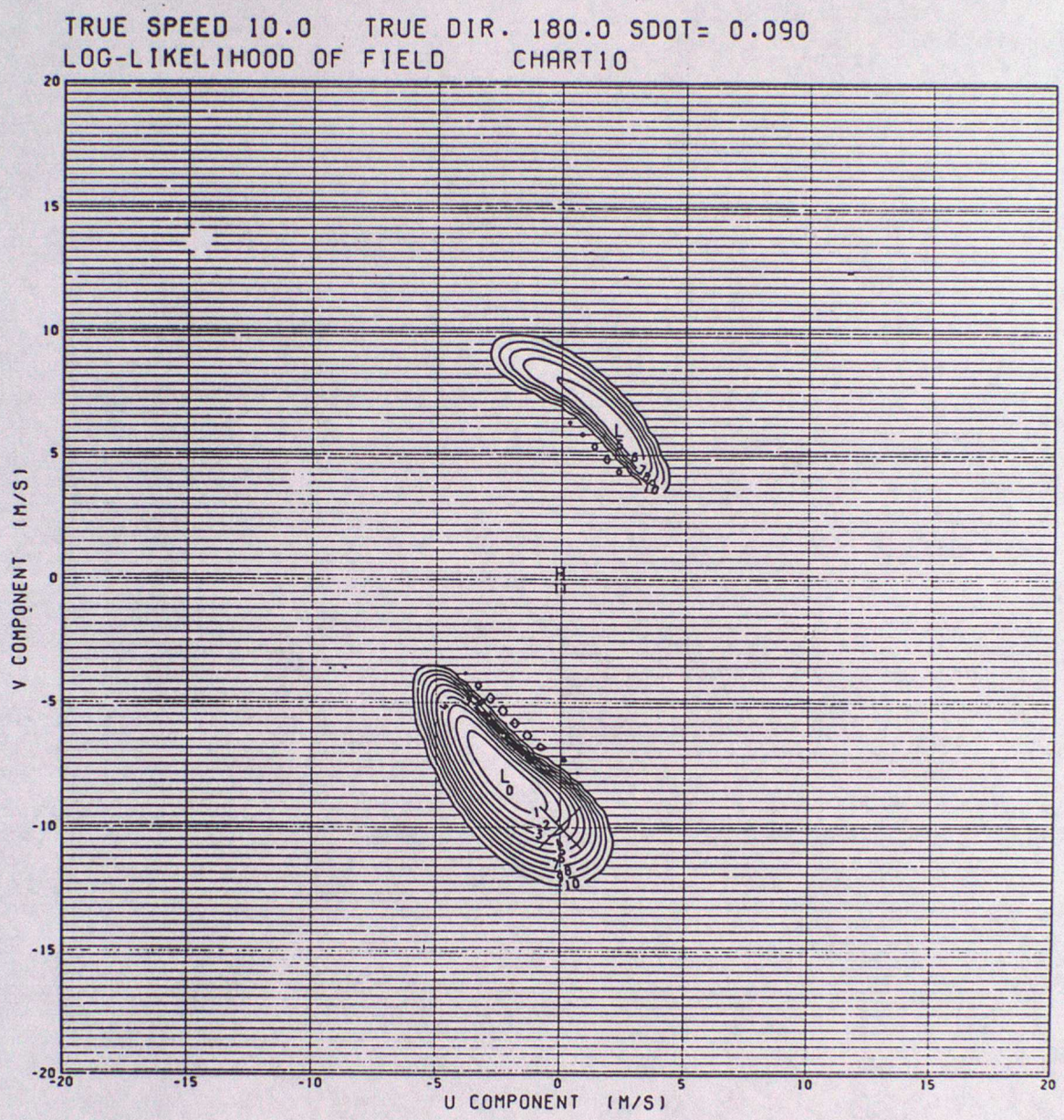
TRUE SPEED 10.0 TRUE DIR. 180.0 SDOT= 0.090
LOG-LIKELIHOOD OF FIELD CHART10
V COMPONENT (M/S)
U COMPONENT (M/S)
20
15
10
5
0
-5
-10
-15
-20
-20
-15
-10
-5
0
5
10
15
20

FIGURE 6-10

TRUE SPEED 10.0 TRUE DIR. 180.0 SDOT= 0.090
LOG-LIKELIHOOD OF FIELD CHART11

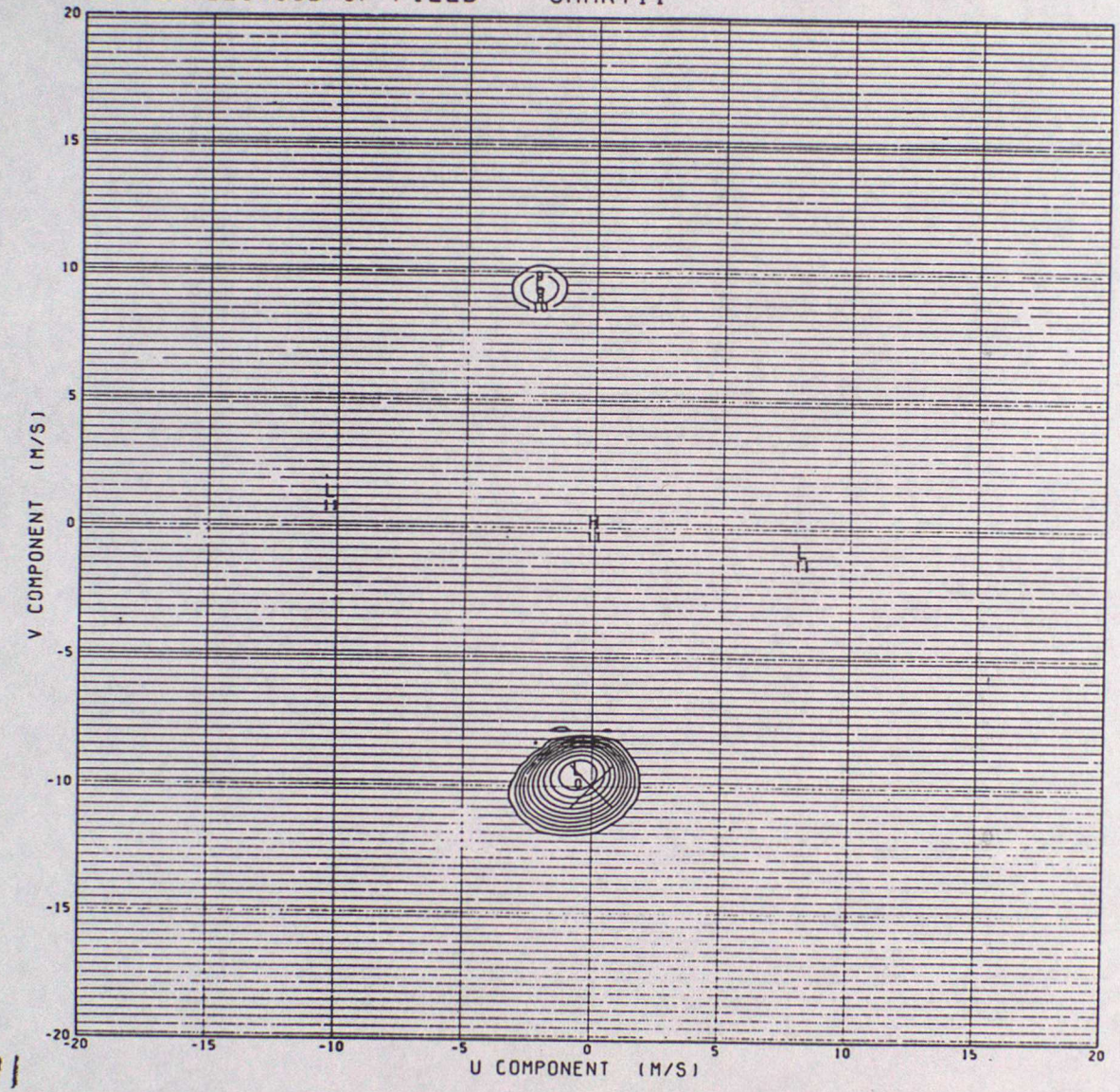

6-11

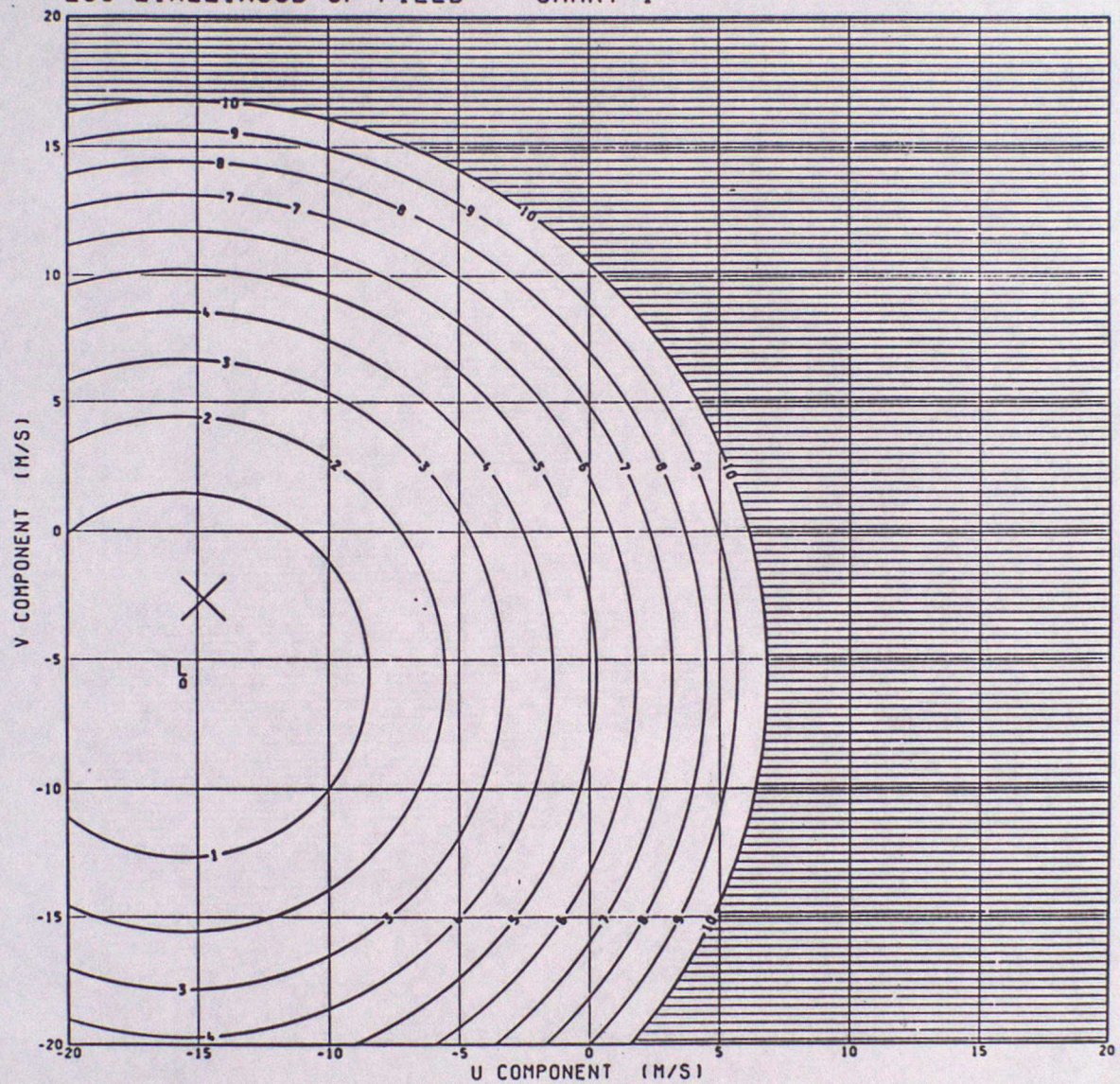
TRUE SPEED 15.0 TRUE DIR. 260.0 SDOT= 0.090
LOG-LIKELIHOOD OF FIELD CHART 1
V COMPONENT (M/S)
U COMPONENT (M/S)
20
15
10
5
0
-5
-10
-15
-20
-20
-15
-10
-5
0
5
10
15
20

Fig 7.1

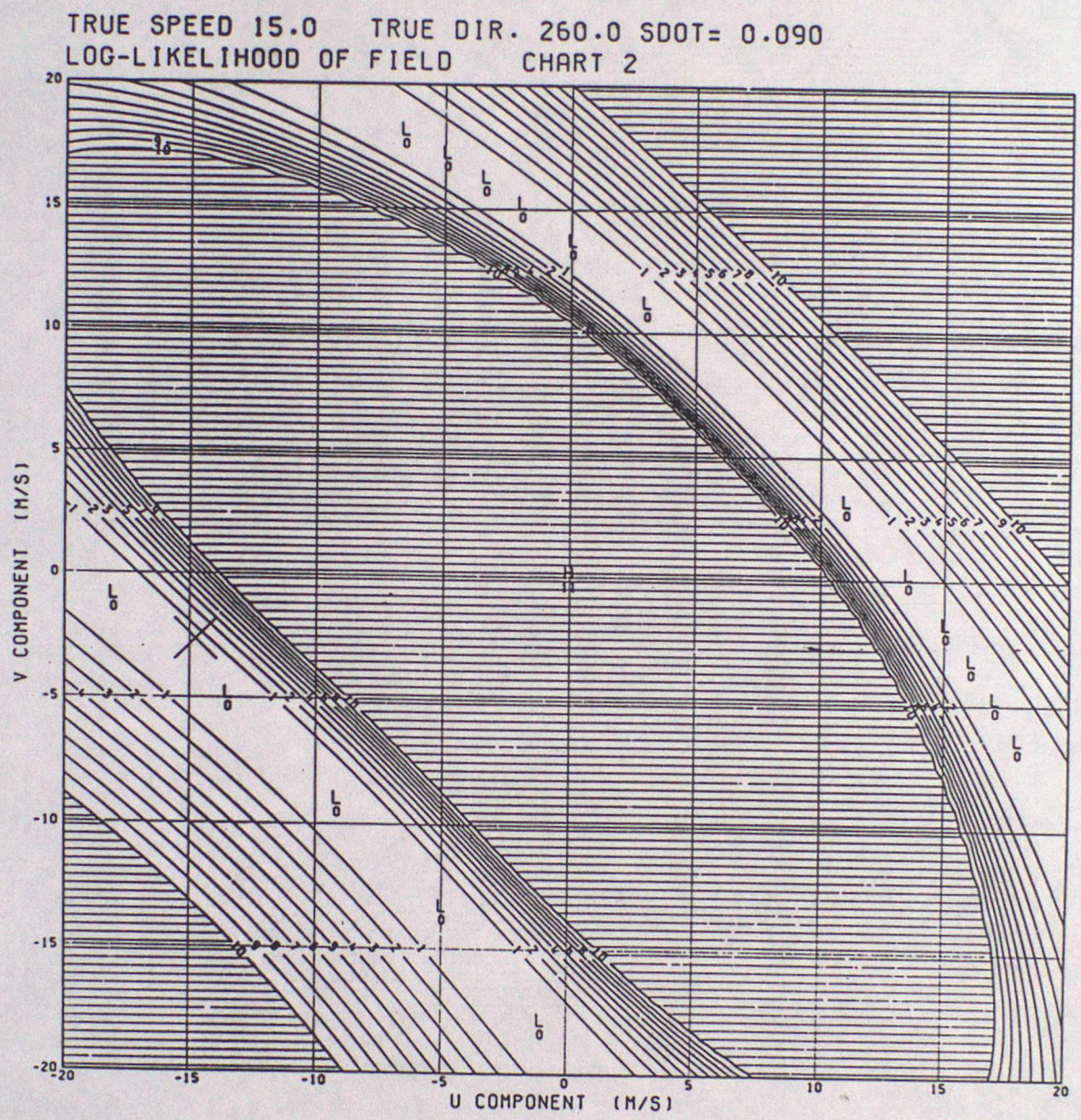
TRUE SPEED 15.0 TRUE DIR. 260.0 SDOT= 0.090
LOG-LIKELIHOOD OF FIELD CHART 2
V COMPONENT (M/S)
U COMPONENT (M/S)
20
15
10
5
0
-5
-10
-15
-20

FIGURE 7-2

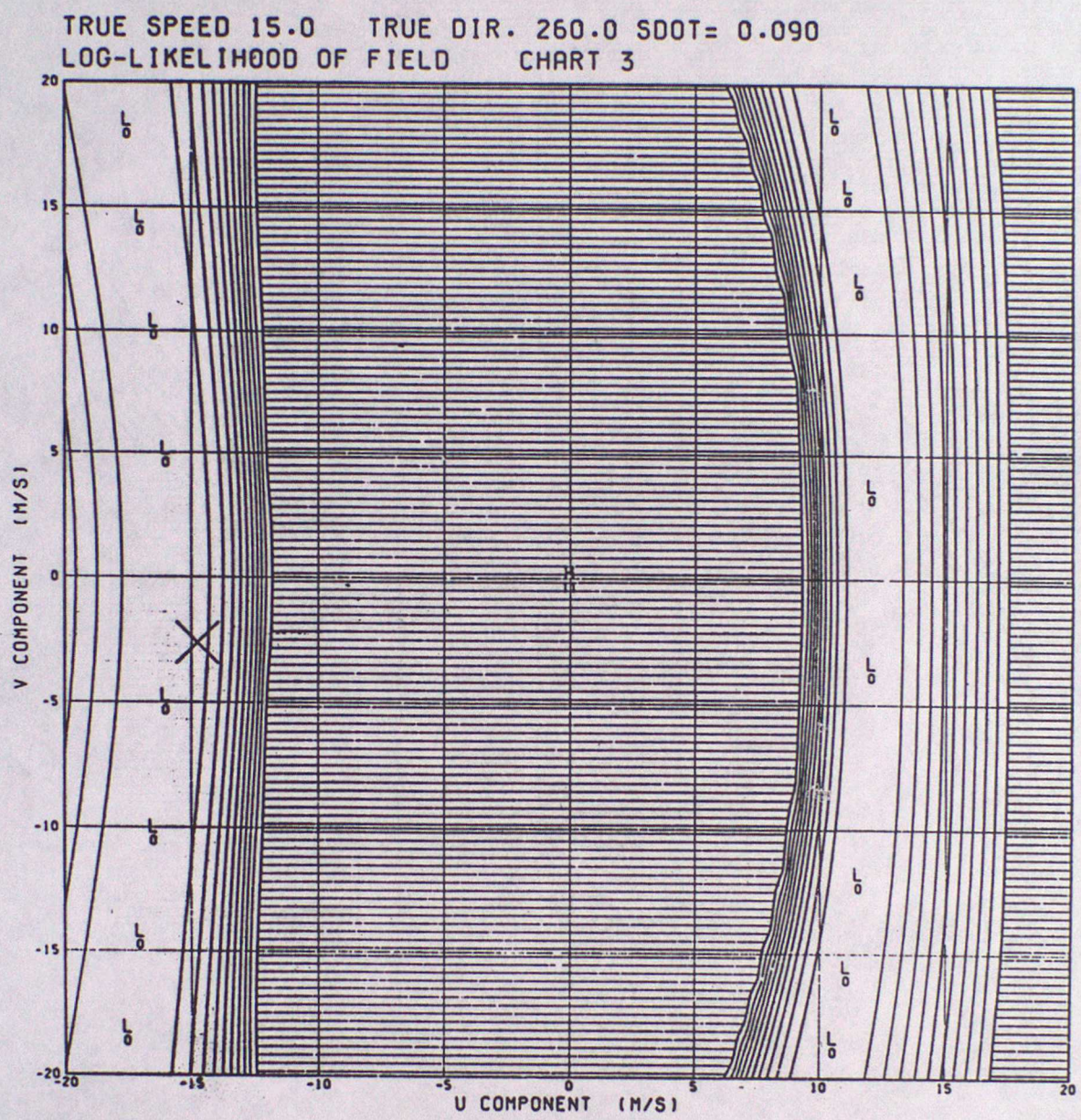
TRUE SPEED 15.0 TRUE DIR. 260.0 SDOT= 0.090
LOG-LIKELIHOOD OF FIELD CHART 3
V COMPONENT (M/S)
U COMPONENT (M/S)
20
15
10
5
0
-5
-10
-15
-20

FIGURE 7.3

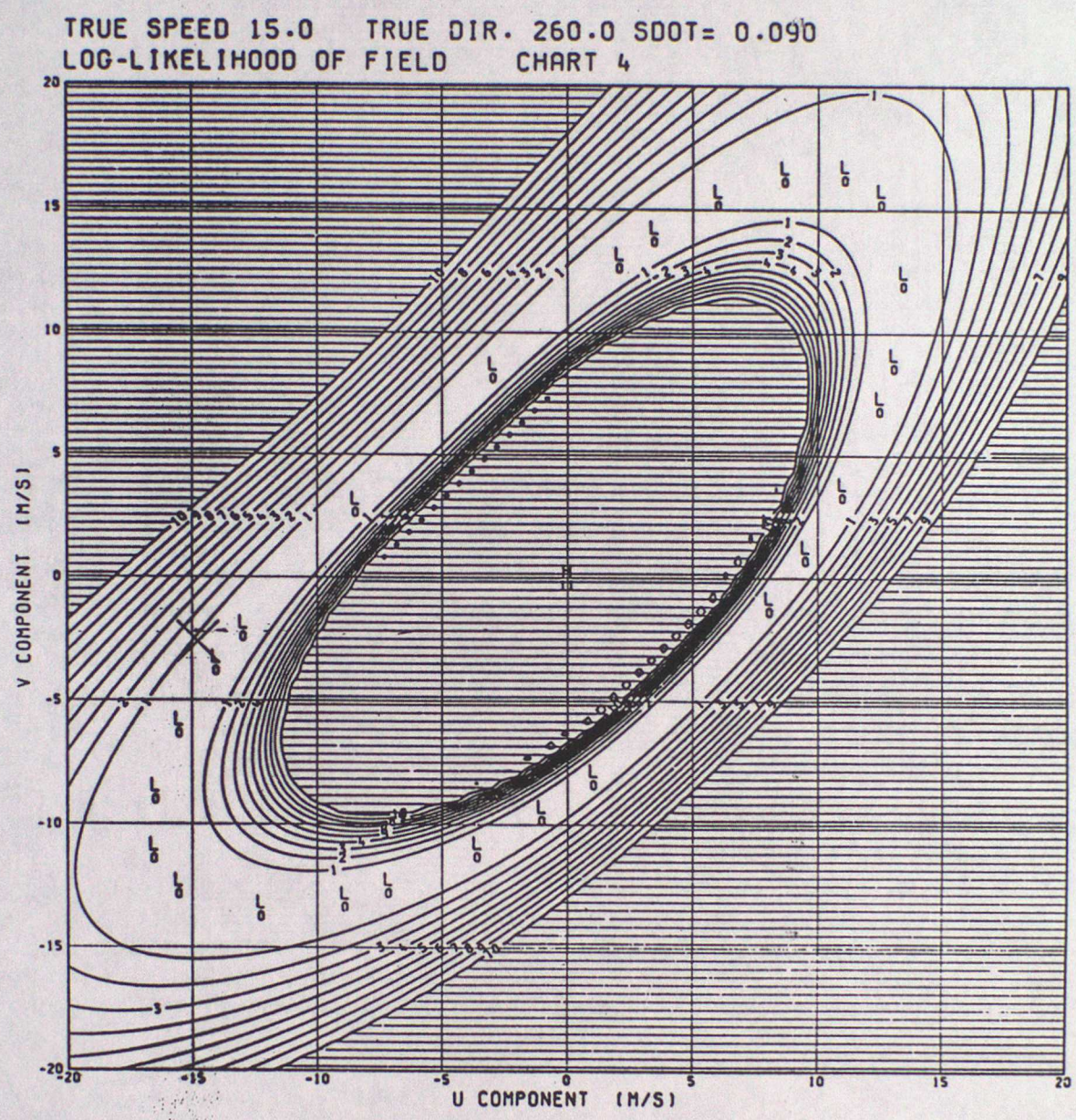
TRUE SPEED 15.0 TRUE DIR. 260.0 SDOT= 0.090
LOG-LIKELIHOOD OF FIELD CHART 4
V COMPONENT (M/S)
U COMPONENT (M/S)
20
15
10
5
0
-5
-10
-15
-20

FIGURE 7.4

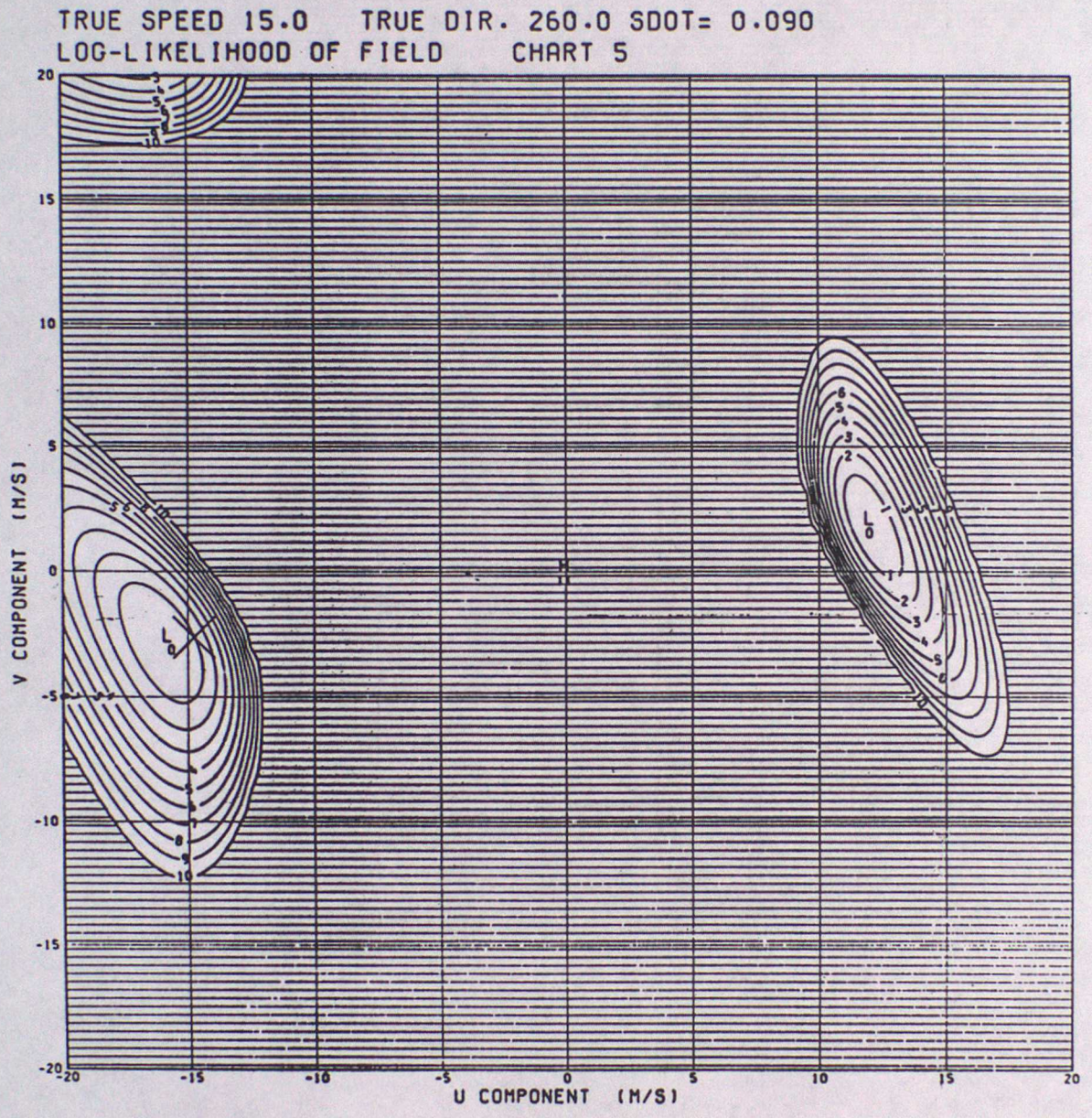
TRUE SPEED 15.0 TRUE DIR. 260.0 SDOT= 0.090
LOG-LIKELIHOOD OF FIELD CHART 5
V COMPONENT (M/S)
U COMPONENT (M/S)
20
15
10
5
0
-5
-10
-15
-20

FIGURE 7-5

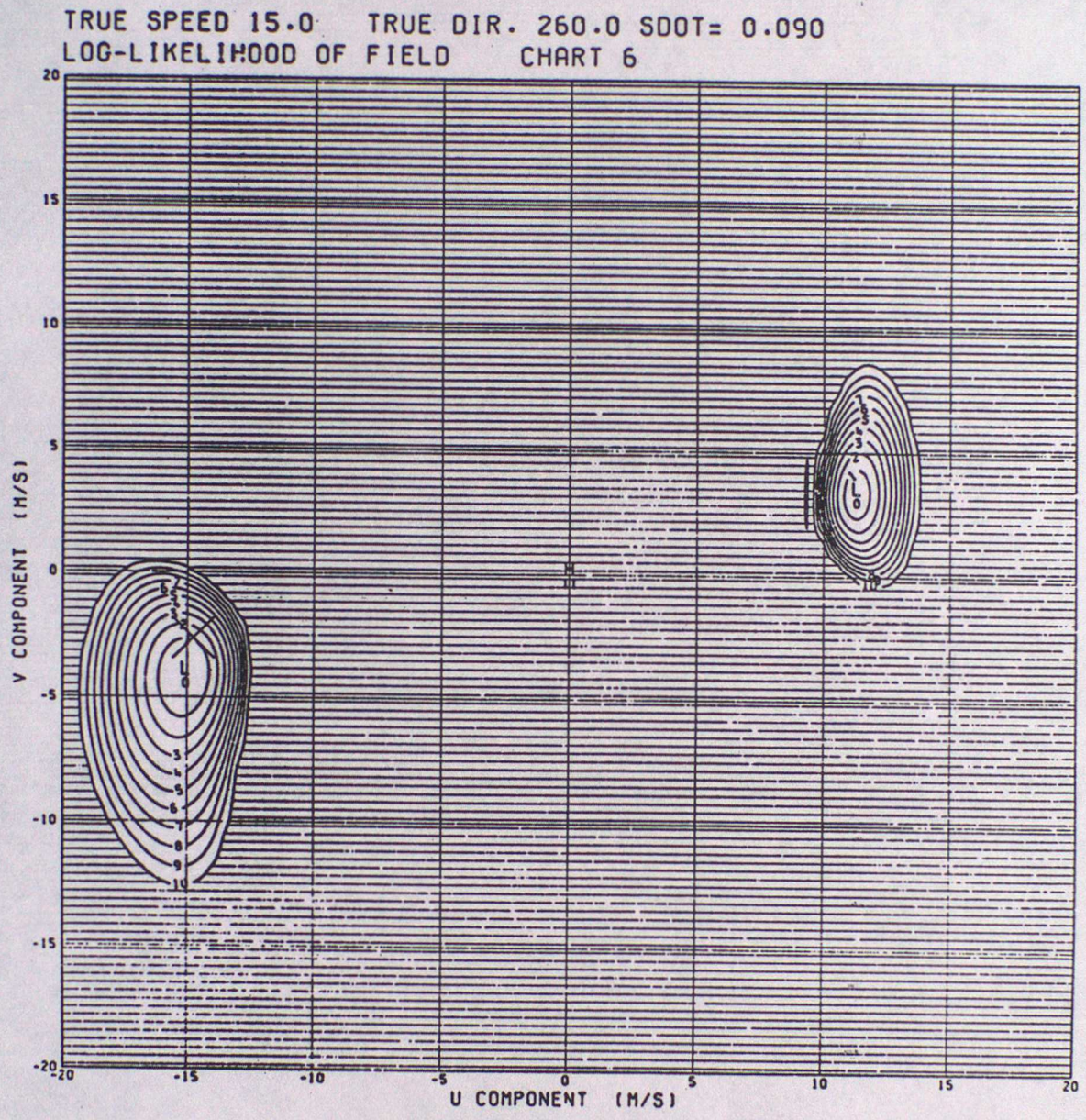
TRUE SPEED 15.0 TRUE DIR. 260.0 SDOT= 0.090
LOG-LIKELIHOOD OF FIELD CHART 6
V COMPONENT (M/S)
U COMPONENT (M/S)
20
15
10
5
0
-5
-10
-15
-20

FIGURE 7.6

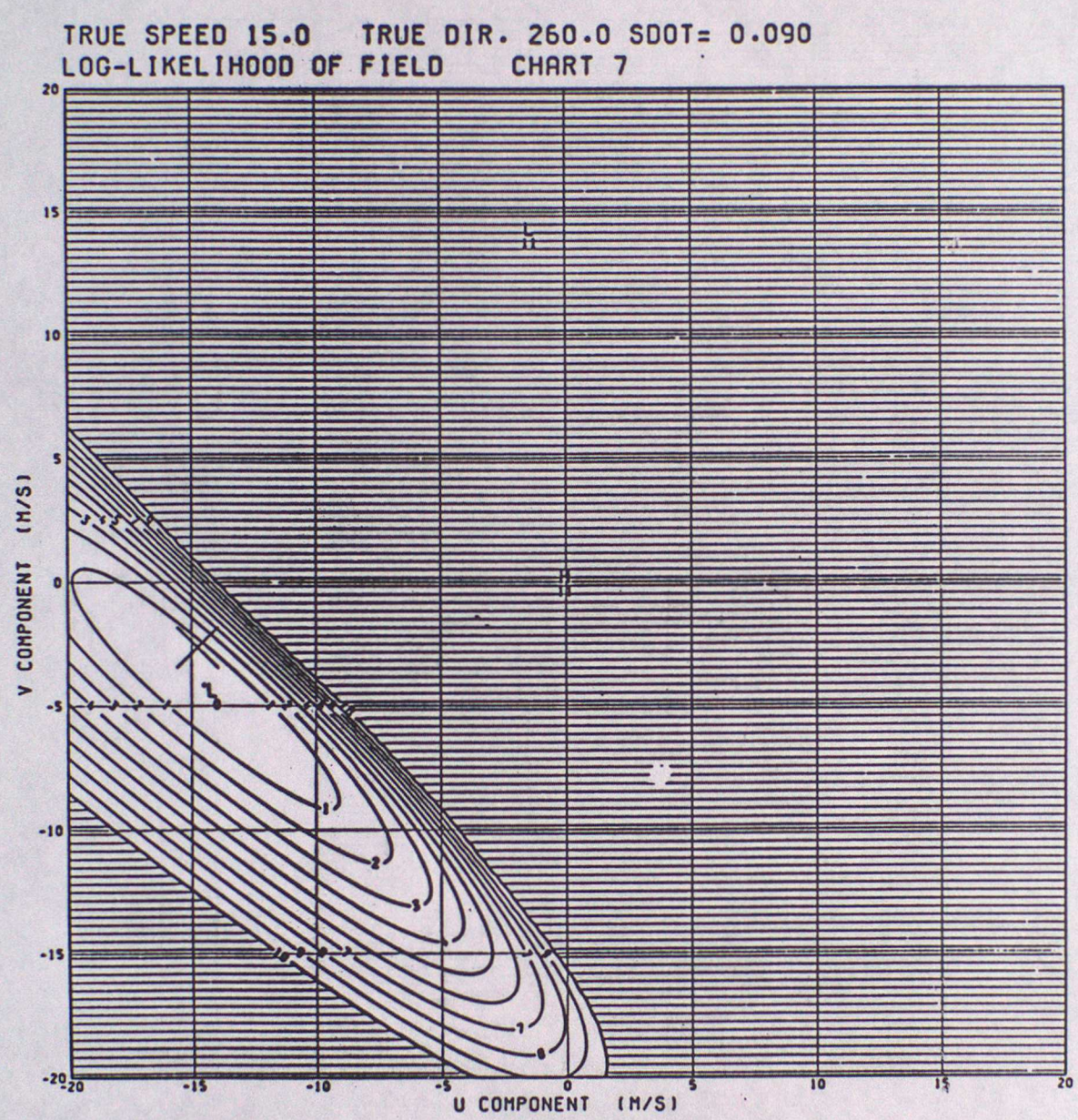
TRUE SPEED 15.0 TRUE DIR. 260.0 SDOT= 0.090
LOG-LIKELIHOOD OF FIELD CHART 7
V COMPONENT (M/S)
U COMPONENT (M/S)
20
15
10
5
0
-5
-10
-15
-20
-20
-15
-10
-5
0
5
10
15
20

FIGURE 7.7

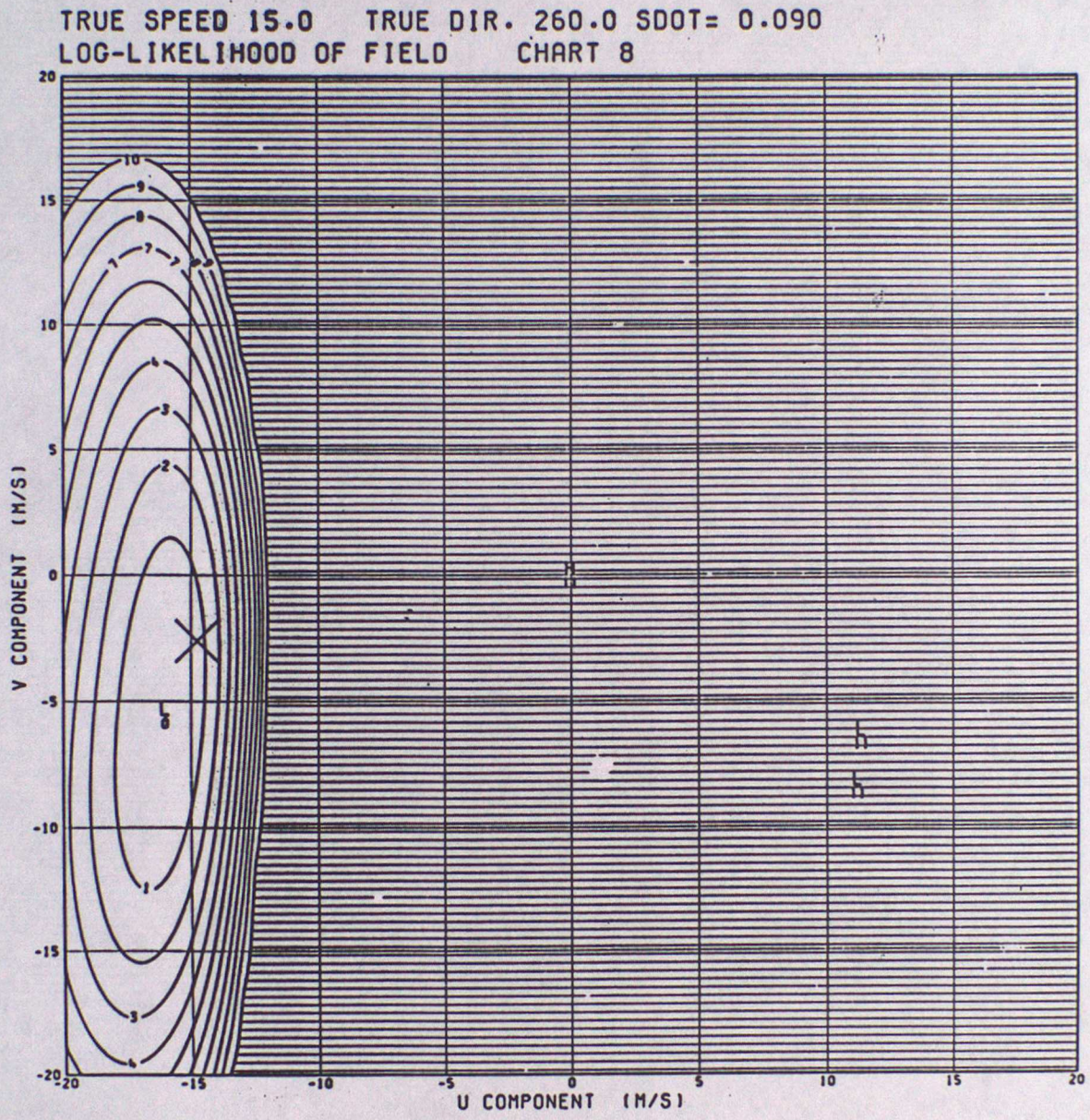
TRUE SPEED 15.0 TRUE DIR. 260.0 SDOT= 0.090
LOG-LIKELIHOOD OF FIELD CHART 8
V COMPONENT (M/S)
U COMPONENT (M/S)
20
15
10
5
0
-5
-10
-15
-20
10
9
8
7
6
5
4
3
2
1
1
2
3
4

FIGURE 7.8

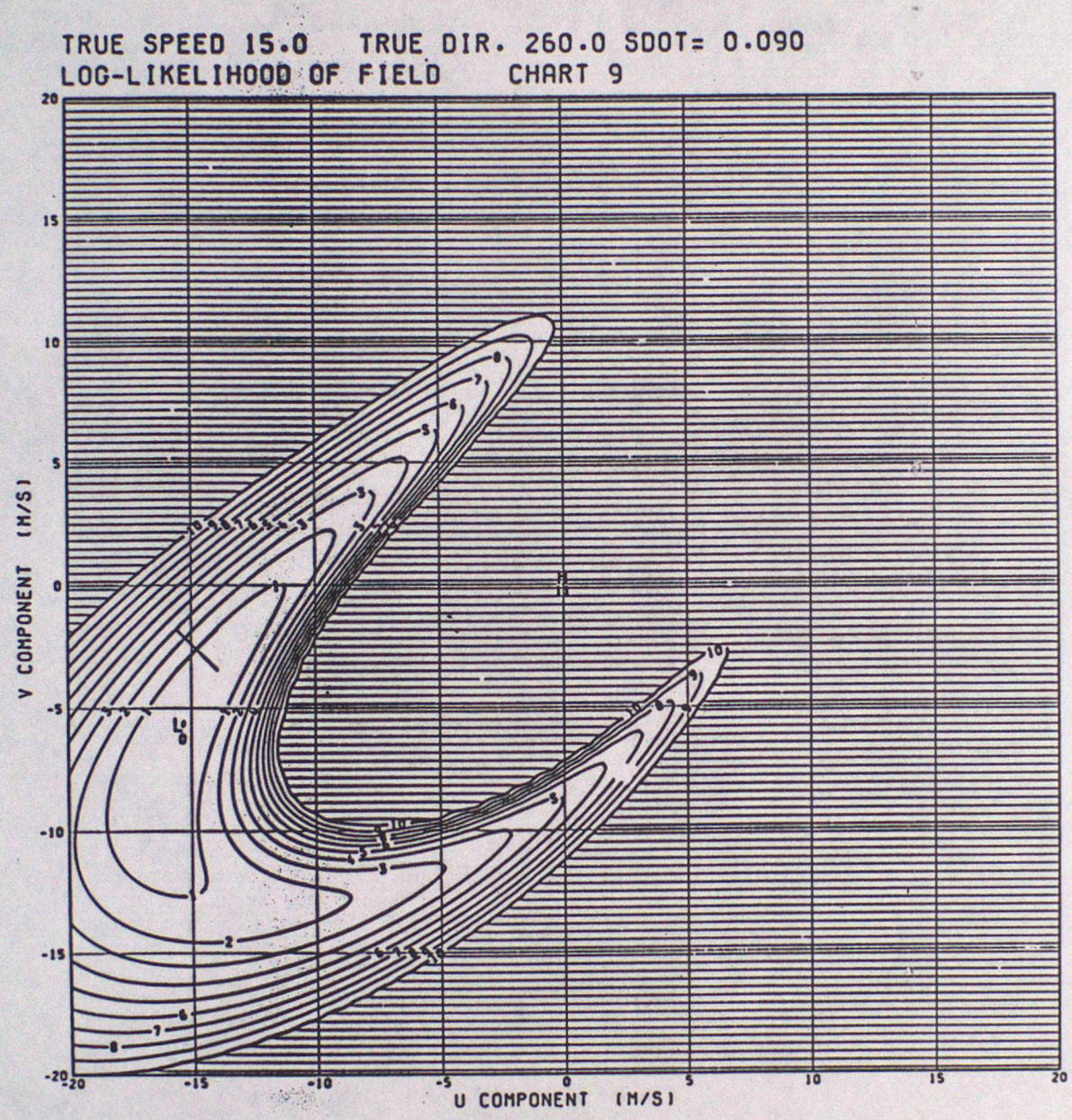
TRUE SPEED 15.0 TRUE DIR. 260.0 SDOT= 0.090
LOG-LIKELIHOOD OF FIELD CHART 9
V COMPONENT (M/S)
U COMPONENT (M/S)
20
15
10
5
0
-5
-10
-15
-20

FIGURE 7.9

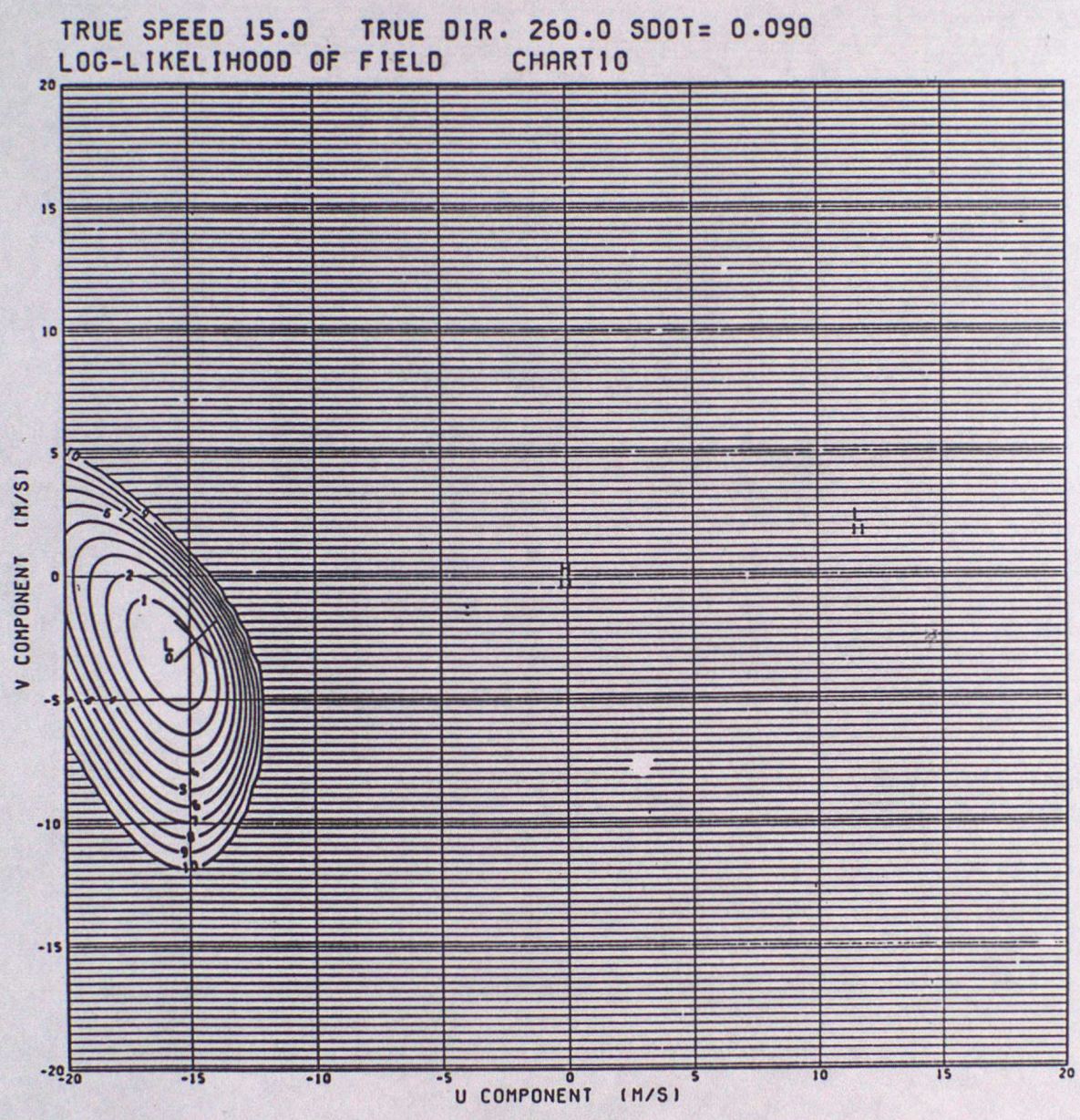
TRUE SPEED 15.0 TRUE DIR. 260.0 SDOT= 0.090
LOG-LIKELIHOOD OF FIELD CHART10
V COMPONENT (M/S)
U COMPONENT (M/S)
20
15
10
5
0
-5
-10
-15
-20

FIGURE 7.10

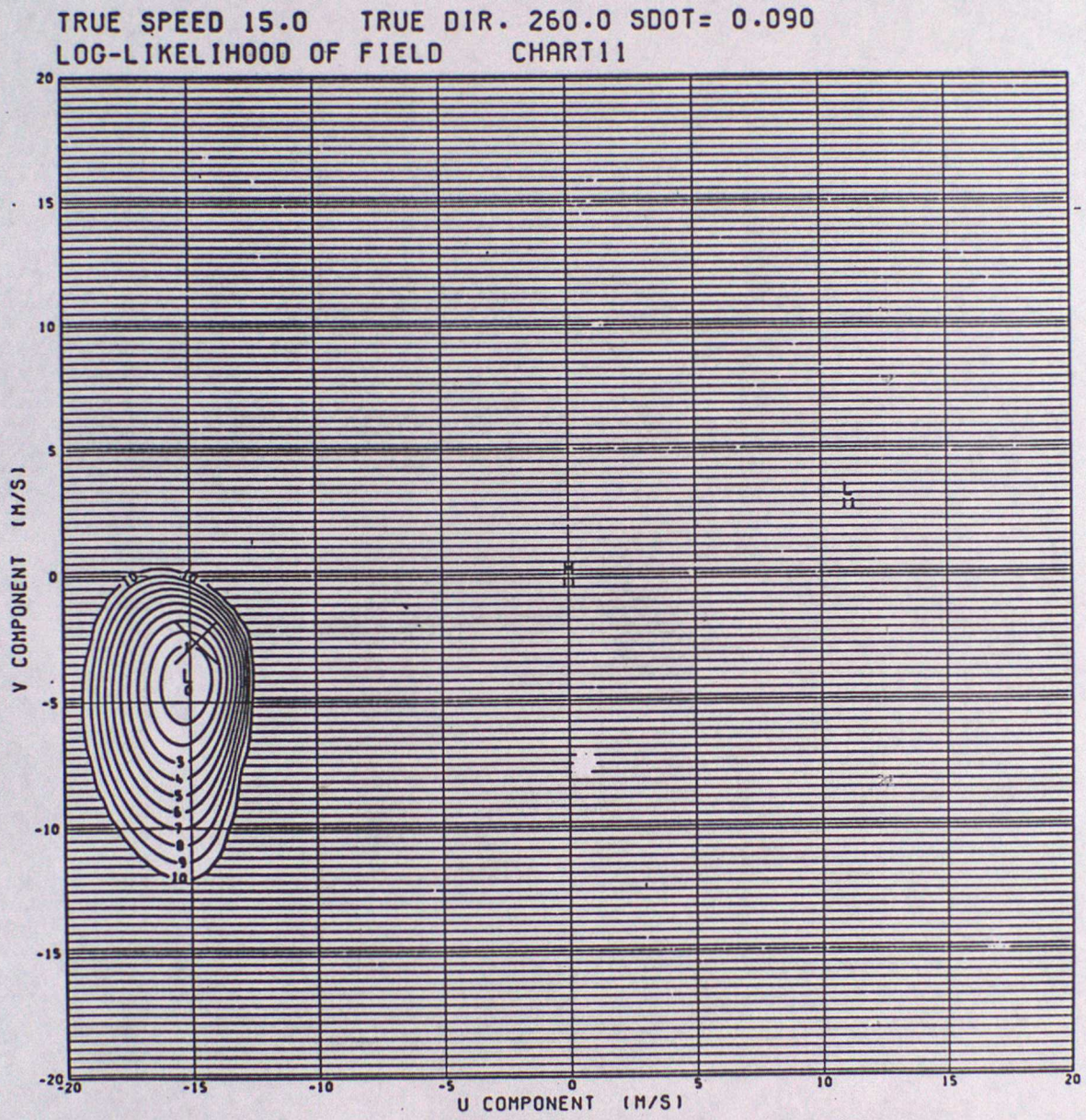
TRUE SPEED 15.0 TRUE DIR. 260.0 SDOT= 0.090
LOG-LIKELIHOOD OF FIELD CHART11
V COMPONENT (M/S)
U COMPONENT (M/S)
20
15
10
5
0
-5
-10
-15
-20

FIGURE 7.11

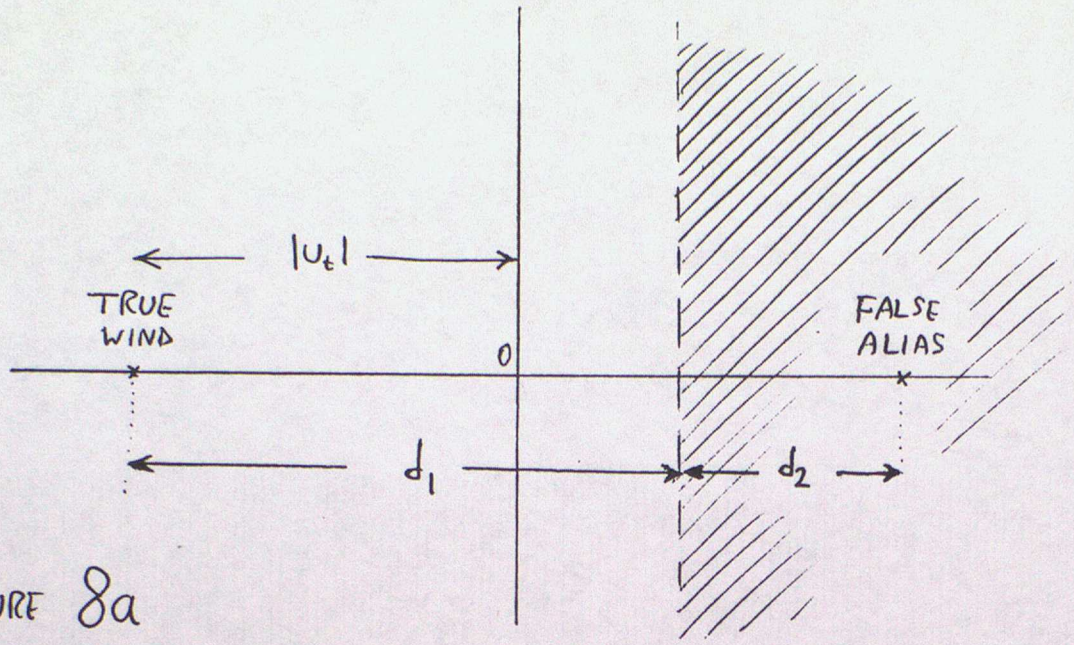

FIGURE 8a

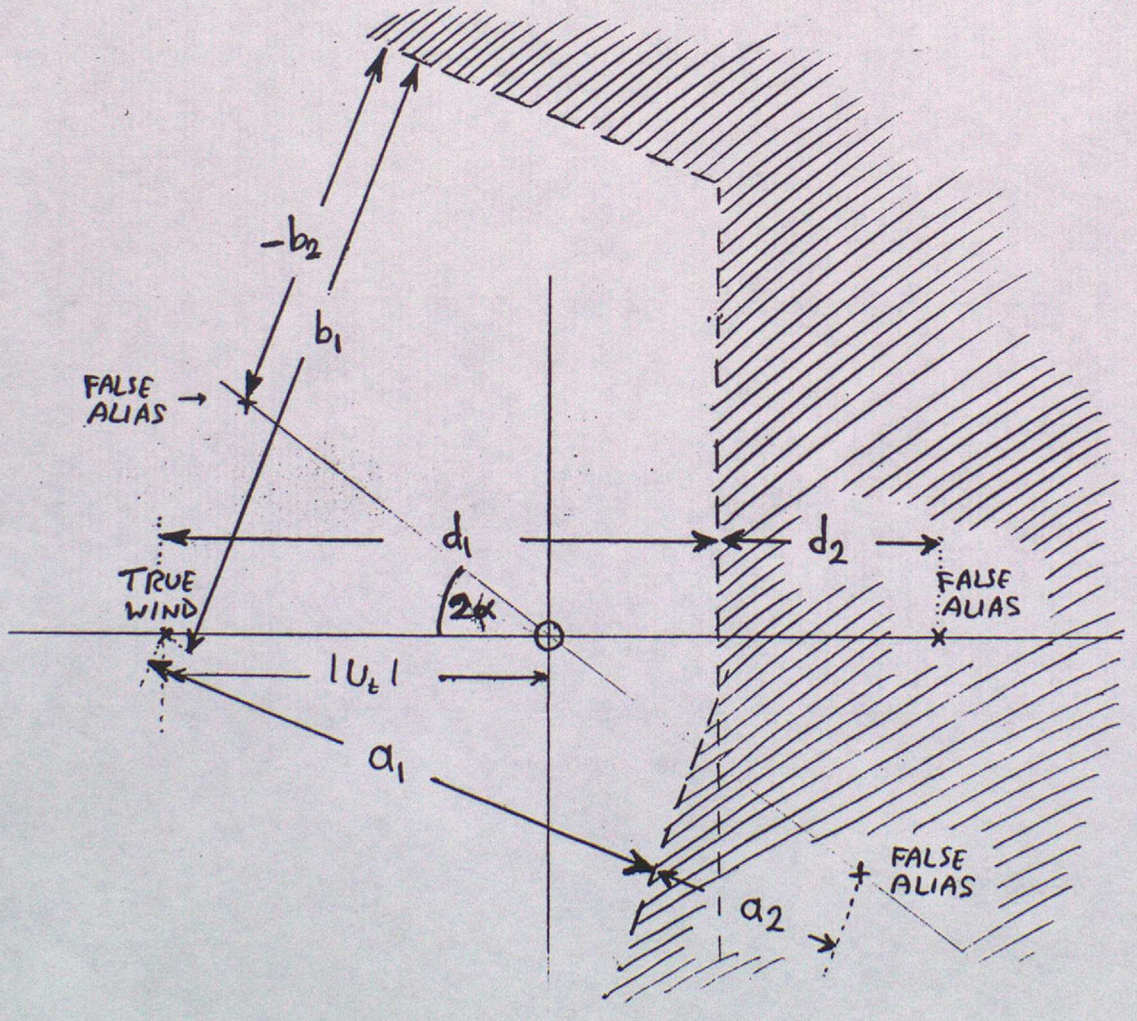

FIGURE 8b

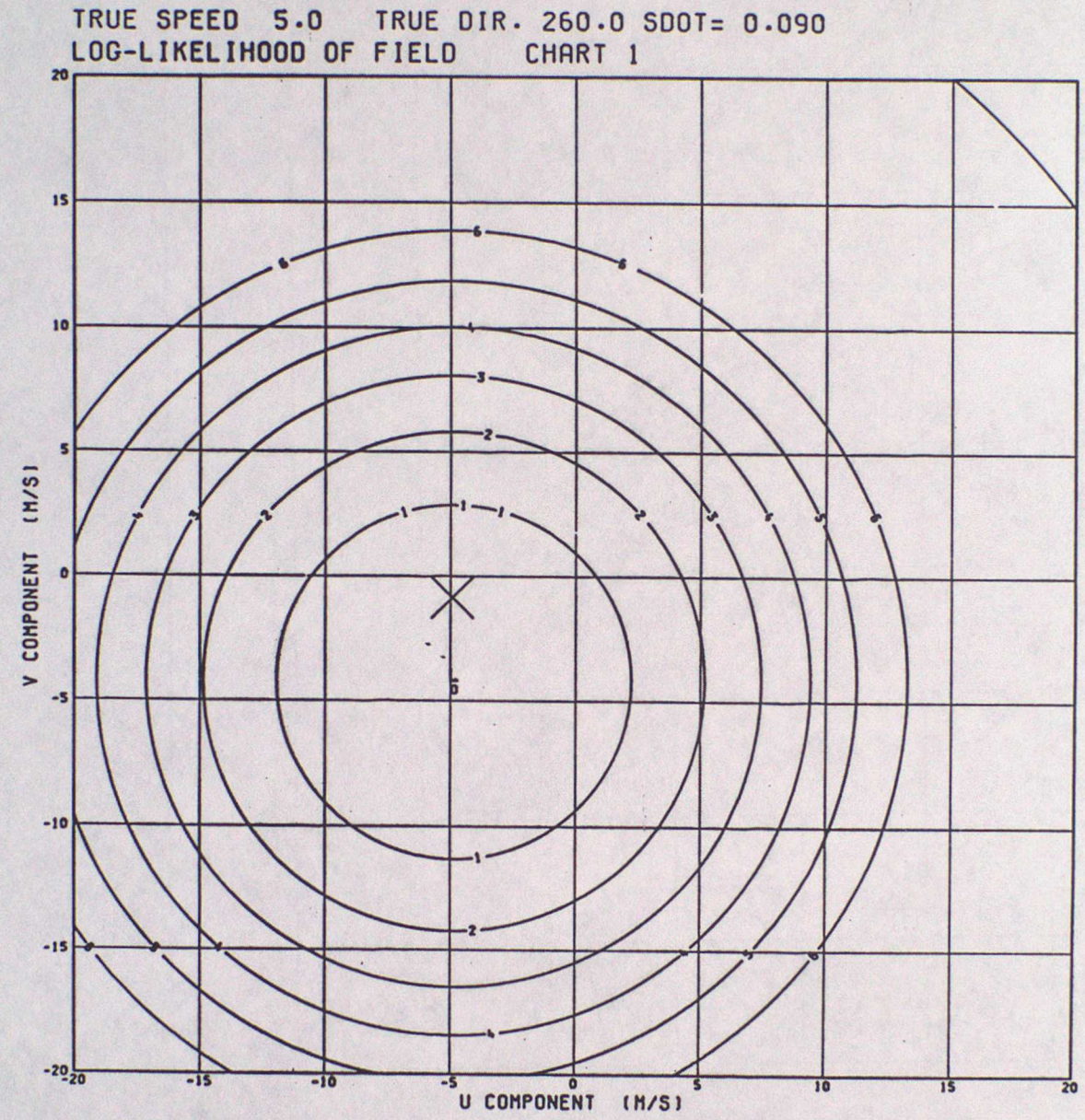
TRUE SPEED 5.0 TRUE DIR. 260.0 SDOT= 0.090
LOG-LIKELIHOOD OF FIELD CHART 1
V COMPONENT (M/S)
U COMPONENT (M/S)
20
15
10
5
0
-5
-10
-15
-20

FIGURE 9.1

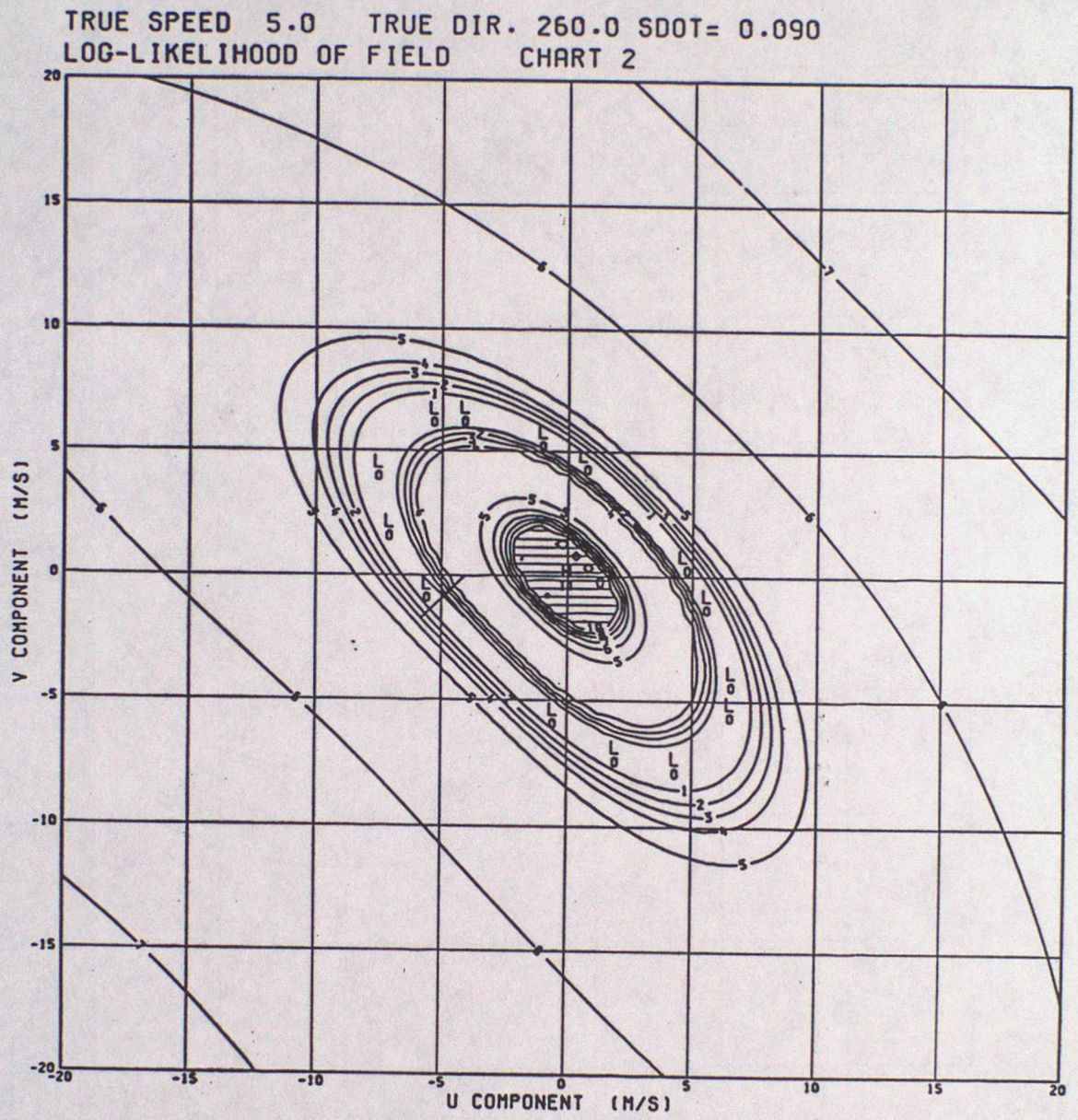
TRUE SPEED 5.0 TRUE DIR. 260.0 SDOT= 0.090
LOG-LIKELIHOOD OF FIELD CHART 2
V COMPONENT (M/S)
U COMPONENT (M/S)
20
15
10
5
0
-5
-10
-15
-20

FIGURE 9.2

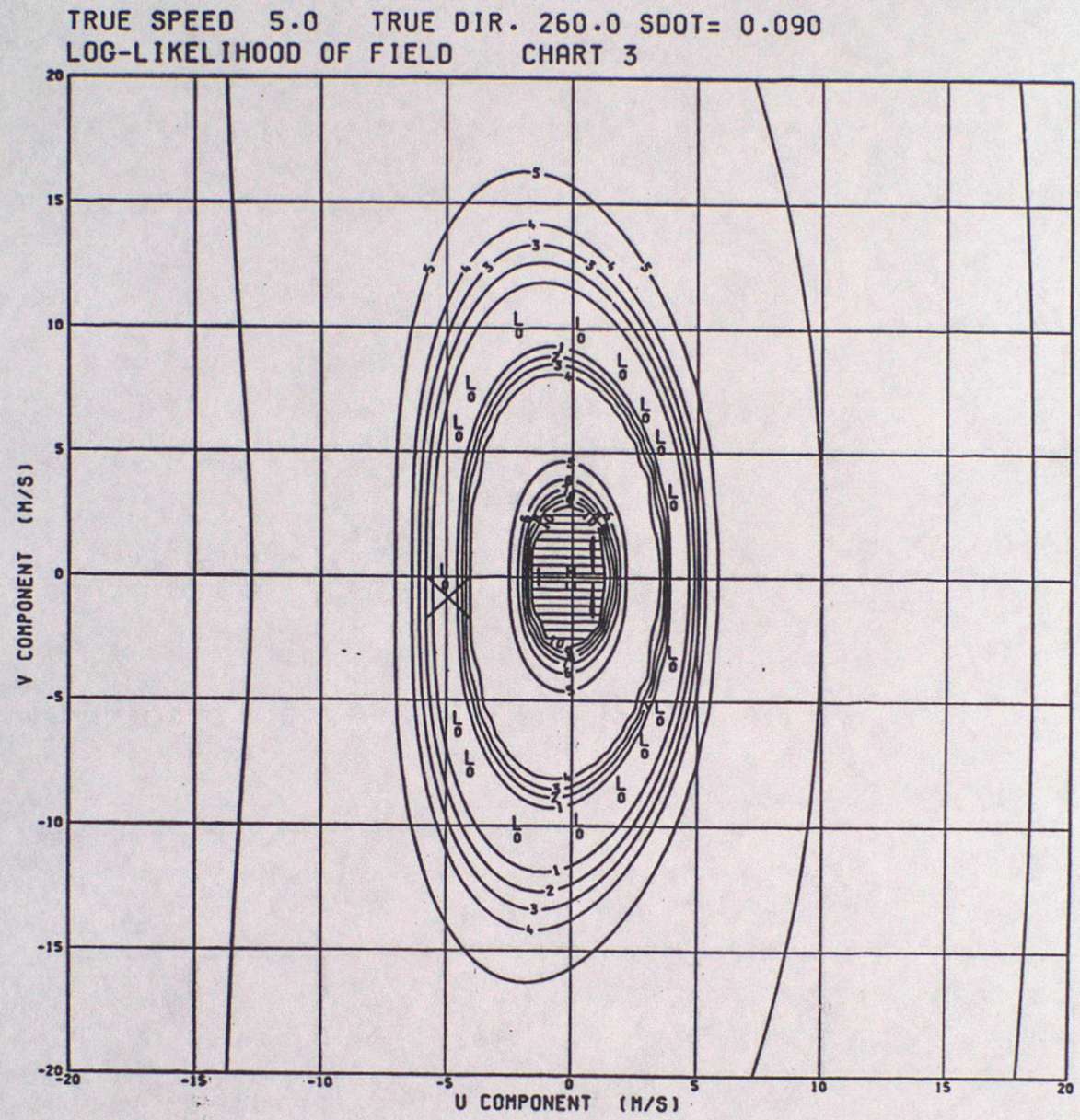
TRUE SPEED 5.0 TRUE DIR. 260.0 SDOT= 0.090
LOG-LIKELIHOOD OF FIELD CHART 3
V COMPONENT (M/S)
U COMPONENT (M/S)
20
15
10
5
0
-5
-10
-15
-20

FIGURE 9.3

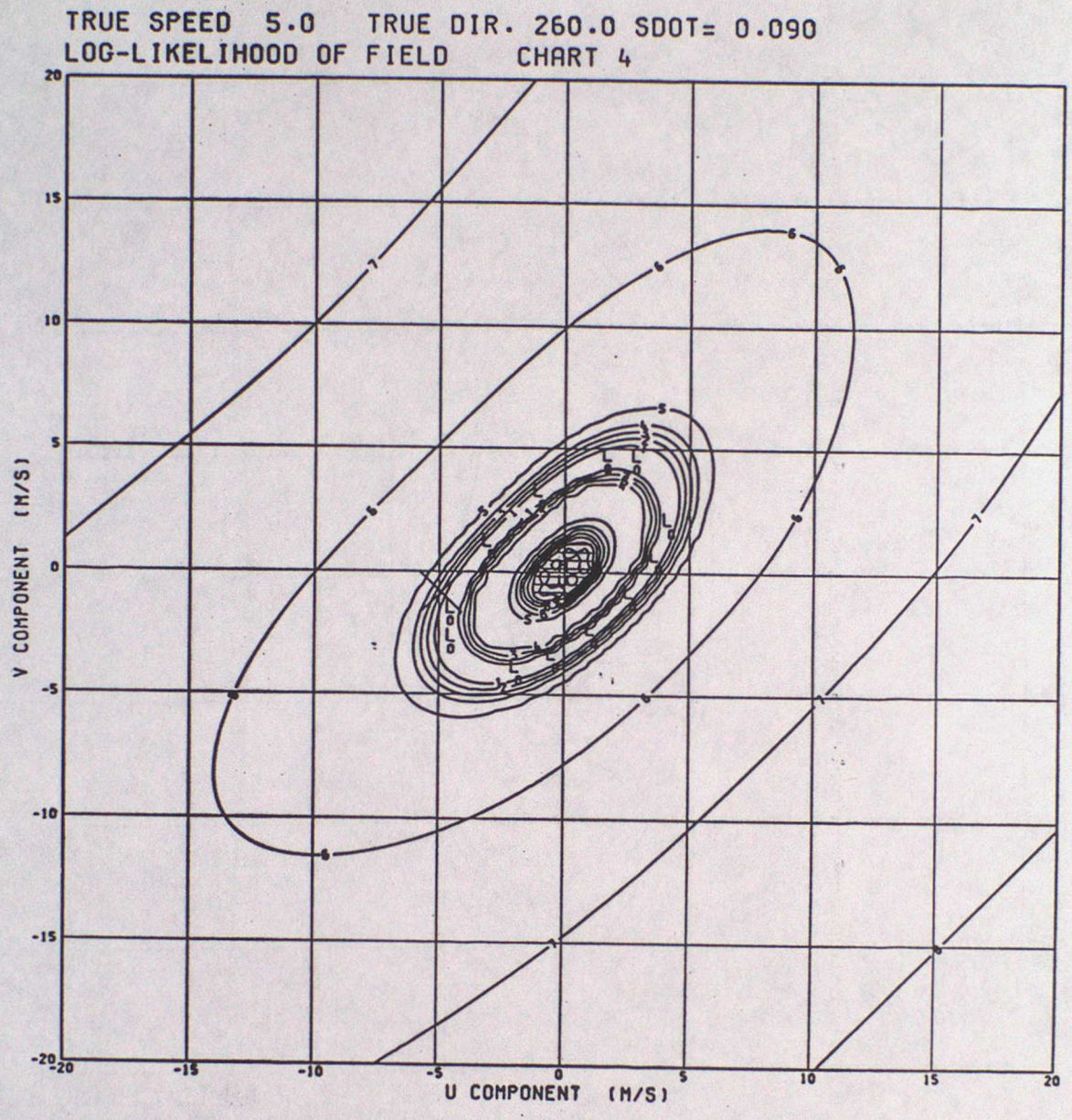
TRUE SPEED 5.0 TRUE DIR. 260.0 SDOT= 0.090
LOG-LIKELIHOOD OF FIELD CHART 4
V COMPONENT (M/S)
U COMPONENT (M/S)
20
15
10
5
0
-5
-10
-15
-20
-20
-15
-10
-5
0
5
10
15
20

FIGURE 9.4

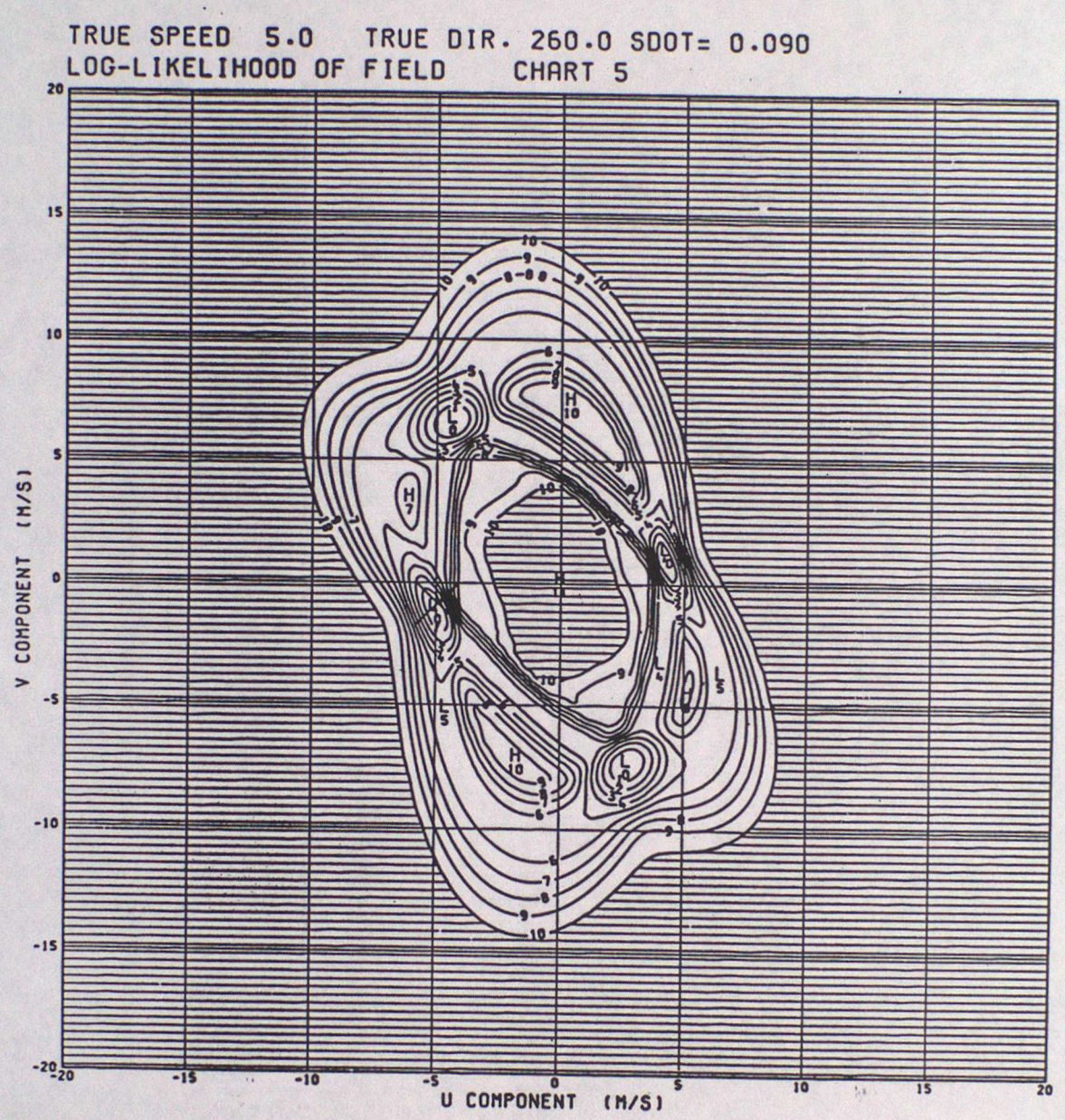
TRUE SPEED 5.0 TRUE DIR. 260.0 SDOT= 0.090
LOG-LIKELIHOOD OF FIELD CHART 5
V COMPONENT (M/S)
U COMPONENT (M/S)
20
15
10
5
0
-5
-10
-15
-20

FIGURE 9.5

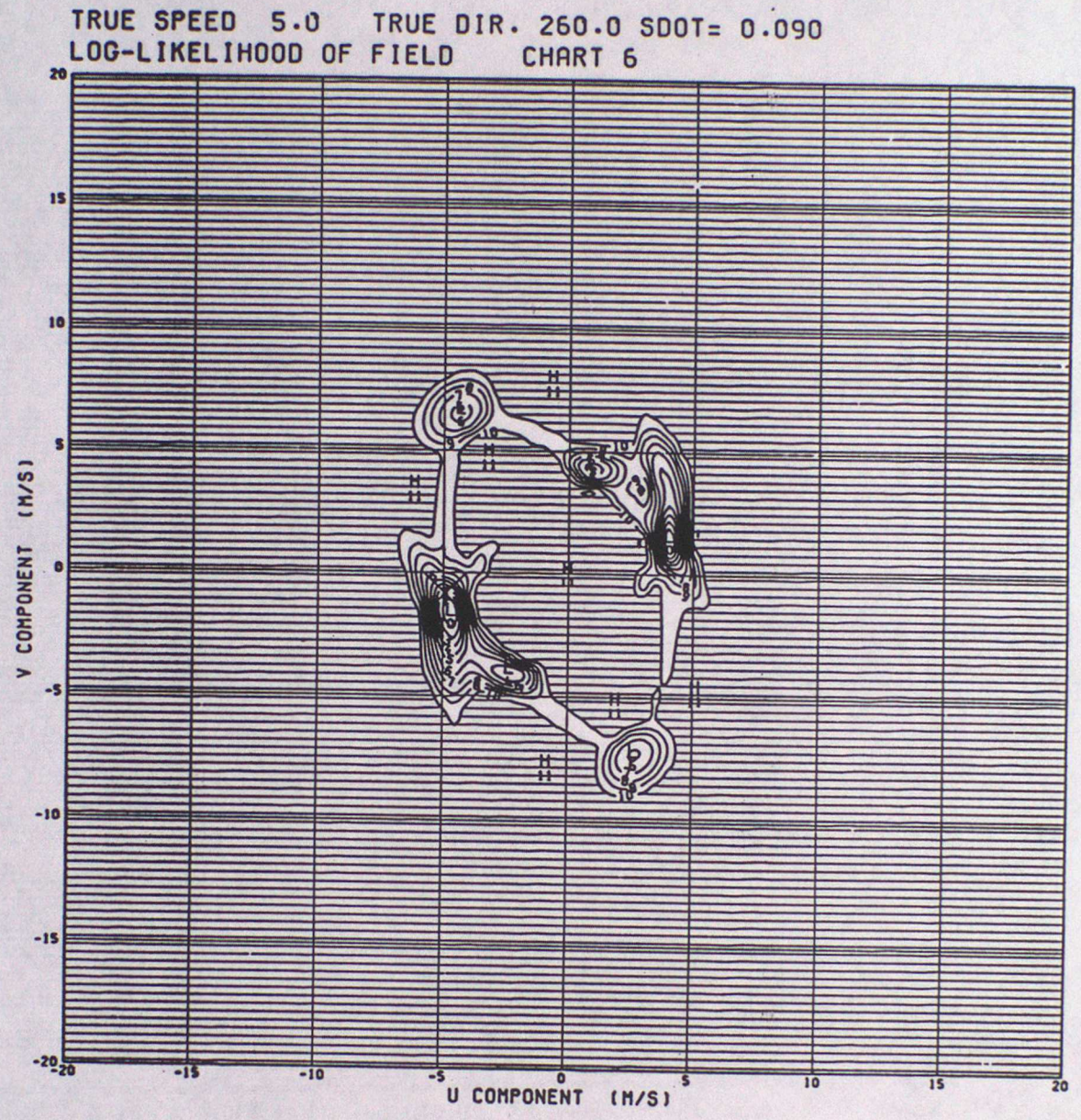
TRUE SPEED 5.0 TRUE DIR. 260.0 SDOT= 0.090
LOG-LIKELIHOOD OF FIELD CHART 6
V COMPONENT (M/S)
U COMPONENT (M/S)
20
15
10
5
0
-5
-10
-15
-20

FIGURE 9.6

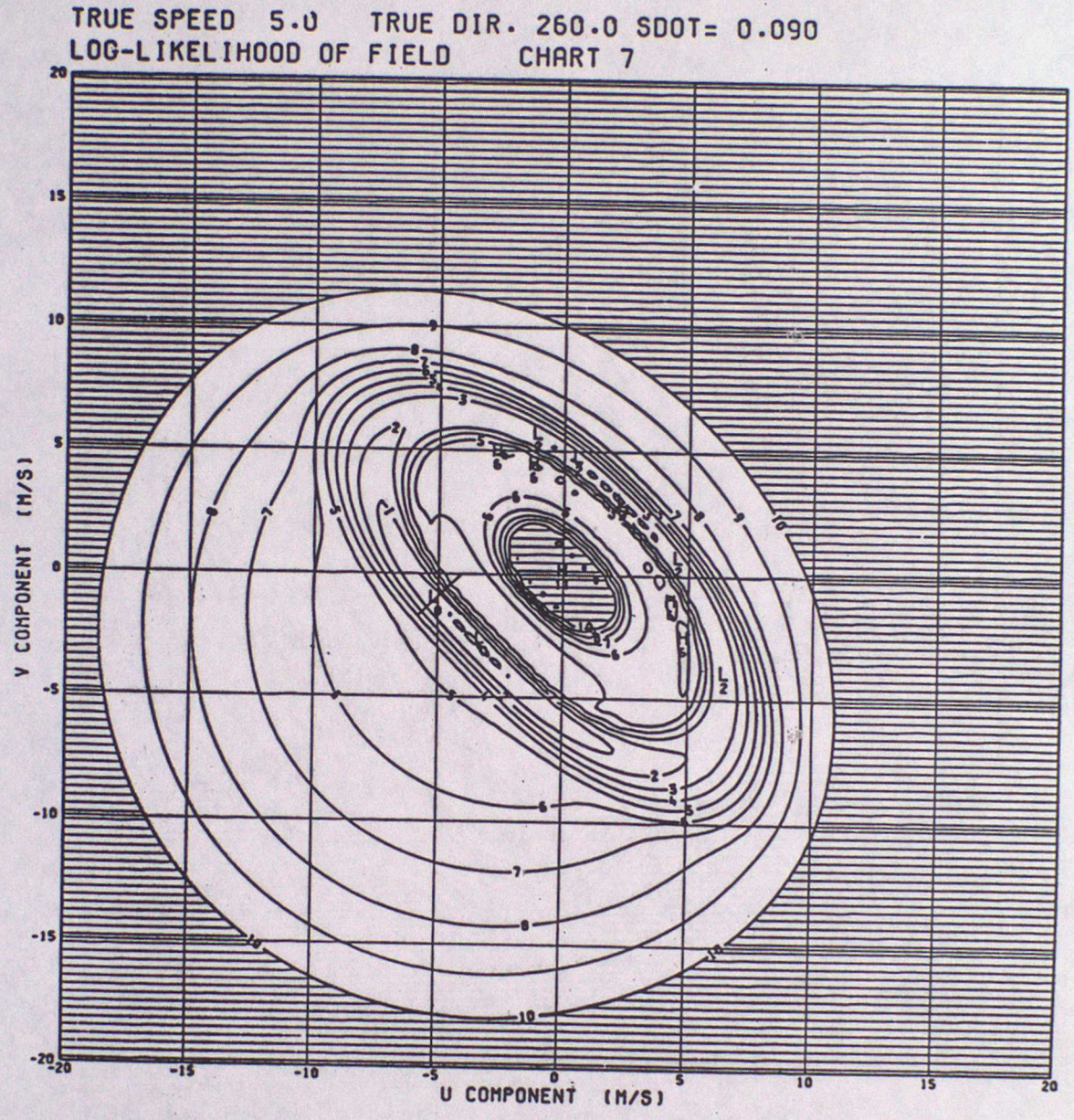
TRUE SPEED 5.0 TRUE DIR. 260.0 SDOT= 0.090
LOG-LIKELIHOOD OF FIELD CHART 7
V COMPONENT (M/S)
U COMPONENT (M/S)
20
15
10
5
0
-5
-10
-15
-20

FIGURE 9.7

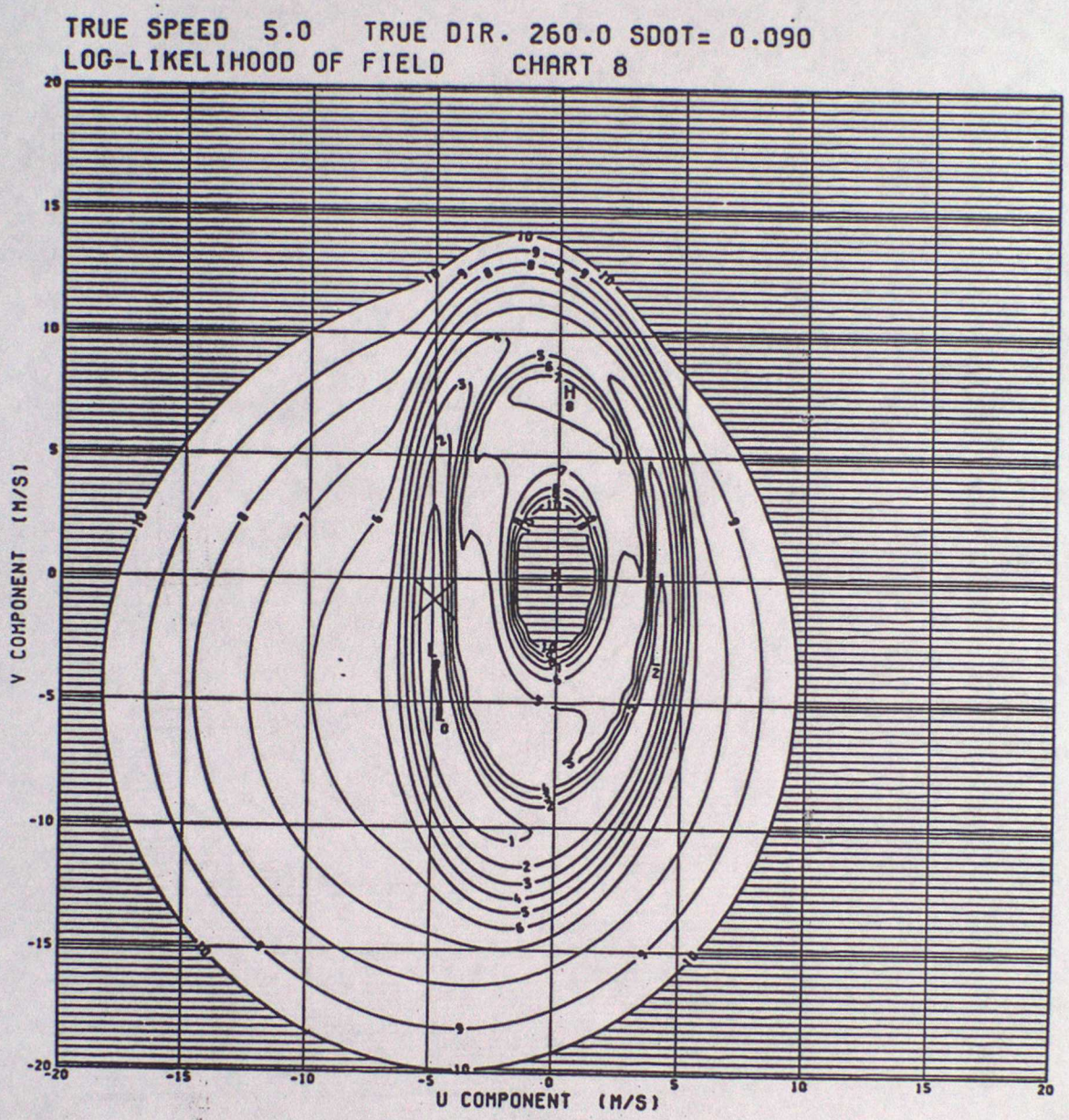
TRUE SPEED 5.0 TRUE DIR. 260.0 SDOT= 0.090
LOG-LIKELIHOOD OF FIELD CHART 8
V COMPONENT (M/S)
U COMPONENT (M/S)
20
15
10
5
0
-5
-10
-15
-20

FIGURE 9.8

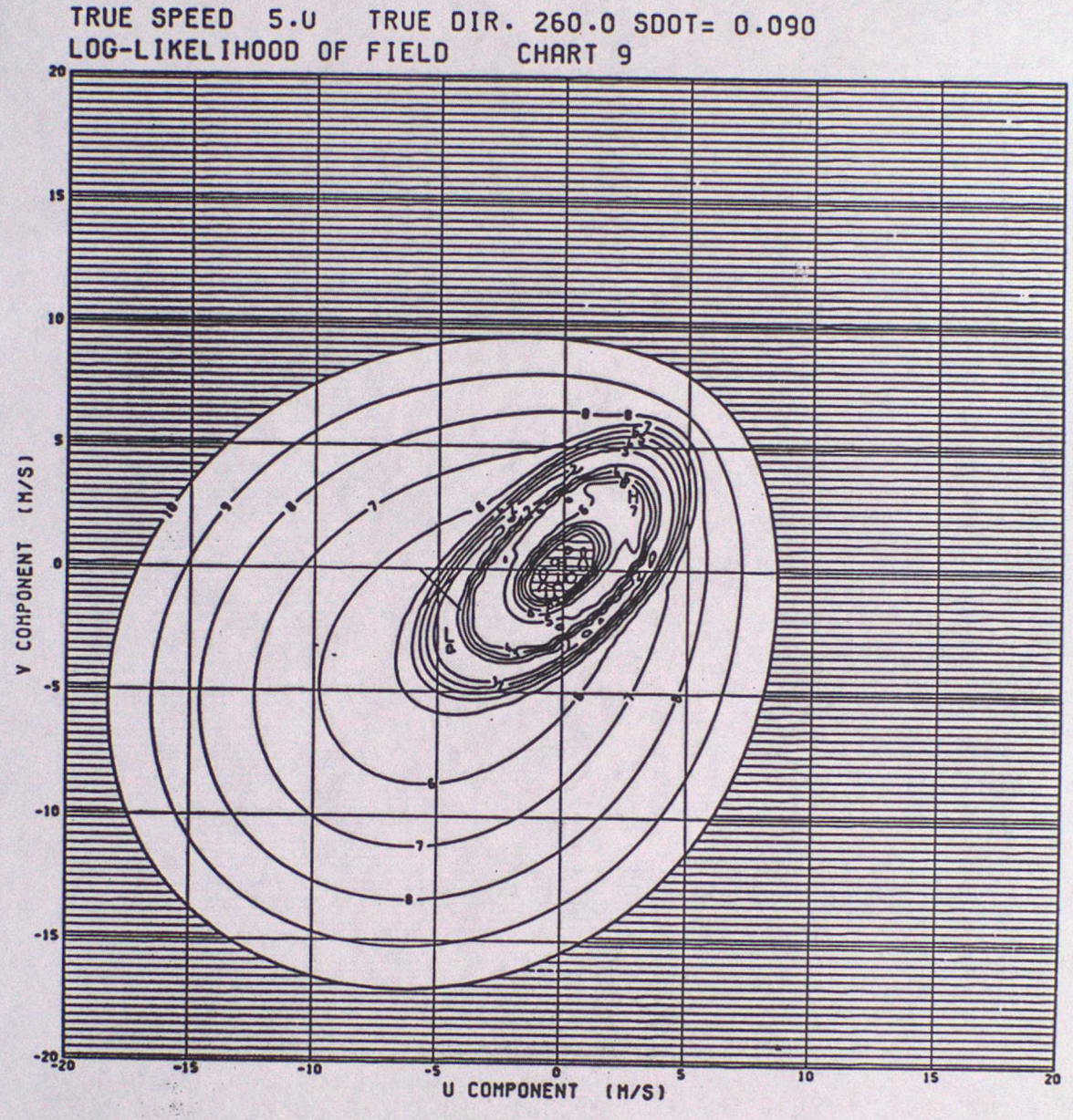
TRUE SPEED 5.0 TRUE DIR. 260.0 SDOT= 0.090
LOG-LIKELIHOOD OF FIELD CHART 9
V COMPONENT (M/S)
U COMPONENT (M/S)
20
15
10
5
0
-5
-10
-15
-20

FIGURE 9.9

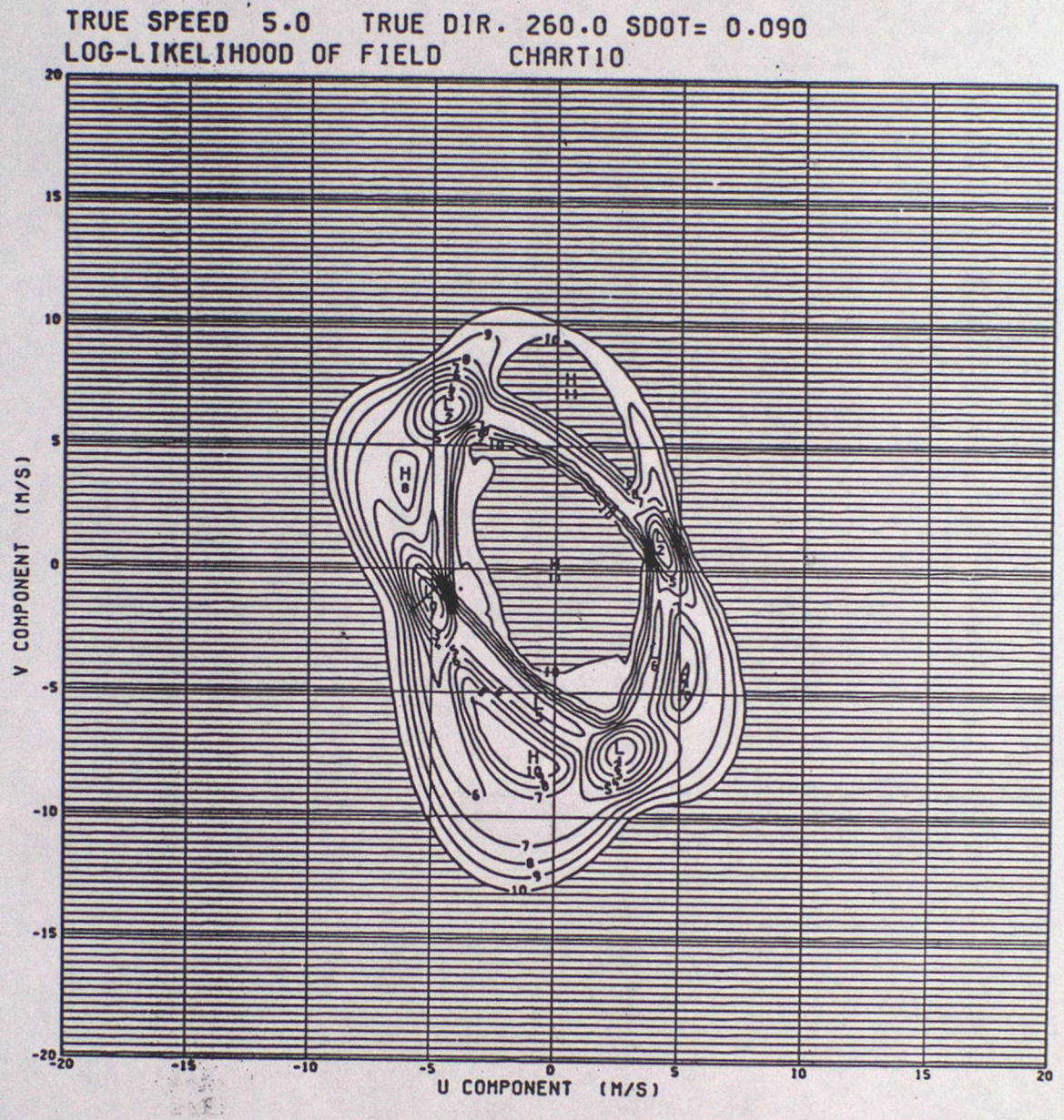
TRUE SPEED 5.0 TRUE DIR. 260.0 SDOT= 0.090
LOG-LIKELIHOOD OF FIELD CHART10
V COMPONENT (M/S)
U COMPONENT (M/S)
20
15
10
5
0
-5
-10
-15
-20

FIGURE 9.10

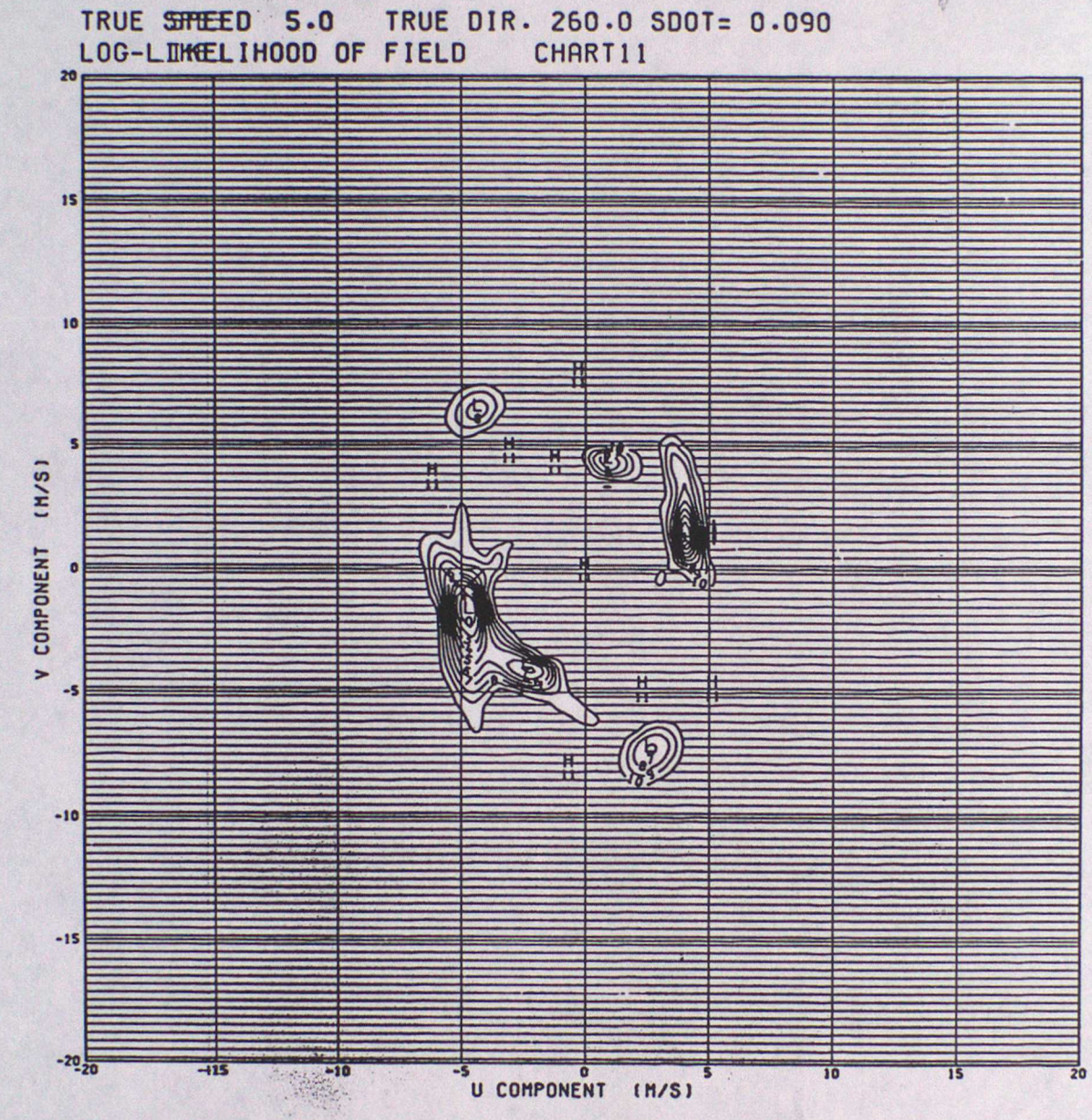
TRUE SPEED 5.0 TRUE DIR. 260.0 SDOT= 0.090
LOG-LIKELIHOOD OF FIELD CHART11
V COMPONENT (M/S)
U COMPONENT (M/S)
20
15
10
5
0
-5
-10
-15
-20

FIGURE 9.11